Model-based control and diagnosis of inland navigation networks

Pablo Segovia Castillo

IMT Lille Douai

Université de Lille

THESE

présentée en vue
d'obtenir le grade de

DOCTEUR

en
Automatique
par

Pablo SEGOVIA CASTILLO

DOCTORAT DE L'UNIVERSITE DE LILLE
DELIVRE PAR IMT LILLE DOUAI

Model-based control and diagnosis of inland navigation networks

Soutenue le 11 Juin 2019 devant le jury d'examen

Rapporteur	Laurent LEFÈVRE	Professeur, Grenoble INP
Rapporteur	Valérie DOS SANTOS MARTINS	M. de Conférences, HDR, Univ. Lyon 1
Examinateur	Rudy R. NEGENBORN	Professeur, TU Delft
Examinateur	José Mª MAESTRE TORREBLANCA	M. de Conférences, Univ. de Sevilla
Directeur de thèse	Vicenç PUIG CAYUELA	Professeur, Univ. Pol. de Catalunya
Directeur de thèse	Éric DUVIELLA	Professeur, IMT Lille Douai
Encadrant	Fatiha NEJJARI AKHI-ELARAB	Professeur, Univ. Pol. de Catalunya
Encadrant	Lala RAJAOARISOA	M. de Conférences, IMT Lille Douai

Unité de Recherche Informatique et Automatique URIA
IMT Lille Douai

Ecole Doctorale Sciences Pour l'Ingénieur EDSPI

Acknowledgements

It is often said that the journey is more important than the destination. Although there is no denying that obtaining a PhD constitutes a rewarding achievement, the three-year journey that leads up to its accomplishment has been a remarkable experience on its own. One of the many lessons is that pursuing a PhD is not about embarking on an individual quest. Rather, it is about interacting, discussing and ultimately learning from others. No matter how many people are acknowledged in this section, the list is likely to remain incomplete. Therefore, before I start, I would like to offer my sincere apologies to anyone who I might have unintentionally left off.

This thesis was carried out in the context of a co-tutoring agreement between two universities: IMT Lille Douai (IMT) in France, and Universitat Politècnica de Catalunya (UPC) in Spain. Therefore, I would like to thank my supervisors and advisors from both universities: Prof. Éric Duviella and Dr. Lala Rajaoarisoa (IMT), and Prof. Vicenç Puig and Prof. Fatiha Nejjari (UPC). Their support, encouragement and exceptional academic guidance have been essential for this thesis to come to fruition. Moreover, they have provided me with excellent working environments, suggesting possible ideas to explore but at the same time leaving space for me to find my own path. They have definitely set high standards regarding what a good supervisor, a good researcher and a good colleague should be.

I would like to acknowledge Prof. Laurent Lefèvre (Grenoble INP) and Prof. Valérie Dos Santos (Univ. Lyon 1) for their time spent reviewing this thesis, providing valuable remarks that helped to improve the quality of the manuscript. I would also like to thank them, together with Prof. Rudy R. Negenborn (TU Delft) and Prof. José Mª Maestre (Univ. de Sevilla), for accepting to be part of the examination panel.

During these years, I have also had the possibility to collaborate with several people. I would like to thank Dr. Joaquim Blesa (UPC) for the opportunity to work with him

in the topic of fault diagnosis, Dr. Klaudia Horváth (Deltares and TU Eindhoven) for the discussions regarding the modeling of navigation canals and Prof. Pierre-Olivier Malaterre (IRSTEA) for receiving me in Montpellier and teaching me the basics of SIC^2.

Given the nature of the co-tutoring agreement, I spent a great deal of time in Douai during the doctoral period. I would like to begin by warmly thanking Éric and Caroline for their hospitality, generosity and kindness, which almost made me feel as if I had never left Barcelona. Besides, upon my arrival, I spent some weeks at the student residence, where I felt at home from the first day thanks to the people I met there, despite the modest accommodation. A special thought goes to the fellow students in the department, who are a source of fond memories: Balsam, Enjie, Guillaume, Houda, Johann, Mónika, Pablo, Tony and Ziad, thank you for all the discussions and fun moments we shared together. Upon my return to Barcelona for the second part of the thesis, I got to known another great group with whom I have also shared many stimulating discussions and unforgettable moments: Asi, Damiano, Hazem, Jenny, José Luis, Julián, Masoud, Miguel, Nikolas, Unni, Wicak and Ye, thank you for everything.

I cannot but acknowledge my parents, Juan Antonio and Julia, and my brother Oscar, for teaching me essential values that have shaped me into the person I am today, and without which I would have never succeeded in completing this thesis. Your unfailing support, understanding and love during all these years have been fundamental. Finally, I want to express my sincerest gratitude to Bet, who has stood beside me all this time, showing more patience than I could have hoped for and never ceasing to provide comforting words. I cannot put into words how much you have contributed to this thesis.

Pablo Segovia Castillo
Douai & Barcelona, 2019

Abstract

This thesis addresses the problem of optimal management of water resources in inland navigation networks from a control theory perspective. In particular, the main objective to be attained consists in guaranteeing the navigability condition of the network, i.e., ensuring that the water levels are such that vessels can travel safely. More specifically, the water levels must be kept within an interval around the setpoint. Other common objectives include minimizing the operational cost and ensuring a long lifespan of the equipment. However, inland navigation networks are large-scale systems characterized by a number of features that complicate their management, namely complex dynamics, large time delays and negligible bottom slopes.

In order to achieve the optimal management, the efficient control of the hydraulic structures, e.g., gates, weirs and locks, must be ensured. To this end, a control-oriented modeling approach is derived based on an existing simplified model obtained from the Saint-Venant equations. This representation reduces the complexity of the original model, provides flexibility and allows to coordinate current and delayed information in a systematic manner. However, the resulting model formulation belongs to the class of delayed descriptor systems, for which standard control and state estimation tools would need to be extended. Instead, model predictive control and moving horizon estimation can be easily adapted for this formulation, as well as being able to deal with physical and operational constraints in a natural manner.

Due to the large dimensionality of inland navigation networks, a centralized implementation is often neither possible nor desirable. In this regard, non-centralized approaches are considered, decomposing the overall system in subsystems and distributing the computational burden among the local agents, each of them in charge of meeting the local objectives. Given the fact that inland navigation networks are strongly coupled systems, a distributed approach is followed, featuring a communication protocol among the agents.

Despite the optimality of the computed solutions, state estimation will only be effective provided that the sensors acquire reliable data. Likewise, the control actions will only be applied correctly if the actuators are not impacted by faults. Indeed, any malfunction can lead to an inefficient management of the system. Therefore, the last part of the thesis is concerned with the design of supervisory strategies that allow to detect and isolate faults in inland navigation networks.

All the presented modeling, centralized and distributed control and state estimation and fault diagnosis approaches are applied to a realistic case study based on the inland navigation network in the north of France to validate their effectiveness.

Keywords: inland navigation networks, large-scale systems, time-delay systems, Saint-Venant equations, control-oriented modeling, model predictive control, moving horizon estimation, system partitioning, distributed control and state estimation, fault diagnosis.

Résumé

Cette thèse contribue à répondre au problème de la gestion optimale des ressources en eau dans les réseaux de navigation intérieure du point de vue de la théorie du contrôle. L'objectif principal à atteindre consiste à garantir la navigabilité des réseaux de voies navigables, c'est à dire, à veiller à ce que les niveaux d'eau de chaque partie des réseaux soient tels que les bateaux puissent naviguer en toute sécurité. Plus spécifiquement, les niveaux d'eau doivent être maintenus dans un intervalle autour de points de consigne. Parmi les autres objectifs de gestion, il est nécéssaire de veiller à la réduction des coûts opérationnels et la longue durée de vie des équipements. Lors de la conception de lois de contrôle, les caractéristiques des réseaux de voies navigables doivent étre prises en compte, à savoir leurs grandes dimensions, leur composition (biefs interconnectés), leurs dynamiques complexes, des retards importants et variables, et parfois l'absence de pente.

Afin de réaliser la gestion optimale de réseaux de voies navigables, le contrôle efficace des structures hydrauliques, par exemple des portes, des déversoirs et des écluses, doit être assuré. À cette fin, une approche de modélisation orientée contrôle est dérivée d'un modèle simplifié existant, obtenu à partir des équations de Saint-Venant. Cette représentation réduit la complexité du modèle d'origine, offrant de la flexibilité et permettant de coordonner les informations actuelles et retardés de manière systématique. Cependant, la formulation du modèle obtenue appartient à la classe des systèmes de descripteurs retardés, pour lesquels les outils de contrôle standard et d'estimation d'état doivent être étendus. La commande prédictive MPC et l'estimation d'état sur horizon glissant MHE peuvent être facilement adaptés à cette formulation, tout en permettant de gérer les contraintes physiques et opérationnelles de manière naturelle.

En raison de la grande dimensionnalité des réseaux de voies navigables intérieures, une mise en œuvre centralisée n'est souvent ni possible ni souhaitable. À cet égard, les approches non centralisées sont considérées, décomposant le système global en sous-systèmes et répartissant la charge de calcul entre les agents locaux, chacun d'entre eux

chargé de garantir les objectifs locaux. Compte tenu du fait que les réseaux de navigation intérieure sont des systèmes fortement couplés, une approche distribuée est proposée, incluant un protocole de communication entre agents.

Malgré l'optimalité des solutions calculées, l'estimation d'état n'est efficace que si les capteurs acquièrent des données fiables. De même, les actions de contrôle ne sont appliquées correctement que si les actionneurs ne sont pas impactés par des défauts. Toute erreur peut entraîner une gestion inefficace du système. Par conséquent, les dernières contributions de la thèse concernent la conception de stratégies de supervision permettant de détecter et d'isoler les pannes des équipements hydrauliques.

Toutes les approches de modélisation, de commande centralisée et distribuée, d'estimation d'état et de diagnostic de pannes présentées sont appliquées à une étude de cas réaliste basée sur le réseau de voies navigables du nord de la France afin de valider leur efficacité.

Mots-clés: réseaux de voies navigables, systèmes à grande échelle, systèmes à retard, équations de Saint-Venant, modélisation orientée contrôle, commande prédictive, estimation d'état sur horizon glissant, partitionnement de systèmes, commande et estimation d'état distribuées, diagnostic de pannes.

Resum

La present tesi versa sobre el problema de la gestió òptima dels recursos hídrics en vies de navegació interior des de la perspectiva de la teoria de control. Concretament, l'objectiu principal radica en garantir la condició de navegabilitat del sistema. Dit d'una altra manera, es vol garantir que els nivells d'aigua siguin tals que les embarcacions puguin navegar-hi de forma segura. Aquest objectiu s'assoleix mantenint els nivells a l'interior d'un interval construït al voltant del punt d'operació. Altres objectius comuns en aquest context aspiren a minimitzar els costos associats a l'operació dels equips, així com a prolongar-ne la seva vida útil. Ara bé, les vies de navegació interior són sistemes a gran escala caracteritzats per dinàmiques complexes, grans retards temporals i pendents negligibles, aspectes que en dificulten la gestió.

Per tal d'assolir la gestió òptima, s'ha de garantir un control eficient de les estructures hidràuliques tals com comportes, dics i rescloses. Amb aquesta finalitat, es deriva un modelat del sistema orientat a control basat en un model existent simplificat, obtingut a partir de les equacions de Saint-Venant. Aquesta nova representació redueix la complexitat del model original, proporciona flexibilitat i permet coordinar informació actual i retardada de manera sistemàtica. Malgrat això, la formulació resultant pertany a la classe de sistemes descriptors amb retard, per als quals les tècniques de control i d'estimació estàndards necessiten ser esteses. En canvi, el control predictiu basat en models i l'estimació d'estat amb horitzó lliscant es poden adaptar fàcilment a la formulació proposada. A més, són capaços de tractar amb restriccions físiques i operacionals de forma natural.

Degut a les grans dimensions de les vies de navegació interior, una implementació centralizada no resulta, tot sovint, ni possible ni desitjada. Per tal de pal·liar aquest problema, es consideren mètodes no centralitzats. D'aquesta manera, es descompon el sistema global en subsistemes i es distribueix la càrrega computacional del problema centralitzat entre els agents locals, de manera que cadascun d'ells s'encarrega de fer

complir els objectius locals. En tant que les vies de navegació interior són sistemes fortament connectats, se segueix un plantejament distribuït, incloent un protocol de comunicació entre els agents.

Malgrat la optimalitat dels resultats que les estratègies proposades puguin proporcionar, l'estimació d'estat només serà efectiva a condició que els sensors proveeixin informació fiable. Igualment, les accions de control únicament es podran aplicar correctament si els actuadors no estan afectats per fallades. En efecte, qualsevol avaria pot conduir a una gestió ineficaç del sistema. És per aquest motiu que la darrera part de la tesi tracta sobre el disseny d'estratègies de supervisió, que permetin detectar i aillar fallades en vies de navegació interior.

Tots els resultats de modelat, control i estimació d'estat centralitzats i distribuïts, així com de diagnòstic de fallades, s'apliquen a un cas d'estudi realista, basat en les vies de navegació interior del nord de França, per tal de provar-ne la seva eficàcia.

Paraules clau: vies de navegació interior, sistemes a gran escala, sistemes amb retards temporals, equacions de Saint-Venant, modelat orientat a control, control predictiu basat en models, estimació d'estat amb horitzó lliscant, partit de sistemes, control i estimació d'estat distribuïts, diagnòstic de fallades.

Resumen

La presente tesis versa sobre el problema de la gestión óptima de los recursos hídricos en vías de navegación interior desde la perspectiva de la teoría de control. En concreto, el objetivo principal consiste en garantizar la condición de navegabilidad del sistema, es decir, garantizar que los niveles de agua de los canales sean tales que las embarcaciones puedan navegar de forma segura. Dicho objetivo se consigue manteniendo los niveles dentro de un intervalo alrededor del punto de operación. Otros objetivos comunes consisten en minimizar los costes asociados a la operación de los equipos, así como a extender su vida útil. Hay que tener en cuenta que las vías de navegación interiores son sistemas a gran escala caracterizados por dinámicas complejas, grandes retardos temporales y pendientes prácticamente nulas, lo que dificulta su gestión.

Para alcanzar la gestión óptima, se debe garantizar un control eficiente de las estructuras hidráulicas tales como compuertas, diques y esclusas, y para ello se deriva un modelado del sistema orientado a control, basado en un modelo simplificado ya existente, obtenido a partir de las ecuaciones de Saint-Venant. Esta nueva representación reduce la complejidad del modelo original, proporciona flexibilidad y permite coordinar información actual y retardada de forma sistemática. Sin embargo, la formulación resultante pertenece a la clase de sistemas descriptores con retardos, para los cuales las técnicas de control y de estimación de estado estándares necesitan ser extendidas. En cambio, el control predictivo basado en modelos y la estimación de estado con horizonte deslizante pueden ser fácilmente adaptadas para la formulación propuesta, además de permitir lidiar con restricciones físicas y operacionales de forma natural.

Hay que tener en cuenta que, debido a las grandes dimensiones de las vías de navegación interior, una implementación centralizada no es, a menudo, ni posible ni deseada, y para paliar este problema se consideran los enfoques no centralizados. De este modo, se descompone el sistema global en subsistemas y se distribuye la carga computacional del problema centralizado entre los agentes locales, de manera que cada uno de ellos se

encarga de cumplir los objetivos locales. Como las vías de navegación interior son sistemas fuertemente conectados, se sigue un enfoque distribuido, incluyendo un protocolo de comunicación entre los agentes.

También se ha de considerar que la estimación de estado sólo será efectiva a condición de que los sensores provean información fiable. Asimismo, las acciones de control únicamente se podrán aplicar correctamente si los actuadores no están afectados por fallas. En efecto, cualquier avería puede conducir a una gestión ineficaz del sistema. Es por ello que la última parte de la tesis trata sobre el diseño de estrategias de supervisión que permitan detectar y aislar fallas en vías de navegación interior.

Todos los resultados de modelado, control y estimación de estado centralizados y distribuidos, así como de diagnóstico de fallas, se aplican a un caso de estudio realista basado en las vías de navegación interior del norte de Francia para probar su eficacia.

Palabras clave: vías de navegación interior, sistemas a gran escala, sistemas con retardos temporales, ecuaciones de Saint Venant, modelado orientado a control, control predictivo basado en modelos, estimación de estado con horizonte deslizante, particionado de sistemas, control y estimación de estado distribuidos, diagnóstico de fallas.

Notation

Symbol	Description
$\{\cdots\}$	set
$a \in \mathcal{A}$	a is an element of the set $\mathcal{A}$
$\mathbb{R}$	set of real numbers
$\mathbb{R}^n$	space of n-dimensional column vectors with real entries
$\mathbb{R}^{n\times m}$	space of n-by-m matrices with real entries
$\mathbb{R}_{\geq 0}$	set of non-negative real numbers, defined as $\mathbb{R}_{\geq 0} \triangleq \mathbb{R} \setminus (-\infty, 0)$
$\mathbb{Z}$	set of integer numbers
$\mathbb{Z}_{\geq 0}$	set of non-negative integer numbers, defined as $\mathbb{Z}_{\geq 0} \triangleq \mathbb{Z} \setminus (-\infty, 0)$
$\mathcal{X} \times \mathcal{Y}$	Cartesian product of the sets $\mathcal{X}$ and $\mathcal{Y}$, defined as $\mathcal{X} \times \mathcal{Y} \triangleq \{(x, y) : x \in \mathcal{X},\ y \in \mathcal{Y}\}$
$\mathcal{X}\,(\subset) \subseteq \mathcal{Y}$	$\mathcal{X}$ is a (strict) subset of $\mathcal{Y}$
$\mathbf{x}_i$	i-th element of the vector $\mathbf{x} \in \mathbb{R}^n$
$\mathbf{X}_{ij}$	element in the i-th row and j-th column of the matrix $\mathbf{X} \in \mathbb{R}^{n\times m}$
$\mathbf{x}^\intercal\,(\mathbf{X}^\intercal)$	transpose of a vector $\mathbf{x} \in \mathbb{R}^n$ (matrix $\mathbf{X} \in \mathbb{R}^{n\times m}$)
$\mathbf{X}^{-1}$	inverse of the matrix $\mathbf{X} \in \mathbb{R}^{n\times m}$
$\max(\cdot)$	operator that returns, among the elements of its argument, the one with maximum value
$\lceil\cdot\rceil$	operator that rounds its argument to the nearest integer greater than or equal to the argument (*ceiling* operator)
$\lvert\cdot\rvert$	operator that returns the cardinality of the argument set
$\mathbb{I}_n$	identity matrix of dimension n
$\dot{x}$	derivative of x with respect to time, defined as $\dot{x} \triangleq \frac{d}{dt}x(t)$
x_k	the subindex k indicates discrete time
$x_{k+j\mid k}$	predicted value of x at time instant $k+j$, performed at the current time instant k

Acronyms

Acronym	Description
ARX	AutoRegressive eXogenous
CMHE	Centralized Moving Horizon Estimation (or Estimator)
CMPC	Centralized Model Predictive Control (or Controller)
DMHE	Distributed Moving Horizon Estimation (or Estimator)
DMPC	Distributed Model Predictive Control (or Controller)
FDI	Fault Detection and Isolation
FTC	Fault-Tolerant Control
HNL	Higher Navigation Level
ID	Integrator Delay
IDZ	Integrator Delay Zero
IR	Integrator Resonance
LNL	Lower Navigation Level
LQR	Linear Quadratic Regulator
LSS	Large-Scale System(s)
MHE	Moving Horizon Estimation (or Estimator)
MPC	Model Predictive Control (or Controller)
NNL	Normal Navigation Level
UIO	Unknown Input Observer

Contents

List of Tables

List of Figures

Part I

Preliminaries

Chapter 1

Introduction

1.1 Context of the thesis

The results presented in this thesis have been developed in a co-tutoring agreement between Institut Mines Télécom Lille Douai (IMT) in France and Universitat Politècnica de Catalunya (UPC) in Spain. The three-year doctoral program is divided into two parts of equal duration: the first part was carried out at IMT, whereas the second was carried out at UPC, both under the supervision of Prof. Vicenç Puig and Prof. Éric Duviella.

1.2 Motivation

Hydrographical networks are large and complex systems used to meet the needs of mankind in terms of irrigation, transport, water supply and responses to the needs of industries. The long-term response to these requirements has resulted in structures and measurement systems that are generally remote, enabling the implementation of strategies for the efficient management of water resources. However, in an increasingly constrained context, notably due to changes in water demand, resource depletion and climate change, the management of hydrographical networks must be carried out optimally.

This thesis focuses on water management in inland waterways, also known as inland navigation networks (both namings are used indistinctly throughout the thesis). Such networks can be located within several watersheds and transport water among these watersheds and towards the sea. They are generally composed of several interconnected

reaches, which can be defined as artificial canals and natural rivers located between two actuators or measurement points. Thus, inland waterways are equipped with a large number of sensors and actuators spatially distributed and connected. The large dimensionality of these systems complicates the collection and transmission of measurements, as well as entailing a considerable computational burden. All these reasons cause the management of inland waterways to be a challenging problem.

More specifically, an efficient management is such that the transportation of passengers and freight can be conducted in a safe manner. Furthermore, water resources must be managed optimally, which means that their misuse should be minimized. To guarantee seamless transport chains, the water levels must be kept within boundaries around a reference level. To this end, cross structures are operated in the waterways to regulate the levels of the reaches. A two-level control architecture is typically considered in this environment [POMN15]: the global control level determines the setpoints and sends them to the local controllers available at each control structure. In turn, these local controllers must ensure that the actuators supply adequate flows. Nevertheless, this thesis deals only with the global control level, thus assuming that the local controllers are able to perform as desired.

The control strategy must also reject the disturbances that affect the system and interfere with the control objectives. In the framework of inland waterways, these disturbances refer to the request of lock operations each time that a boat reaches a lock. Indeed, vessels navigate along the network until their final destination, probably along several reaches in their way. The access from one reach to the adjacent one is granted by means of locks, i.e., enclosures that enable boats to overcome the difference in elevation between the reaches. Lock operations require large water volumes to be withdrawn from the origin reach, which are then discharged into the destination reach. The reason for considering lock operations as disturbances is that they cannot be postponed for a long time from the moment a boat reaches a lock, according to existing policies. Therefore, it is not possible to schedule lock operations in an optimal manner.

Taking into account all these issues, the problem that this thesis intends to solve is that of designing control strategies that guarantee an optimal management of inland waterways. To do so, a model of the system is needed. Then, control strategies must be designed based on this model, bearing in mind physical and operational constraints that might limit the performance of the system. Moreover, possible unmeasurable states of the system have to be estimated based on available measurements of the inputs and

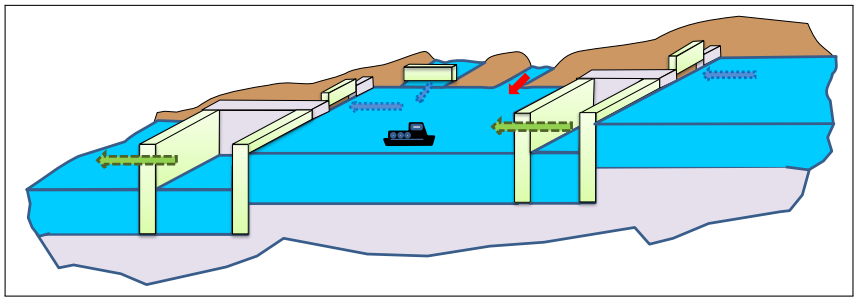

Figure 1.1: Navigation canal and its water-resource exchanges

outputs. Furthermore, the occurrence of faults in the system must be considered, leading to strategies that allow to diagnose whether the system is in faulty condition.

To illustrate the framework within which this thesis rests, Fig. 1.1 depicts part of a network consisting of three reaches, separated from one another by cross structures. The red solid arrows represent uncontrolled inputs and outputs such as natural bifurcations. On the other hand, the green dashed arrows indicate the flows generated due to the lock operations. Finally, the blue dotted arrows represent controlled actions, carried out by gates and weirs in order to regulate the water levels. Note that the locks are often built next to a control structure.

1.3 Thesis objectives

The main objectives of the thesis are described below:

— Characterize the dynamics of inland waterways by means of a precise mathematical representation that is both simple and flexible.

— Design a control strategy that allows to guarantee the navigability condition, as well as fulfilling other operational goals.

— Enhance the control design by means of a state estimation approach that supplies the controller with the unmeasurable states of the system.

— Take into account the large dimensionality of inland waterways in the implementation of the proposed solutions. In this regard, consider non-centralized approaches.

— Address the occurrence of faults in the system to ensure that the proposed approaches are able to perform as expected.

1.4 Outline of the thesis

The contents of the thesis, which tackle the objectives described in Section 1.3, are arranged in three parts, which in turn are further divided in chapters. The list of publications upon which they are based are given below each chapter.

Part I presents the framework of the thesis and introduces preliminary concepts regarding the management of inland waterways. It is organized in two chapters:

— **Chapter 1** justifies the motivation behind the topic considered in this thesis, states the problem to be solved and introduces briefly the subsequent chapters.

— **Chapter 2** provides some background on the main topics that are covered in this thesis, namely modeling, control and state estimation using both centralized and non-centralized approaches, and fault diagnosis. Moreover, a review of the literature is carried out, aiming at identifying relevant works in the context of this thesis.

Part II constitutes the central core, as it gathers all the results derived in this thesis. It is organized in four chapters:

— **Chapter 3** addresses the modeling of open-flow water systems for control, state estimation and fault diagnosis purposes. More specifically, a modeling methodology based on an existing simplified model is derived. The main improvements that this novel approach offers with respect to the original methodology lie in reducing the complexity of the resulting model, providing more flexibility and allowing to coordinate current and delayed information in a systematic manner. The content of this chapter has been featured in the following works:

  ◦ P. Segovia, K. Horváth, L. Rajaoarisoa, F. Nejjari, V. Puig, and E. Duviella. Modeling of two sub-reach water systems: application to navigation canals in the north of France. In *14th International Conference on Informatics in Control, Automation and Robotics (ICINCO)*, pages 459–467, 2017.

- P. Segovia, L. Rajaoarisoa, F. Nejjari, V. Puig, and E. Duviella. Modeling of interconnected flat open-channel flow: application to inland navigation canals. In *Advances in Hydroinformatics*, pages 75–90. Springer Singapore, 2018.
- P. Segovia, L. Rajaoarisoa, F. Nejjari, V. Puig, and E. Duviella. Decentralized control of inland navigation networks with distributaries: application to navigation canals in the north of France. In *American Control Conference*, pages 3341–3346. IEEE, 2017.
- P. Segovia, L. Rajaoarisoa, F. Nejjari, E. Duviella, and V. Puig. Model predictive control and moving horizon estimation for water level regulation in inland waterways. *Journal of Process Control*, 76C:1–14, 2019.
- P. Segovia, J. Blesa, E. Duviella, L. Rajaoarisoa, F. Nejjari, and V. Puig. Sensor fault diagnosis in inland navigation networks based on a grey-box model. *IFAC-PapersOnLine*, 51(24):742–747, 2018.

— **Chapter 4** proposes a centralized control and state estimation approach based on the model formulation derived in the previous chapter. The goal is to ensure the navigability of inland waterways. In this regard, the proposed approaches are of predictive nature, as they have proven to perform well in the past for these kinds of systems, given their features. The obtained results have been published in:

- P. Segovia, L. Rajaoarisoa, F. Nejjari, E. Duviella, and V. Puig. Input-delay model predictive control of inland waterways considering the backwater effect. In *2018 IEEE Conference on Control Technology and Applications (CCTA)*, pages 589–594. IEEE, 2018.
- P. Segovia, L. Rajaoarisoa, F. Nejjari, E. Duviella, and V. Puig. Model predictive control and moving horizon estimation for water level regulation in inland waterways. *Journal of Process Control*, 76C:1–14, 2019.

— **Chapter 5** discusses the limitations of the centralized implementation designed in the previous chapter. In this regard, a non-centralized strategy that belongs to the family of distributed approaches is proposed. To this end, the overall system is partitioned into subsystems, which are coordinated by means of local agents that solve smaller optimization problems with regard to the centralized one, and exchange information with one another. The results are gathered in:

- P. Segovia, L. Rajaoarisoa, F. Nejjari, E. Duviella, and V. Puig. Distributed Input-Delay Model Predictive Control of Inland Waterways. In Goffredo La Loggia, Gabriele Freni, Valeria Puleo, and Mauro De Marchis, editors,

HIC 2018. 13th International Conference on Hydroinformatics, volume 3 of *EPiC Series in Engineering*, pages 1893–1901. EasyChair, 2018.

- P. Segovia, L. Rajaoarisoa, F. Nejjari, E. Duviella, and V. Puig. A communication-based distributed model predictive control approach for large-scale systems. In *2019 IEEE Conference on Decision and Control (CDC)*, 2019. Submitted.
- P. Segovia, L. Rajaoarisoa, F. Nejjari, E. Duviella, and V. Puig. A distributed model predictive control and moving horizon estimation approach for the optimal management of inland waterways. *To be submitted.*

— **Chapter 6** is concerned with the design of supervisory strategies that allow to diagnose whether the system is in faulty condition. Indeed, the centralized and state estimation approaches described in previous sections will only be effective provided that the sensors and actuators are not affected by faults. Two different strategies, both based on the general model formulation derived in Chapter 3, are tested. The outcome of this work has been published in:

- P. Segovia, L. Rajaoarisoa, E. Duviella, J. Blesa, F. Nejjari, V. Puig, and K. Horváth. Fault detection and isolation in flat navigation canals. In *2017 4th International Conference on Control, Decision and Information Technologies (CoDIT)*, pages 427–432, 2017.
- P. Segovia, J. Blesa, K. Horváth, L. Rajaoarisoa, F. Nejjari, V. Puig, and E. Duviella. Modeling and fault diagnosis of flat inland navigation canals. *Proceedings of the Institution of Mechanical Engineers, Part I: Journal of Systems and Control Engineering*, 232(6):761–771, 2018.
- P. Segovia, J. Blesa, E. Duviella, L. Rajaoarisoa, F. Nejjari, and V. Puig. Sensor fault diagnosis in inland navigation networks based on a grey-box model. *IFAC-PapersOnLine*, 51(24):742–747, 2018.
- P. Segovia, J. Blesa, E. Duviella, L. Rajaoarisoa, F. Nejjari, and V. Puig. Sliding window assessment for sensor fault model-based diagnosis in inland waterways. *IFAC-PapersOnLine*, 51(5):31–36, 2018.

The approaches and strategies derived in Part II are tested using a realistic case study, which allows to discuss the obtained results and draw conclusions.

Part III, which is only composed of **Chapter 7**, draws the concluding remarks of this dissertation. Moreover, some topics that were left outside of the scope of this thesis

are presented, opening the door to possible future works.

Part IV gathers the two appendices:

— **Appendix A** completes the modeling results in Chapter 3. In particular, a model that links the discharges and the depths at the boundaries of a system characterized by a distributary is derived. This model is expressed using the external representation.

— **Appendix B** is also linked to Chapter 3. In this case, an alternative structure for a model characterized by the state-space representation is obtained. Such formulation provides a more compact notation and is to be used for parameter estimation purposes.

The connections among chapters are illustrated by means of the road map presented in Fig. 1.2, suggesting the appropriate reading order.

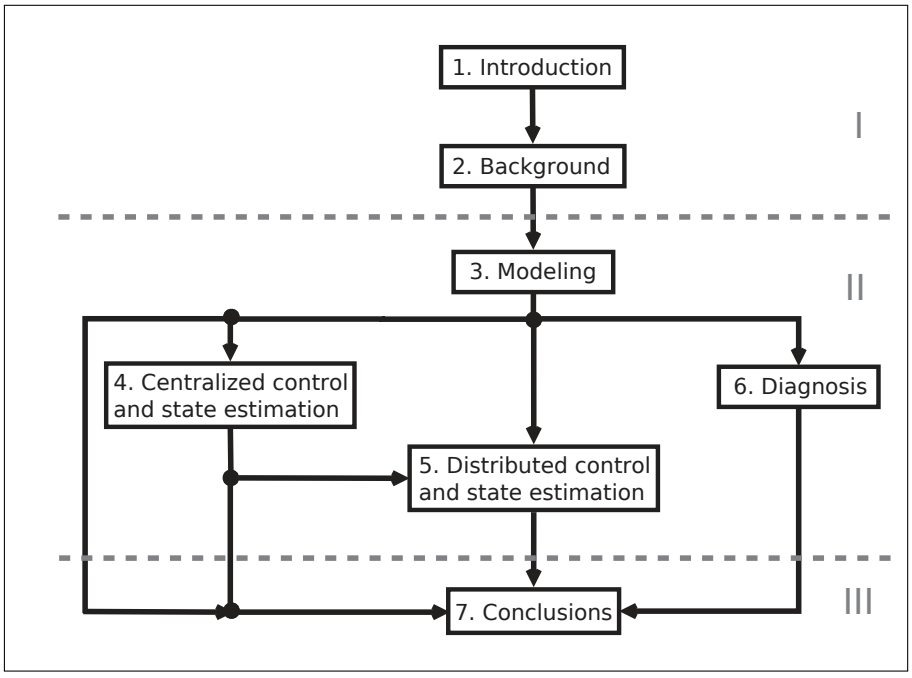

Figure 1.2: Road map of the thesis

Chapter 2

Literature review and background

This chapter provides some background on the main topics that are tackled in this thesis. For each of them, relevant works are presented and discussed. First, the modeling of open-flow water systems is discussed in Section 2.1: the nonlinear differential equations that govern their dynamics are presented, from which the existing simplified control-oriented modeling approaches are derived. Afterward, a review of model predictive control (MPC) and moving horizon estimation (MHE) is carried out in Section 2.2. The main features of these control and state estimation approaches are described, and their suitability to solve the inland waterways management problem is discussed. Then, Section 2.3 discusses the limitations of a centralized implementation, and hence the non-centralized paradigm is introduced. Finally, the issue of fault diagnosis in water systems is analyzed in Section 2.4. Indeed, it is necessary to design supervisory methods that enable the detection and prediction of faults to guarantee that the aforementioned tools yield reliable results.

2.1 Modeling

It was in 1871 that Adhémar Jean Claude Barré de Saint-Venant, a French mechanician and mathematician, published the seminal paper in which he derived the unsteady open-channel flow shallow water equations in unidirectional form [dSV71]. This is a set

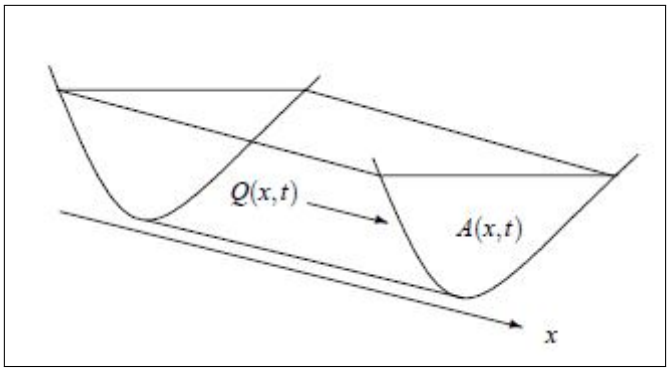

Figure 2.1: Open-channel flow along the longitudinal axis x (taken from [LF09])

of coupled nonlinear partial derivative equations that can be obtained from the application of conservation of mass and linear momentum principles, and is commonly used to model transient open-channel flow. Its formulation is as follows [Cho59]:

$$\frac{\partial A(x,t)}{\partial t} + \frac{\partial Q(x,t)}{\partial x} = 0, \tag{2.1a}$$

$$\frac{\partial Q(x,t)}{\partial t} + \frac{\partial}{\partial x}\left[\frac{Q^2(x,t)}{A(x,t)}\right] + gA(x,t)\left[\frac{\partial Y(x,t)}{\partial x} + S_f(x,t) - S_b(x)\right] = 0, \tag{2.1b}$$

with x the longitudinal abscissa and t the time. Relation (2.1a) is the mass conservation equation, whereas (2.1b) is the momentum conservation equation, and is the summation of the descriptions for the inertia, advection, gravitational force and friction force, respectively. According to Fig. 2.1, the following notation is used: $A(x,t)$ represents the wetted area $[m^2]$, $Q(x,t)$ the discharge $[m^3/s]$ across section A, $V(x,t)$ the average velocity $[m/s]$ in section A, $Y(x,t)$ the water depth $[m]$, $S_f(x,t)$ the friction slope $[m/m]$, $S_b(x)$ the bed slope $[m/m]$ and g the gravitational acceleration $[m/s^2]$.

In addition, the friction slope S_f is modeled with the classical Manning formula [Man91]:

$$S_f = \frac{Q^2 n^2}{A^2 R^{4/3}}, \tag{2.2}$$

with n the Manning coefficient $[s/m^{1/3}]$ and R the hydraulic radius $[m]$, defined by $R = A/P_w$, where P_w is the wetted perimeter $[m]$.

The Saint-Venant equations remain to this day as the most accurate mathematical representation of the dynamics of open-flow water systems. Alas, they suffer from a number of drawbacks that render them inadequate for control purposes. First of all, an analytical solution only exists in the uniform case (constant flow and water depth), a situation seldom encountered in practice [LF04a]. Furthermore, they are extremely sensitive to geometry errors and unmodeled dynamics. All these reasons have fostered the design of simpler models. Indeed, the main goal is to approximate the dominant dynamical behavior while retaining most of the system response behavior required for control needs [DRBG17].

A survey of the existing literature on the topic shows a considerable attention from the community. In this regard, one of the first proposals was the Integrator Delay (ID) model, an approximation model for flow in an open channel with backwater effect [SBB95, SCD+99]. As its name implies, the ID model uses two parameters to capture the main features of the dynamics of a canal: an integrator, which reflects the change in volume of the canal according to the variation of the water level, and a time delay, which measures the required time for actions at one end of the canal to have an impact at the other end.

However, as it was discussed in [LF04b], while the ID model is able to characterize satisfactorily the low frequency behavior, it fails to represent the high frequency phenomena. Indeed, the authors proposed in [LF04a] a modification of the original ID model that was able to describe a canal in any flow condition. This model, known as the Integrator Delay Zero (IDZ) model, was obtained from mathematical approximations of the exact transfer matrix. It extended the ID model formulation with a zero, which represents the direct influence of the discharge on the water level in high frequencies. Among others, it was successfully employed to design controllers for an irrigation canal with H_∞ performance in [LF06].

More recently, the Integrator Resonance (IR) model was proposed in [vOMB+10, vOB12], aiming at determining the properties of reflecting waves, which dominate the behavior of short and deep open water canals. The testing of this model resulted in good estimations of the frequency and magnitude of the first resonant peak, and was used in [vOHA14] to design predictive controllers for water level regulation purposes.

The presented approaches fall into the category of *white-box* models, which can be perfectly constructed using prior knowledge and physical insight. Two other cases can

be distinguished according to the level of assumed prior knowledge [SZL+95]: on the one hand, *gray-box* models can be used when some physical insight is possessed, but several parameters remain to be determined from observed data. On the other hand, *black-box* models do not apply any physical insight, although they might resort to model structures that have proved to perform well in the past. Such approaches have also found some success in the field of open-flow water systems [OW01, Wey01, BBPE02, DBSM+13, RPFBCGLS14, HDB+14].

Other techniques aim at providing a representation of the dynamics of canals in various operating points. Indeed, it can be argued that these systems do not always work close to the same operating point, and hence linear models, which are obtained by linearizing the Saint-Venant equations around a setpoint, yield predictions that are far from the real behavior in these situations. In this regard, Linear Parameter-Varying (LPV) models, which describe a class of nonlinear systems that can be modeled as parametrized linear systems, each of them designed at a different operating point (average flow along the canal), can be used. This approach has been applied in [PQE+05, BMGGMG09, BPB14, BP16] for real-time control of irrigation and navigation canals. Other approaches linked to the control of open-channel systems characterized by several operating modes have been proposed in [DCCC05, DPC+10, DSMRD12], where multi-models are considered.

Finally, numerical approaches in which spatial and temporal discretizations of the original shallow equations are performed have also been employed for control purposes. Although these techniques do not fall under the scope of the thesis, several related works are recalled here for convenience [CN09, HDLM10, PCL+10, DSMWR14, PGB14].

2.2 Centralized control and state estimation

Once the system has been modeled using one of the approaches presented in Section 2.1, the problem at stake is that of designing control strategies that allow to fulfill the management policy. Typically, two management scales are considered:

— The lower management scale is concerned with the water level control. Indeed, water levels must be kept within a predefined interval known as the navigation rectangle, which is depicted in Fig. 2.2. This interval is bounded by the lower and the higher navigation levels (NNL and HNL, respectively), which set the

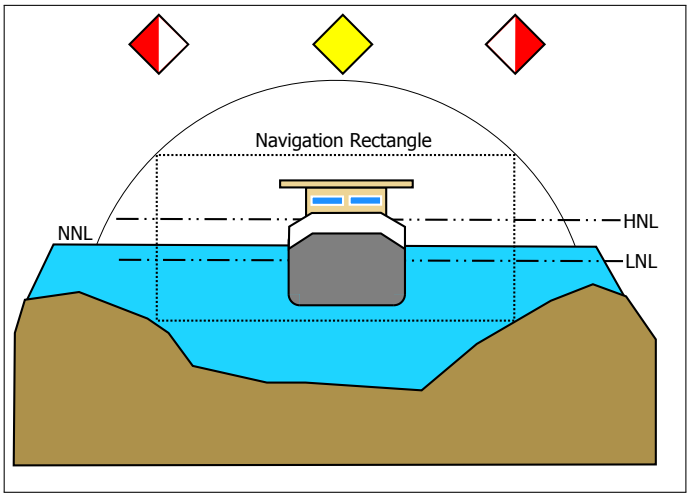

Figure 2.2: Navigation rectangle, delimited by the LNL and the HNL

admissible minimum and maximum water levels in the reaches that allow vessels to travel safely. This thesis falls within the context of a lower management scale policy.

— The higher management scale aims at dispatching the water resources in an optimal manner, i.e., minimizing their losses. Indeed, it is of the utmost importance that these resources are carefully managed, especially in the current context of climate change [Int14].

Several approaches have been reported in the literature to deal with this problem. From the many existing possibilities, MPC is chosen for this purpose. Its adequacy to deal with these kinds of systems as well as the basic features of its formulation are discussed next. This approach requires the vector of states to be known at current time, which are not always measurable. Thus, the MHE approach, which is often regarded as the dual problem of MPC, is also presented. These tools are introduced in a centralized manner in this section. By contrast, Section 2.3 discusses its suitability to deal with large-scale systems (LSS) and introduces the non-centralized philosophy.

2.2.1 Centralized model predictive control

Centralized model predictive control (CMPC) is one of the most widespread control techniques in many fields due to its ease of understanding and application. In

the framework of water systems, it has been employed in irrigation and drainage canals [BRB+07, LMN+09, vOCS+10, ÁRRS13, OMPCQ13], navigation canals and rivers [PRQ+09, VONDSVDG10, HRD+15, POMN15] and water distribution networks [GOMPJ14, WOP16, WPC17, KPPC18].

The following interesting features, among others, can be stated [CB98, Mac02]:

— The model of the system captures the dynamic and static interactions between input, output and disturbance variables.

— The physical constraints on inputs and outputs can be handled in a systematic manner.

— Multiple operational goals can be taken into account simultaneously.

— It is particularly suitable for those systems for which the disturbances can be forecast.

The main principle of this optimization-based technique resides in computing an optimal sequence of inputs that minimizes the value of a cost function, often composed of several weighted terms, subject to physical and operational constraints over a temporal horizon.

To begin with, the general linear discrete-time state-space representation

$$\mathbf{x}_{k+1} = \mathbf{A}\mathbf{x}_k + \mathbf{B}\mathbf{u}_k, \tag{2.3a}$$

$$\mathbf{y}_k = \mathbf{C}\mathbf{x}_k + \mathbf{D}\mathbf{u}_k \tag{2.3b}$$

is considered, where $k \in \mathbb{Z}_{\geq 0}$ denotes the discrete time instant. The vectors $\mathbf{x}_k \in \mathcal{X} \subseteq \mathbb{R}^{n_x}$, $\mathbf{u}_k \in \mathcal{U} \subseteq \mathbb{R}^{n_u}$ and $\mathbf{y}_k \in \mathcal{Y} \subseteq \mathbb{R}^{n_y}$ represent the system states, control inputs and system outputs, respectively, while $\mathbf{A}$, $\mathbf{B}$, $\mathbf{C}$ and $\mathbf{D}$ are the system matrices of appropriate dimensions. Moreover, $\mathcal{X}$, $\mathcal{U}$ and $\mathcal{Y}$ define, using set membership, the feasible sets according to the physical and operational constraints [RM09]. Note that (2.3a) and (2.3b) represent the state and the output equations, respectively.

Remark 2.1. The justification of the use of a linear model follows from Section 2.1, where it was stated that the use of a simpler linear model is preferred for control purposes. □

Then, the solution of the CMPC is computed by solving the following optimization problem:

$$\min_{\{\mathbf{u}_{i|k}\}_{i=k}^{k+H_p-1},\, \{\mathbf{x}_{i|k}\}_{i=k}^{k+H_p},\, \{\mathbf{y}_{i|k}\}_{i=k}^{k+H_p-1}} J\left(\mathbf{u}_{i|k}, \mathbf{x}_{i|k}, \mathbf{y}_{i|k}\right) \tag{2.4a}$$

subject to:

$$\mathbf{x}_{i+1|k} = \mathbf{A}\mathbf{x}_{i|k} + \mathbf{B}\mathbf{u}_{i|k},\ i \in \{k, ..., k+H_p-1\}, \tag{2.4b}$$

$$\mathbf{y}_{i|k} = \mathbf{C}\mathbf{x}_{i|k} + \mathbf{D}_u\mathbf{u}_{i|k},\ i \in \{k, ..., k+H_p-1\}, \tag{2.4c}$$

$$\mathbf{u}_{i|k} \in \mathcal{U},\ i \in \{k, ..., k+H_p-1\}, \tag{2.4d}$$

$$\mathbf{x}_{j|k} \in \mathcal{X},\ j \in \{k, ..., k+H_p\}, \tag{2.4e}$$

$$\mathbf{y}_{i|k} \in \mathcal{Y},\ i \in \{k, ..., k+H_p-1\}, \tag{2.4f}$$

$$\mathbf{x}_{k|k} = \mathbf{x}_k, \tag{2.4g}$$

with $\{\mathbf{u}_{i|k}\}_{i=k}^{k+H_p-1} \triangleq \{\mathbf{u}_{k|k}, \mathbf{u}_{k+1|k}, \cdots, \mathbf{u}_{k+H_p-1|k}\}$, and $\mathbf{x}_{i|k}$ and $\mathbf{y}_{i|k}$ are defined in the same manner. As stated before, the CMPC yields the optimal sequence of inputs to be applied to the system, provided that (2.4) is feasible. However, only $\mathbf{u}_{k|k}$ is applied to the system and the rest of components are disregarded, according to the receding philosophy $\mathbf{u}_k^{MPC} \triangleq \mathbf{u}_{k|k}$. This procedure is repeated at the next time instant.

2.2.2 Centralized moving horizon estimation

The CMPC presented in Section 2.2.1 uses the current state to compute the set of future inputs that moves the system to the setpoint in an optimal manner with respect to the chosen criteria. In general, the measurements of all states are not available, which motivates the design of observers to estimate the values of the unmeasured states.

There is little doubt that the work of Kalman [Kal60, KB61] constitutes the seminal result in state estimation [Rao00]. However, Kalman filtering does not address the issue of constraints. As it has been discussed before, physical and operational constraints limit the system performance, and thus the design of the observer must take this matter into account.

Therefore, the chosen observer is no other than the centralized moving horizon estimation approach (CMHE). The combination of CMPC and CMHE is especially attractive since the MHE formulation corresponds also to an online optimization problem that

can explicitly handle constraints [CH17]. Unlike MPC, this technique started receiving wider attention only a few years ago [TR02]. Indeed, the combination of MPC and MHE has been applied in diverse fields such as autonomous agricultural vehicles [KFK+13], unmanned aerial vehicles [QCH15], preventive sensor maintenance [LEDC15], airborne wind energy systems [VGH+15] and blood glucose regulation [CGH17]. Concerning water systems, the combination of these techniques is not so common, although it has been used for flood prevention in rivers [BBM10], pollution mitigation for combined sewer networks [JDOMC14] and to deal with offset problems due to a mismatch between the real system and a model [AvORT17].

Considering the general state-space representation introduced in (2.3), the CMHE can be easily formulated using the CMPC problem (2.4) as follows:

$$\min_{\{\hat{\mathbf{x}}_{i|k}\}_{i=k-N}^{k}} \left(\hat{\mathbf{x}}_{k-N|k} - \mathbf{x}_{k-N}\right)^{\intercal} \mathbf{P}^{-1} \left(\hat{\mathbf{x}}_{k-N|k} - \mathbf{x}_{k-N}\right) + \sum_{i=k-N}^{k-1} \left(\mathbf{w}_{i|k}^{\intercal} \mathbf{Q}^{-1} \mathbf{w}_{i|k} + \mathbf{v}_{i|k}^{\intercal} \mathbf{R}^{-1} \mathbf{v}_{i|k}\right) \tag{2.5a}$$

subject to:

$$\mathbf{w}_{j|k} = \hat{\mathbf{x}}_{j+1|k} - \left(\mathbf{A}\hat{\mathbf{x}}_{j|k} + \mathbf{B}\mathbf{u}_{j|k}\right), \; j \in \{k-N, ..., k-1\}, \tag{2.5b}$$

$$\mathbf{v}_{j|k} = \mathbf{y}_{j|k} - \left(\mathbf{C}\hat{\mathbf{x}}_{j|k} + \mathbf{D}\mathbf{u}_{j|k}\right), \; j \in \{k-N, ..., k-1\}, \tag{2.5c}$$

$$\hat{\mathbf{x}}_{i|k} \in \mathcal{X}, \; i \in \{k-N, ..., k\}, \tag{2.5d}$$

where $\mathbf{w}_k$ represents the system noise (disturbances) and $\mathbf{v}_k$ accounts for the measurement noise.

The CMHE problem is formulated as a quadratic program using a sliding window of a fixed size to take into account only the most recent measurements. Indeed, the amount of data processed with time can result in a high computational burden, which might render the full-information problem intractable. Instead, a truncated sequence of state estimates is computed at each time step.

Therefore, at the current time instant k, N input-output pairs $[(\mathbf{u}_{k-N}, \mathbf{y}_{k-N}) : (\mathbf{u}_{k-1}, \mathbf{y}_{k-1})]$ shall be available. Note that N is the length of the moving estimation window, thus bounding the size of the problem. The solution of the CMHE is given by the sequence $\{\hat{\mathbf{x}}_{i|k}\}_{i=k-N}^{k} \triangleq \{\hat{\mathbf{x}}_{k-N|k}, \hat{\mathbf{x}}_{k-N+1|k}, \cdots, \hat{\mathbf{x}}_{k|k}\}$.

However, as in the CMPC, only one value in the sequence is considered, and the rest are discarded. Therefore, $\hat{\mathbf{x}}_k^{MHE} \triangleq \hat{\mathbf{x}}_{k|k}$. In the next time instant, the sequence of input-output pairs is shifted in time to consider the most recent data, and a new estimation problem is solved.

2.3 Non-centralized control and state estimation

Centralized approaches such as those presented in Section 2.2 might not be practical to implement in the case of LSS such as inland navigation networks [MN14]. Indeed, these systems spread over large areas, and thus their models often involve a large number of states and control signals. Aside from the computational burden that this may cause on a centralized control agent, which may even compromise its reliability, a centralized approach also would require to rebuild the control-oriented model when the system configuration changes, thus complicating its maintenance [OMBP11].

To overcome the aforementioned issues, non-centralized approaches have been proposed. These consider multiple agents, each of them in charge of a different part of the network. An *agent* can be defined as a computing system within an environment that is capable of performing certain actions, aiming at attaining its objectives [WJ95]. In this context, agents are controllers and estimators.

Two main types of non-centralized strategies can be distinguished based on the interactions between the local agents [NvOKDS09, CSMndlPnL13]:

— *Decentralized* strategies often solve the subproblems by considering other subsystems' inputs as external disturbances. Depending on the degree of coupling, i.e., how closely linked the different subsystems are, this approach might lead to a poor overall performance [Sil11].

— *Distributed* strategies take into account the effects of local actions at the systemwide level. Indeed, the exchange of information among local agents is possible nowadays thanks to the developments in information and communication technologies, which allows them to cooperate and negotiate with each other, aiming at achieving the best global performance.

Indeed, both approaches have found success in the framework of water systems, as the review of the literature reveals. For instance, the decentralized approach has

been used for open-flow systems in [SFMC01, GRM02, BFR07, PLGB14] and water distribution networks [OMBP11, OMBPB12]. On the other hand, the distributed approach has also been applied to the control of open-flow systems [NvOKDS09, NvODS09, ZCMR$^+$11, FMH$^+$14, NPLGC17, VTSM19] and water distribution networks [GOMP17a, GOMP17b, TOMCP18].

Bearing in mind the differences between decentralized and distributed control, the latter is preferred in the context of this thesis. Inland waterways are strongly coupled systems, as each reach is physically connected to the adjacent ones at its boundaries, which causes local control actions to have an effect on the adjacent reaches that cannot be neglected without compromising the overall performance of the system. Therefore, it is desirable that the agents perform negotiation and cooperation at the benefit of optimality. Nevertheless, due to the many iterations that might be required for the agents to find a common satisfactory solution, distributed approaches usually result in higher computation times compared to their decentralized counterparts.

In order to perform distributed control and state estimation, the overall system must be decomposed into subsystems. To this end, partitioning strategies that aim at minimizing the number of couplings among subsystems can be looked at. Of course, this additional step might increase the computation time of non-centralized approaches.

Most of the system partitioning approaches are based on graph-theoretic methods, and thus the problem of system decomposition often leads to the problem of graph partitioning. Indeed, the structural properties of a linear dynamic system S such as (2.3) can be interpreted by means of the associated graph $\mathscr{G} = (\mathcal{V}, \mathcal{E})$, whose elements are defined in the following manner:

— $\mathcal{V} = \mathcal{U} \times \mathcal{X} \times \mathcal{Y}$ is the set of *vertices*, where $\mathcal{U} = \{u_1, u_2, ..., u_{n_u}\}$, $\mathcal{X} = \{x_1, x_2, ..., x_{n_x}\}$ and $\mathcal{Y} = \{y_1, y_2, ..., y_{n_y}\}$ are the nonempty input, state and output sets of $\mathscr{G}$, respectively.

— $\mathcal{E}$ is the set of *edges*, i.e., the set of arcs that connect the vertices of $\mathscr{G}$.

The system partitioning approach followed in this thesis consists in formulating the structural properties of the system by means of the adjacency matrix. Then, a permutation of the elements of this matrix allows to divide the overall system into smaller sets $\mathscr{G}_i$, $i = \{1, ..., M\}$. Assuming that the overall system can be decomposed into M subsystems, each of them defining a different subproblem, distributed model

predictive controllers (DMPC) and distributed moving horizon estimators (DMHE) can be designed based on the centralized problems given by (2.4) and (2.5), respectively. However, it is possible that one or more variables appear in more than one subproblem (coupled variables). Then, each agent must exchange information with the rest of agents with whom a coupled input or state is shared, aiming at obtaining a common solution that satisfies all subproblems.

2.4 Fault diagnosis

Given the large dimensionality of inland waterways, a large number of sensors and actuators are placed throughout the system in order to collect data and to operate the hydraulic equipment, respectively. However, these devices are subject to measurement errors and faults. This fact justifies the need for tools or procedures that are able to detect the occurrence of a fault. Faults can be of varied nature, e.g., internal events, environmental conditions and undetected design errors, but they all change the behavior of a system such that it no longer performs as expected, and thus it no longer satisfies its purpose.

Fault detection and isolation (FDI) allows, under certain circumstances, to detect whether or not a fault appears in the system and to be able to isolate it from the rest of possible faults, i.e., to identify in which component the fault occurs. Many different diagnosis methods exist, but they all follow the principle of consistency [CP99, BKLS06, Din08]. First, the nominal behavior of the system needs to be characterized by means of a plant model. Next, it is checked whether the measurements (input-output pairs) and the nominal behavior are consistent: if so, no inconsistency is detected. However, it is possible that two (or more) different faults cause the same pair, and thus an ambiguity in the diagnosis result exists. Thus, it is not possible to detect a fault with just the information about the nominal behavior of the system.

On the other hand, fault isolation requires information about the faults and their impact on the system, which means that models of the faults are required. Unfortunately, this information is not always enough to isolate faults, since more than one fault may generate the same effect, which means that, again, an ambiguity is present.

An additional issue to be taken into account is that of distinguishing faults from model uncertainties. Indeed, environmental systems such as open-flow water systems are

subject to uncertainties, which stem from natural unmodeled phenomena, e.g., seepage, evapotranspiration and rain.

In general, two main approaches are used to solve the FDI problem, model-based and data-driven methods [BKLS06]:

— Model-based approaches compare the measured data with the estimated data from the knowledge of the nominal behavior of the system. This comparison generates a residual, which is an expression that is close to zero when no fault is present in the system, and that deviates from zero when a fault occurs. However, since it is necessary to compute a model that represents the normal behavior of the plant in order to contrast the measured data, a deep knowledge of the physical principles governing the system is required.

— On the other hand, data-driven methods rely on the use of experimental data. One possible approach consists in using part of these data to estimate the parameters of a model that describes the faultless behavior of the system. Of course, it must be ensured that the used data are not impacted by faults. Moreover, the structure of the model can be based on previous physical knowledge. Other possibilities regard, for instance, building a classifier that is able to characterize the normal and faulty models, and to detect and localize in which component the fault occurs [SFCB+17]. However, the main drawback of this approach is that the applicability of this problem is restricted by the available data. This means that only past faults may be detected, as they are the only ones that have been experimented by the system.

Fault diagnosis in inland waterways is mostly concerned with the occurrence of sensor and actuator faults. Indeed, any error caused by a failure in a level sensor or in a flow control device can lead to inefficient management of the water resources, which can affect the navigation. Therefore, sensor and actuator fault diagnosis represents an important issue for inland navigation systems monitoring and supervision. This topic has attracted considerable attention in the past years, and an extensive body of literature dedicated to fault diagnosis in open-flow water systems has been produced. Several different strategies have been applied to diagnose faults in irrigation [BLKM06, BPB10, BW11, NMB12] and navigation canals [DRBC13, BHD+14, HBD+14].

2.5 Summary

This chapter has discussed some preliminary concepts regarding the main topics that will be covered in this thesis. More precisely, a general background on modeling, centralized and distributed control and state estimation, and fault diagnosis in the framework of water systems has been introduced. The study of these topics aims at dealing with the management of inland waterways, which requires the water levels to be kept within an interval to guarantee that vessels travel safely. Moreover, a general literature review has been carried out not only to familiarize with the existing approaches, but also to identify novel strategies proposed in this thesis with respect to the current state of the art.

Part II

Inland navigation networks: modeling, control, state estimation and fault diagnosis

Chapter 3

Modeling

This chapter addresses the problem of modeling open-flow water systems for control, state estimation and fault diagnosis purposes. First of all, the IDZ model is chosen and described in Section 3.1. This model, formulated as a continuous-time transfer function matrix, was originally conceived for single-reach systems. The original formulation is extended in Section 3.2 to deal with larger portions of inland waterways. A modeling strategy for systems with several reaches in cascade is proposed, which can be used, for instance, to model reaches with secondary inputs along its course. These contributions have been published in [SHR+17] and [SRN+18c]. Furthermore, inland waterways are characterized by water streams that branch off from the main stream and flow away (distributaries), as well as water streams that flow into other larger streams or lakes (tributaries). Imposing boundary conditions at the nodes, i.e., the locations in which these mergings and splittings take place, allows to extend the original IDZ formulation to model these topologies. These results have been collected in [SRN+17].

Nevertheless, it becomes apparent that this procedure is rather inadequate even in the case of small networks. It is therefore required to devise an alternative modeling approach that provides more flexibility in terms of adding reaches to or removing them from the considered system. For this purpose, a more suitable state-space representation is derived in Section 3.3 by taking into account the full model to account for the backwater effect. Indeed, a standard transformation leads to the equivalent IDZ model in the state-space form, which can then be used to model each reach separately. The rest of elements that integrate the system are also described mathematically to complete the model. Then, the links between reaches are established by means of mass balances at the nodes, which can be either incorporated into the model or formulated by means of

equality constraints. This static behavior leads to a delayed descriptor formulation, for which the appropriate control and state estimation techniques are designed in Chapter 4. All these modeling contributions have been published in [SRN+19b]. Furthermore, a parameter estimation approach is discussed in Section 3.4, which can be used in those cases where the lack of knowledge of a physical parameter prevents the computation of the IDZ model. This methodology was presented in [HDB+14] and has been further extended in [SBD+18a]. Finally, the modeling results for the approaches presented in Sections 3.3 and 3.4 are gathered in Section 3.5.

3.1 Modeling a canal: the IDZ model

The IDZ input-output model links the discharges and the water levels at the boundaries of a reach and is given by:

$$\begin{bmatrix} y_1(s) \\ y_2(s) \end{bmatrix} = \underbrace{\begin{bmatrix} p_{11}(s) & p_{12}(s) \\ p_{21}(s) & p_{22}(s) \end{bmatrix}}_{\mathbf{R}_r} \begin{bmatrix} q_1(s) \\ q_2(s) \end{bmatrix}, \tag{3.1}$$

where the subscripts 1 and 2 indicate the initial (upstream) and final (downstream) ends of the reach, $y_1(s)$ and $y_2(s)$ are the upstream and downstream water levels, $q_1(s)$ and $q_2(s)$ are the upstream inflow and downstream outflow, and the several IDZ terms are given by:

$$\begin{aligned} p_{11}(s) &= \frac{z_{11}s+1}{A_u s}, & p_{12}(s) &= \frac{z_{12}s+1}{A_u s}e^{-\tau_u s}, \\ p_{21}(s) &= \frac{z_{21}s+1}{A_d s}e^{-\tau_d s}, & p_{22}(s) &= \frac{z_{22}s+1}{A_d s}. \end{aligned} \tag{3.2}$$

Remark 3.1. $q_1(s) \in \mathbb{R}_{\geq 0}$ and $q_2(s) \in \mathbb{R}_{\geq 0}$. However, the latter is an outflow, which means that it causes the water levels to diminish. Therefore, $p_{12}(s)$ and $p_{22}(s)$ are negative. □

Remark 3.2. The parameters linked to the upstream level equation are denoted with a subscript u, whereas those linked to the downstream level are denoted with a subscript d. □

Remark 3.3. The terms $p_{11}(s)$ and $p_{22}(s)$ do not include a time delay as the discharges are assumed to have an immediate effect at the locations where they take place. □

The IDZ model contains an integrator, a time delay and a zero. The system can be

characterized by two different behaviors in the frequency domain. In low frequencies, the behavior of the system is similar to a tank that is being filled and/or emptied. In this situation, the integrator gain and the time delay have a predominant role. The former reflects how the volume changes according to the water level variation, whereas the latter expresses the minimum time that a perturbation requires to travel from one end of the canal to the other one. Two different time delays are defined:

$$\begin{aligned} \tau_u &= \frac{L}{C_w - V} \,, \\ \tau_d &= \frac{L}{C_w + V} \,, \end{aligned} \tag{3.3}$$

where L [m] is the length of the reach, C_w $[ms^{-1}]$ is the wave celerity and V $[ms^{-1}]$ is the wave velocity. Additionally, (3.3) corresponds to the case in which both the celerity and the velocity are constant. More precisely, the celerity is defined as the relative velocity of a wave with respect to the fluid in which it travels, whereas the velocity measures the variation of the particles' position of a fluid with respect to time. In particular, τ_u is measured from the downstream end to the upstream end, while τ_d is measured in the inverse direction.

Finally, the high frequency phenomena is approximated by the zero of $p_{ij}(s)$. More specifically, its constant gain approximates the oscillating modes caused by the gravity waves, which are predominant in high frequencies. Therefore, the IDZ model is not capable of representing the subsequent attenuated peaks that can be observed in the evolution of the water levels.

It is worth noting that the complete model is taken into consideration. Indeed, it is common practice to design only downstream water level controllers [LF09] for other systems such as irrigation and drainage canals and sewage networks, as their bottom slopes are usually non-negligible. Navigation reaches, on the other hand, are usually characterized by negligible bottom slopes, and therefore the backwater effect becomes of increasing importance. This effect takes place at the downstream hydraulic structure of a reach: when the water waves impact upon the structure, the water can flow back to the upstream end, resulting in a back-and-forth mass transport known as the resonance phenomena. Therefore, considering the full model allows to take into account the backwater effect in the upstream water level, which constitutes a novel feature of the modeling and control approaches that will be derived in the following.

In order to compute all the IDZ model parameters, it is necessary to know where the transition between the upstream uniform and downstream backwater flows occurs. The value of this abscissa is named x_1 [LF04b] and can be obtained as follows:

$$x_1 = \begin{cases} \max\left(L - \frac{y_L - y_n}{s_L}, 0\right) & if s_L \neq 0 \\ L & if s_L = 0 \end{cases}, \tag{3.4}$$

with y_L $[m]$ the downstream boundary condition, y_n $[m]$ the normal depth and s_L (dimensionless) the deviation from bed slope of the line tangent to the water curve at the downstream end of the pool. More details about the computation of these magnitudes can be found in [LF04b].

According to (3.4), x_1 can either be 0, L or take an intermediate value between 0 and L. The reach is completely under backwater flow if $x_1 = 0$, completely under uniform flow if $x_1 = L$ or present both kinds of flow if $0 < x_1 < L$. In particular, the interval $(0,\ x_1)$ is under uniform flow whereas the interval $(x_1,\ L)$ is under backwater flow. This is an important fact in the computation of the parameters, as they have to be computed for each kind of flow: the same formulas are applied for the uniform and backwater parts, but are evaluated according to the length of each part. The partial uniform and backwater parameters are merged into the so-called equivalent parameters, which represent the whole pool. In the event that $x_1 = 0$ or $x_1 = L$, they will only have to be computed once, for the whole length of the reach.

3.2 Modeling inland navigation networks using the IDZ model

Model (3.1) is used to characterize systems with reaches in cascade, as well as systems with tributaries and distributaries.

3.2.1 Networks with reaches in cascade

Figure 3.1 depicts a reach with a finite number of intermediate flows (either inflows or outflows) between the initial and final ends of the reach. Each of the abscissas in which these flows take place will be called a *section*. It is assumed that all these intermediate

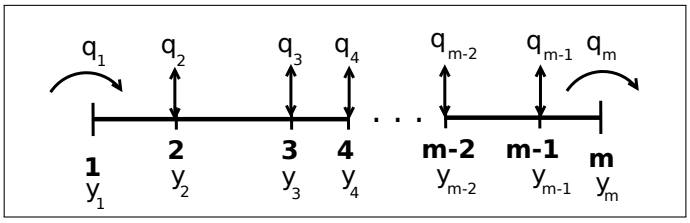

Figure 3.1: Scheme of a reach with m sections

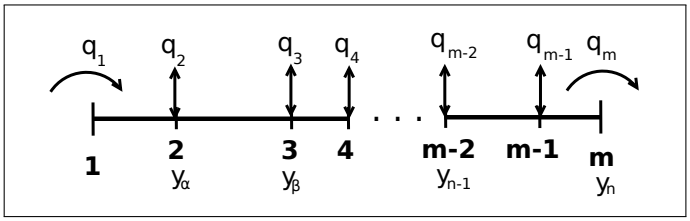

Figure 3.2: Scheme of a reach with only n measured water levels

flows can be controlled, and thus they are regarded as m known inputs of the system. However, it is also considered that it is not always possible to measure the water level for each section, but only for n of them ($n \leq m$). This fact justifies the notation introduced in Fig. 3.2:

The model that describes the system depicted in Fig. 3.2 can be written as follows:

$$\begin{bmatrix} y_\alpha \\ y_\beta \\ \vdots \\ y_n \end{bmatrix} = \underbrace{\begin{bmatrix} p_{\alpha,1} & p_{\alpha,2} & \cdots & p_{\alpha,m} \\ p_{\beta,1} & p_{\beta,2} & \cdots & p_{\beta,m} \\ \vdots & \vdots & \ddots & \vdots \\ p_{n,1} & p_{n,2} & \cdots & p_{n,m} \end{bmatrix}}_{\mathbf{R}} \begin{bmatrix} q_1 \\ q_2 \\ \vdots \\ q_m \end{bmatrix}, \tag{3.5}$$

with each of the p_{ij} elements as in (3.2), for $i = \{1, ..., n\}$ and $j = \{1, ..., m\}$.

To obtain all the p_{ij} terms, it is necessary to compute (3.1) between each pair of sections. After that, each of these elements is placed inside $\mathbf{R}$ in the position that links the corresponding pair. However, following these steps results in computing $m-1$ times the terms that link the input and the output in the same section, which leads to an

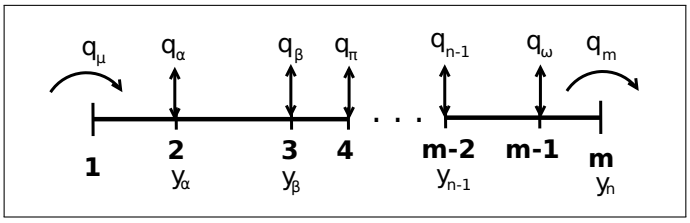

Figure 3.3: Scheme of a reach with n measured levels and final notation

overlapping problem. Consider, for instance, the term that links the water level and the discharge in section 2: it can be computed considering the part of the stream comprised between sections 1 and 2, but also between sections 2 and 3, between sections 2 and 4, and so on.

The position of these overlapped terms inside $\mathbf{R}$ depends on the measurable water levels, and therefore no fixed pattern can be established. For the sake of convenience, the variables in Fig. 3.2 are renamed so that the numbering of water levels and discharges match:

Equation (3.5) is modified according to the change of notation introduced in Fig. 3.3:

$$\begin{bmatrix} y_\alpha \\ y_\beta \\ \vdots \\ y_n \end{bmatrix} = \underbrace{\begin{bmatrix} p_{\alpha,\alpha} & p_{\alpha,\beta} & \cdots & p_{\alpha,n} \\ p_{\beta,\alpha} & p_{\beta,\beta} & \cdots & p_{\beta,n} \\ \vdots & \vdots & \ddots & \vdots \\ p_{n,\alpha} & p_{n,\beta} & \cdots & p_{n,n} \end{bmatrix}}_{\mathbf{R}_1} \begin{bmatrix} q_\alpha \\ q_\beta \\ \vdots \\ q_n \end{bmatrix} + \underbrace{\begin{bmatrix} p_{\alpha,\mu} & p_{\alpha,\pi} & \cdots & p_{\alpha,\omega} \\ p_{\beta,\mu} & p_{\beta,\pi} & \cdots & p_{\beta,\omega} \\ \vdots & \vdots & \ddots & \vdots \\ p_{n,\mu} & p_{n,\pi} & \cdots & p_{n,\omega} \end{bmatrix}}_{\mathbf{R}_2} \begin{bmatrix} q_\mu \\ q_\pi \\ \vdots \\ q_\omega \end{bmatrix} \tag{3.6}$$

The interesting fact about this new formulation is that $\mathbf{R}$ is split into two matrices $\mathbf{R}_1$ and $\mathbf{R}_2$, where the former is a square matrix whose diagonal elements link the input-output pair for the same section, and thus the overlapped terms are always placed in this diagonal. In this way, it is only necessary to define a criterion to select one of the $m-1$ possibilities for each term in the diagonal of $\mathbf{R}_1$. These elements satisfy the property that the time delay is equal to zero. Hence, they only consist of a zero and an integrator:

— The integrator gain accounts for the storage of water in low frequencies. Therefore,

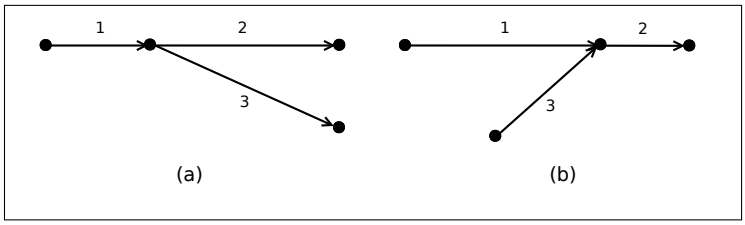

Figure 3.4: Schematic view of a: (a) Distributary. (b) Tributary.

the total area of the canal should be considered, and not any other area comprised between two intermediate sections.

— The zero of each transfer function depends, according to [LF04b], on the length of the reach, which again means the total length should be considered in order to account for the whole canal.

3.2.2 Networks with distributaries and tributaries

Schematic views of a distributary and a tributary are depicted in Fig. 3.4. These two topologies are regarded as composed of three reaches: a main reach, which is divided into two parts at the node, and a secondary reach, which either branches off from the main stream and flows away (distributary) or flows into the main reach (tributary). Since there exists a parallelism between both situations, they are studied together. However, only the first case is dealt with, as it is rather straightforward to derive analogous expressions for the tributary case.

The goal is to obtain a model that links the discharges and the depths at the boundaries by imposing certain conditions in the central node, where a natural bifurcation takes place. The complete procedure to derive such model is detailed in Appendix A. As a result, the global model

$$\begin{aligned} y_1^{(1)} &= p_{11}^{(G)} q_1^{(1)} + p_{12}^{(G)} q_2^{(2)} + p_{13}^{(G)} q_2^{(3)}, \\ y_2^{(2)} &= p_{21}^{(G)} q_1^{(1)} + p_{22}^{(G)} q_2^{(2)} + p_{23}^{(G)} q_2^{(3)}, \\ y_2^{(3)} &= p_{31}^{(G)} q_1^{(1)} + p_{32}^{(G)} q_2^{(2)} + p_{33}^{(G)} q_2^{(3)} \end{aligned} \tag{3.7}$$

is obtained, with

$$p_{11}^{(G)} = p_{11}^{(1)} + p_{12}^{(1)} p_{21}^{(1)} \left(\frac{\lambda}{\lambda p_{11}^{(2)} + p_{22}^{(1)}} + \frac{1-\lambda}{(1-\lambda) p_{11}^{(3)} + p_{22}^{(1)}} \right) \tag{3.8a}$$

$$p_{12}^{(G)} = \frac{\lambda p_{12}^{(1)} p_{12}^{(2)}}{\lambda p_{11}^{(2)} + p_{22}^{(1)}} \tag{3.8b}$$

$$p_{13}^{(G)} = \frac{(1-\lambda) p_{12}^{(1)} p_{12}^{(3)}}{(1-\lambda) p_{11}^{(3)} + p_{22}^{(1)}} \tag{3.8c}$$

$$p_{21}^{(G)} = \lambda p_{21}^{(1)} p_{21}^{(2)} \left(\frac{\lambda}{\lambda p_{11}^{(2)} + p_{22}^{(1)}} + \frac{1-\lambda}{(1-\lambda) p_{11}^{(3)} + p_{22}^{(1)}} \right) \tag{3.8d}$$

$$p_{22}^{(G)} = p_{22}^{(2)} + \frac{\lambda^2 p_{12}^{(2)} p_{21}^{(2)}}{\lambda p_{11}^{(2)} + p_{22}^{(1)}} \tag{3.8e}$$

$$p_{23}^{(G)} = \frac{\lambda(1-\lambda) p_{21}^{(2)} p_{12}^{(3)}}{(1-\lambda) p_{11}^{(3)} + p_{22}^{(1)}} \tag{3.8f}$$

$$p_{31}^{(G)} = (1-\lambda) p_{21}^{(1)} p_{21}^{(3)} \left(\frac{\lambda}{\lambda p_{11}^{(2)} + p_{22}^{(1)}} + \frac{1-\lambda}{(1-\lambda) p_{11}^{(3)} + p_{22}^{(1)}} \right) \tag{3.8g}$$

$$p_{32}^{(G)} = \frac{\lambda(1-\lambda) p_{12}^{(2)} p_{21}^{(3)}}{\lambda p_{11}^{(2)} + p_{22}^{(1)}} \tag{3.8h}$$

$$p_{33}^{(G)} = p_{22}^{(3)} + \frac{(1-\lambda)^2 p_{12}^{(3)} p_{21}^{(3)}}{(1-\lambda) p_{11}^{(3)} + p_{22}^{(1)}}. \tag{3.8i}$$

Remark 3.4. Note that the dependance of the terms in (3.7) and (3.8) on the Laplace variable s is omitted for readability. □

3.3 Limitations and equivalent state-space representation

It becomes apparent at this point that the modeling approaches introduced in Section 3.2 are rather inadequate. Indeed, not only the derivation of (3.8) involves painstaking algebraic manipulations, but also these formulas can only be applied to the particular configuration depicted in Fig. 3.4. If a fourth reach is added to the system, additional

conditions must be imposed, increasing the size and complexity of the model. Therefore, it is necessary to find an alternative modeling approach in order to circumvent this issue.

The proposed alternative consists in transforming the original IDZ model (3.2) into its equivalent state-space representation. This new formulation offers some interesting features:

— The complexity of the model is reduced, as it makes use of a more compact representation.

— It also provides more flexibility in terms of adding reaches to or removing them from the considered system. Although the size of the matrices increases with the number of considered reaches, it is much easier to link reaches. Indeed, it is only required to impose mass balances at the nodes, which can be either incorporated into the model (performing the necessary substitutions) or formulated by means of equality constraints, which are then added to the rest of constraints.

— It allows to coordinate current and delayed information in a systematic manner. Indeed, the model is described by variables with an immediate and a delayed effect. Those variables with a delayed effect are provided to the control and state estimation algorithms as parameters, ensuring that their values are taken into account adequately, which is crucial for a satisfactory performance of the algorithms.

The final control-oriented modeling approach is presented below. An inland waterways model can be regarded as composed of a set of elements, which are introduced and described below. Note that the physical nature of the variables, e.g., water levels, flows, openings and elevations, as well as other elements in the waterways, constrains the performance of the system.

3.3.1 Actuators

Gates and weirs are used to regulate the water levels in the reaches. In particular, two kinds of structures are considered: undershot gates and sharp crested weirs. An undershot gate is a bottom opening in a wall, whose height can be regulated. Conversely, in the case of a weir, the water flows over its crest, whose elevation is also adjustable. A schematic representation of an undershot gate and a weir is given in Fig. 3.5. Note that q is the flow through the cross structure, u is the opening/elevation, and y_1 and y_2 are the upstream and downstream water levels, respectively.

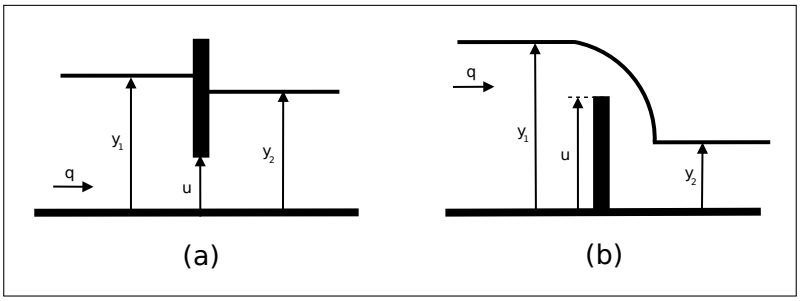

Figure 3.5: Water level regulation with: (a) an undershot gate. (b) a sharp crested weir.

Discharges, openings and elevations can be used in the automated control of canals. The global control level must compute the optimal action and send it to the slave controller that operates the gate or weir. If the discharge is used as the control variable, the slave controller must convert the given discharge into an equivalent opening or elevation, which is not as straightforward as inverting the discharge equation [LMBRB08]. Furthermore, choosing the openings and elevations allows to link them with the local discharges and the upstream and downstream water levels at the structure, thus taking into account such complex dynamics [Mal95]. For these reasons, the openings and elevations are chosen as control variables in this thesis. The conversion is carried out following the methodology described in [BPB14], which basically consists in using linearized equations that describe the relationship between openings and discharges.

The lower and upper operating limits of these elements are characterized as follows:

$$\underline{\mathbf{u}}^m \leq \mathbf{u}_k^m \leq \overline{\mathbf{u}}^m \,, \quad m = 1, ..., N_m \,, \tag{3.9}$$

where $\underline{\mathbf{u}}^m$ and $\overline{\mathbf{u}}^m$ are the lower and upper opening or elevation limits of the m-th actuator, and N_m is the total number of actuators in the system.

The type of flow at the structure determines the general linearized equation to be used:

— The *free-flow* case is characterized by critical or super-critical flow at the structure, which overrides the effect of the downstream water level on the gate discharge. The linearized expression reads as

$$q_2^{(1)}(s) \approx q_1^{(2)}(s) = k_y^{(1)} y_2^{(1)}(s) + k_u u(s). \tag{3.10}$$

— The *submerged flow* case is characterized by sub-critical flow at the structure. In this case, the discharge is affected by the downstream water level:

$$q_2^{(1)}(s) \approx q_1^{(2)}(s) = k_y^{(1)} y_2^{(1)}(s) + k_y^{(2)} y_1^{(2)}(s) + k_u u(s). \tag{3.11}$$

In both cases, $q_2^{(1)}$ is the inflow of the structure at the downstream end of reach 1, $q_1^{(2)}$ is the outflow of the structure at the upstream end of reach 2, $y_2^{(1)}$ is the water level upstream of the structure, $y_1^{(2)}$ is the water level downstream of the structure, u is the opening or elevation and $k_y^{(1)}$, $k_y^{(2)}$ and k_u are the coefficients obtained in the linearization of the nonlinear equations of the gates and weirs. Indeed, (3.10) and (3.11) are derived from the corresponding nonlinear equations of the gates and the weirs, which are introduced in [LF09] and are given in (3.12) and (3.13), respectively. Note that the notation used corresponds to the variables in the general representation depicted in Fig. 3.5.

$$\text{Free flow case} \begin{cases} \text{Undershot gate: } q = C_{dg} L_g u \sqrt{2 g y_1} \\ \text{Weir: } q = C_{dw} \sqrt{2g} \left(y_1 - u\right)^{3/2} \end{cases} \tag{3.12}$$

$$\text{Submerged flow case} \begin{cases} \text{Undershot gate: } q = C_{dg} L_g u \sqrt{2 g \left(y_1 - y_2\right)} \\ \text{Weir: } q = C_{dw} \sqrt{2g} \left(y_1 - y_2\right)^{3/2} \end{cases} \tag{3.13}$$

3.3.2 Disturbances

Systems are usually affected by disturbances, denoted here by $\mathbf{d}_k$. Therefore, the control strategy must minimize their effect on the system. As mentioned before, these disturbances correspond to lock operations, which makes it more difficult to stay close to the setpoints. Although lock operations are rather unpredictable and cannot be postponed for a long time, they can be somewhat anticipated. Indeed, when a boat passes through a lock, its manager informs the rest of the managers. In this way, the arrival time of the boat to the adjacent locks can be predicted, taking into account the distance and the average speed of the boat, which yields a close approximation, with an error of only several minutes. This allows the lock managers to elaborate lock operation time-series profiles ahead of time.

3.3.3 Nodes

Inland waterways are characterized by distributaries, i.e., streams that branch off from the main stream and flow away. When water streams flow into larger streams or lakes, they are referred to as tributaries. The locations in which these splittings and mergings take place are called nodes. They are regarded as mass balance relations modeled as equality constraints given by:

$$\mathbf{0} = \mathbf{E}_u \mathbf{u}_k + \mathbf{E}_{un} \mathbf{u}_{k-n} + \mathbf{E}_d \mathbf{d}_k + \mathbf{E}_{dn} \mathbf{d}_{k-n}. \tag{3.14}$$

Matrices $\mathbf{E}_u$ and $\mathbf{E}_{un}$ have as many rows as nodes are in the studied system, and as many columns as controlled inputs are available. Therefore, each equation in (3.14) establishes a link among the variables involved (mass balance at the node), and thus reduces one degree of freedom. Note that both the controlled inputs and the disturbances have an immediate and a delayed effect on the system. The delayed effect must be taken into account at the controller and estimator design stages.

3.3.4 Reaches

An accurate mathematical representation of the dynamics of inland waterways is required in order to design effective controllers and observers. Indeed, a model of the system is needed in the control design stage to compute the predicted output at future time instants. Likewise, it is used to align measured and predicted values of the process, which results in the optimal state estimates. Since the IDZ model has been described in detail in Section 3.1, its formulation is not repeated here for the sake of convenience.

It is important to take into account the performance constraints that the reaches introduce in the model formulation. Indeed, the navigability condition imposes some restrictions on the water levels. This constraint might be relaxed for a short period of time, depending on factors such as the weather condition. Thus, a relaxation parameter $\boldsymbol{\alpha}_k$ is considered in the constraint, and a quadratic penalty on this parameter is included in the objective function.

The navigability condition is formulated as

$$\underline{\mathbf{y}}_r - \boldsymbol{\alpha}_k \leq \mathbf{y}_k \leq \overline{\mathbf{y}}_r + \boldsymbol{\alpha}_k, \tag{3.15}$$

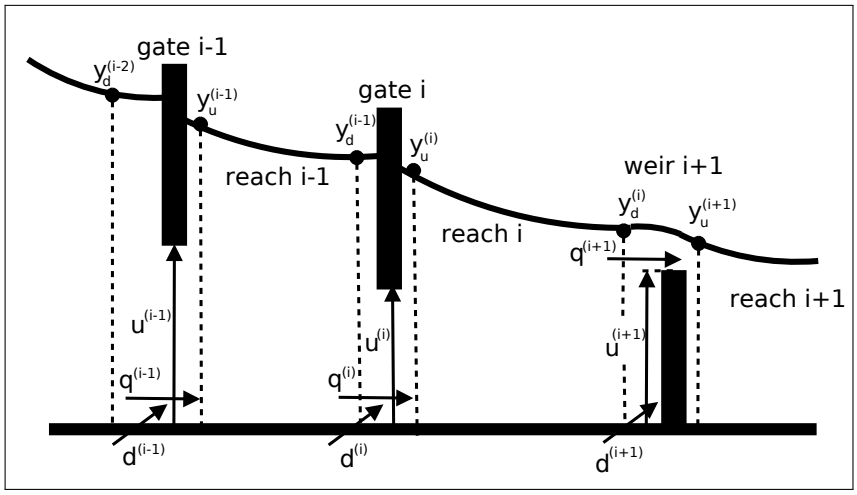

Figure 3.6: Navigation canal schematic with the variables involved

with $\underline{\mathbf{y}}_r$ and $\overline{\mathbf{y}}_r$ the LNL and HNL bounds around the NNL values, respectively. These relaxation parameters $\boldsymbol{\alpha}_k$ must satisfy

$$\boldsymbol{\alpha}_k \geq \mathbf{0}. \tag{3.16}$$

Figure 3.6 depicts a waterway composed of several reaches for a better understanding of the variables introduced to formulate the problem, and how they are linked to one another. Note that the locks are not depicted in this figure, but their operations are labeled using the variable $\mathbf{d}$, as defined before.

Remark 3.5. The direction of the disturbance arrows indicates that their effect is that of an additional but uncontrolled input to the downstream reach. □

3.3.5 Final formulation

After describing all the elements, the final, equivalent state-space representation is derived step by step.

Remark 3.6. In the state-space model formulation, the notation $\mathbf{q}$ represents the discharges, whereas the variable $\mathbf{u}$ is saved for the openings and elevations, and will be used later on. □

Model (3.1) can be rewritten as

$$\begin{aligned} y_1(s) &= p_{11}(s)\, q_1(s) - p_{12}(s)\, q_2(s), \\ y_2(s) &= p_{21}(s)\, q_1(s) - p_{22}(s)\, q_2(s). \end{aligned} \tag{3.17}$$

Note that the complete model is taken into consideration. Indeed, it is common practice to design only downstream water level controllers [LF09]. Instead, the full model allows to take into account the backwater effect in the upstream water level, which is of relevance due to the negligible bottom slope of the reaches. Then, (3.2) is substituted in (3.17), taking into account the parameter naming adopted before, leading to

$$\begin{aligned} y_1(s) &= \frac{z_{11}s+1}{A_u s} q_1(s) - \frac{z_{12}s+1}{A_u s} e^{-\tau_u s} q_2(s), \\ y_2(s) &= \frac{z_{21}s+1}{A_d s} e^{-\tau_d s} q_1(s) - \frac{z_{22}s+1}{A_d s} q_2(s). \end{aligned} \tag{3.18}$$

In order to simplify the task, the delays are initially dropped, and then reincorporated when the state-space representation is obtained. Additionally, a convenient manipulation of (3.18) leads to

$$\begin{aligned} y_1(s) &= \left(\frac{1/A_u}{s} + \frac{z_{11}}{A_u}\right) q_1(s) - \left(\frac{1/A_u}{s} + \frac{z_{12}}{A_u}\right) q_2(s), \\ y_2(s) &= \left(\frac{1/A_d}{s} + \frac{z_{21}}{A_d}\right) q_1(s) - \left(\frac{1/A_d}{s} + \frac{z_{22}}{A_d}\right) q_2(s). \end{aligned} \tag{3.19}$$

A standard transformation of (3.19) (see Section 2.5 in [Oga02] for more details) yields the state-space representation

$$\begin{aligned} \dot{\mathbf{x}}(t) &= \begin{bmatrix} 0 & 0 \\ 0 & 0 \end{bmatrix} \mathbf{x}(t) + \begin{bmatrix} 1 & -1 \\ 1 & -1 \end{bmatrix} \mathbf{q}(t), \\ \mathbf{y}(t) &= \begin{bmatrix} \frac{1}{A_u} & 0 \\ 0 & \frac{1}{A_d} \end{bmatrix} \mathbf{x}(t) + \begin{bmatrix} \frac{z_{11}}{A_u} & -\frac{z_{12}}{A_u} \\ \frac{z_{21}}{A_d} & -\frac{z_{22}}{A_d} \end{bmatrix} \mathbf{q}(t). \end{aligned} \tag{3.20}$$

Model (3.20) is discretized with a sampling time T_s as follows:

$$\begin{aligned}\mathbf{x}_{k+1} &= \begin{bmatrix}1 & 0\\ 0 & 1\end{bmatrix}\mathbf{x}_k + \begin{bmatrix}T_s & -T_s\\ T_s & -T_s\end{bmatrix}\mathbf{q}_k,\\ \mathbf{y}_k &= \begin{bmatrix}\frac{1}{A_u} & 0\\ 0 & \frac{1}{A_d}\end{bmatrix}\mathbf{x}_k + \begin{bmatrix}\frac{z_{11}}{A_u} & -\frac{z_{12}}{A_u}\\ \frac{z_{21}}{A_d} & -\frac{z_{22}}{A_d}\end{bmatrix}\mathbf{q}_k.\end{aligned} \tag{3.21}$$

The time delays are re-incorporated into (3.21), which yields

$$\begin{aligned}\mathbf{x}_{k+1} &= \begin{bmatrix}1 & 0\\ 0 & 1\end{bmatrix}\mathbf{x}_k + \begin{bmatrix}T_s & 0\\ 0 & -T_s\end{bmatrix}\mathbf{q}_k + \begin{bmatrix}0 & -T_s\\ T_s & 0\end{bmatrix}\mathbf{q}_{k-n},\\ \mathbf{y}_k &= \begin{bmatrix}\frac{1}{A_u} & 0\\ 0 & \frac{1}{A_d}\end{bmatrix}\mathbf{x}_k + \begin{bmatrix}\frac{z_{11}}{A_u} & 0\\ 0 & -\frac{z_{22}}{A_d}\end{bmatrix}\mathbf{q}_k + \begin{bmatrix}0 & -\frac{z_{12}}{A_u}\\ \frac{z_{21}}{A_d} & 0\end{bmatrix}\mathbf{q}_{k-n}\ ,\end{aligned} \tag{3.22}$$

where $\mathbf{q}_{k-n}$ is the vector of discharges delayed n samples, with $n = \lceil \tau / T_s \rceil$. In the case of inland waterways, $\tau_d \approx \tau_u$, which leads to a single value of n. Indeed, the bottom slope of these reaches is usually negligible, which allows to make this assumption, depending on the chosen sampling time. The proposed approach works also for different upstream and downstream time delays, being only necessary to adapt the formulation.

Remark 3.7. One of the most widespread approaches in order to model systems with delay consists in deriving an augmented representation. Although this representation is well suited for classical control and state estimation approaches, the order of the system scales linearly with dead-time length [SLNRA12]. Furthermore, augmented representations do not allow for a flexible LPV formulation, as the order of the system (the maximum delay in the network) varies with the operating point, thus being necessary to reconfigure its structure at each variation. Conversely, model representation (3.22) does not suffer from these drawbacks, although additional effort may be required in order to prove properties such as the controllability and the observability. □

Finally, the disturbances are incorporated to the model. Since these lock operations are also flows, and the locks are generally next to the actuators, their effect on the system can be assumed to be the same as the controlled discharges. Thus, the matrices for controlled discharges and disturbances are the same, leading to

$$
\begin{aligned}
\mathbf{x}_{k+1} &= \begin{bmatrix} 1 & 0 \\ 0 & 1 \end{bmatrix} \mathbf{x}_k + \begin{bmatrix} T_s & 0 \\ 0 & -T_s \end{bmatrix} \mathbf{q}_k + \begin{bmatrix} 0 & -T_s \\ T_s & 0 \end{bmatrix} \mathbf{q}_{k-n} \\
&+ \begin{bmatrix} T_s & 0 \\ 0 & -T_s \end{bmatrix} \mathbf{d}_k + \begin{bmatrix} 0 & -T_s \\ T_s & 0 \end{bmatrix} \mathbf{d}_{k-n}, \\
\mathbf{y}_k &= \begin{bmatrix} \frac{1}{A_u} & 0 \\ 0 & \frac{1}{A_d} \end{bmatrix} \mathbf{x}_k + \begin{bmatrix} \frac{z_{11}}{A_u} & 0 \\ 0 & -\frac{z_{22}}{A_d} \end{bmatrix} \mathbf{q}_k + \begin{bmatrix} 0 & -\frac{z_{12}}{A_u} \\ \frac{z_{21}}{A_d} & 0 \end{bmatrix} \mathbf{q}_{k-n} \\
&+ \begin{bmatrix} \frac{z_{11}}{A_u} & 0 \\ 0 & -\frac{z_{22}}{A_d} \end{bmatrix} \mathbf{d}_k + \begin{bmatrix} 0 & -\frac{z_{12}}{A_u} \\ \frac{z_{21}}{A_d} & 0 \end{bmatrix} \mathbf{d}_{k-n}.
\end{aligned} \tag{3.23}
$$

As mentioned before, (3.23) must be obtained for each reach in the case study. Then, $\mathbf{q}_k$ and $\mathbf{q}_{k-n}$ must be substituted in each case by either (3.10) or (3.11) accordingly. It can be anticipated that this substitution will cause delayed states to appear in the model. Indeed, $\mathbf{q}_k = f(\mathbf{y}_k, \mathbf{u}_k)$, and thus $\mathbf{q}_{k-n} = f(\mathbf{y}_{k-n}, \mathbf{u}_{k-n})$, with $\mathbf{y}_{k-n} = g(\mathbf{x}_{k-n})$, and f and g are the corresponding relationships.

Remark 3.8. The well-posedness of (3.23) may be proved following the ideas in [LF12]. □

More generally, the model formulation of a system with n_x states, n_u inputs and n_y outputs is

$$\mathbf{x}_{k+1} = \mathbf{A}\mathbf{x}_k + \mathbf{A}_n\mathbf{x}_{k-n} + \mathbf{B}_u\mathbf{u}_k + \mathbf{B}_{un}\mathbf{u}_{k-n} + \mathbf{B}_d\mathbf{d}_k + \mathbf{B}_{dn}\mathbf{d}_{k-n}, \tag{3.24a}$$

$$\mathbf{y}_k = \mathbf{C}\mathbf{x}_k + \mathbf{C}_n\mathbf{x}_{k-n} + \mathbf{D}_u\mathbf{u}_k + \mathbf{D}_{un}\mathbf{u}_{k-n} + \mathbf{D}_d\mathbf{d}_k + \mathbf{D}_{dn}\mathbf{d}_{k-n}, \tag{3.24b}$$

with $\mathbf{x}_k \in \mathbb{R}^{n_x}$, $\mathbf{u}_k \in \mathbb{R}^{n_u}$, $\mathbf{y}_k \in \mathbb{R}^{n_y}$, and $\mathbf{A}$, $\mathbf{A}_n$, $\mathbf{B}_u$, $\mathbf{B}_{un}$, $\mathbf{B}_d$, $\mathbf{B}_{dn}$, $\mathbf{C}$, $\mathbf{C}_n$, $\mathbf{D}_u$, $\mathbf{D}_{un}$, $\mathbf{D}_d$ and $\mathbf{D}_{dn}$ are time-invariant matrices of suitable dimensions. The state equation is given by (3.24a), and (3.24b) is the output equation. The mass balances given by (3.14) can be either formulated by means of constraints or incorporated into (3.24) as shown in [GOMPJ14].

Model (3.24) corresponds to the case of only one delay in the network. The general case for a system with multiple delays given by the set $S = \{n_1, n_2, ..., n_p\}$ reads as

$$\mathbf{x}_{k+1} = \mathbf{A}\mathbf{x}_k + \mathbf{B}_u\mathbf{u}_k + \mathbf{B}_d\mathbf{d}_k + \sum_{n_i \in S} \left(\mathbf{A}_{n_i}\mathbf{x}_{k-n_i} + \mathbf{B}_{un_i}\mathbf{u}_{k-n_i} + \mathbf{B}_{dn_i}\mathbf{d}_{k-n_i}\right), \tag{3.25a}$$

$$\mathbf{y}_k = \mathbf{C}\mathbf{x}_k + \mathbf{D}_u\mathbf{u}_k + \mathbf{D}_d\mathbf{d}_k + \sum_{n_i \in S} \left(\mathbf{C}_{n_i}\mathbf{x}_{k-n_i} + \mathbf{D}_{un_i}\mathbf{u}_{k-n_i} + \mathbf{D}_{dn_i}\mathbf{d}_{k-n_i}\right). \tag{3.25b}$$

Furthermore, (3.14) must be modified as

$$\mathbf{0} = \mathbf{E}_u \mathbf{u}_k + \mathbf{E}_d \mathbf{d}_k + \sum_{n_i \in S} (\mathbf{E}_{un_i} \mathbf{u}_{k-n_i} + \mathbf{E}_{dn_i} \mathbf{d}_{k-n_i}) \tag{3.26}$$

in order to take into account multiple time delays.

Finally, and because of the delayed terms, (3.24) and (3.25) are not representable using the standard state-space formulation. While the theory of other classical state feedback control techniques might not be used for this representation, the combination of MPC and MHE can deal with these models in a suitable manner. Furthermore, this formulation also allows a flexible and more compact notation of a system with delayed variables. Indeed, a common approach to represent such systems consists in the augmentation procedure described in [SNRL10], where the delay effect is incorporated as a dead-beat dynamic to obtain an undelayed representation. However, a downside of this methodology lies in the large dimensionality of the resulting description. By contrast, no augmented model needs to be derived in the case of MPC and MHE.

3.4 An alternative grey-box modeling approach

The IDZ model described in Section 3.1 relies on the knowledge of the physical characteristics of the system to compute the model parameters. However, it can happen that certain physical data are unavailable. Hence, a grey-box modeling approach can be used to estimate model parameters, as these strategies allow to incorporate previous physical knowledge and to apply statistical methods for parameter estimation purposes [KMJ04].

Therefore, this section is concerned with the estimation of the model parameters of a grey-box model in those cases in which experimental data are available. The complete derivation of its structure is carried out in Appendix B and is recalled here for convenience:

$$\hat{\mathbf{y}}_{k+1} = \tilde{\mathbf{A}} \overline{\mathbf{y}}_{k|\kappa} + \tilde{\mathbf{B}} \overline{\mathbf{q}}_{k|\kappa}, \tag{3.27}$$

with $\tilde{\mathbf{A}} \in \mathbb{R}^{n_y \times (n_y \times n_\kappa)}$, $\tilde{\mathbf{B}} \in \mathbb{R}^{n_y \times (n_u \times n_\kappa)}$, $\overline{\mathbf{y}}_{k|\kappa} = \left[\overline{\mathbf{y}}^{(1)}_{k|\kappa}\ \overline{\mathbf{y}}^{(2)}_{k|\kappa}\ \cdots\ \overline{\mathbf{y}}^{(n_y)}_{k|\kappa}\right]^\mathsf{T}$ and $\overline{\mathbf{q}}_{k|\kappa} = \left[\overline{\mathbf{q}}^{(1)}_{k|\kappa}\ \overline{\mathbf{q}}^{(2)}_{k|\kappa}\ \cdots\ \overline{\mathbf{q}}^{(n_u)}_{k|\kappa}\right]^\mathsf{T}$.

Remark 3.9. The general description given in Appendix B is particularized in this thesis

by assuming that each actuator is equipped with one level sensor. Therefore, $n_y = n_u = n$. □

The grey-box modeling approach is formulated as follows: the time delays are determined according to the well-known relations given in [LF09]. On the other hand, matrices $\tilde{\mathbf{A}}$ and $\tilde{\mathbf{B}}$ are estimated using available input-output data. To this end, (3.27) can be rewritten as follows:

$$\hat{\mathbf{y}}_{k+1} \quad = \quad \mathbf{M}\ \mathbf{\Phi}_k. \tag{3.28}$$

According to the structure of $\tilde{\mathbf{A}}$ and $\tilde{\mathbf{B}}$ given in Appendix B, the i-th level $\hat{y}^{(i)}_{k+1}$ can be estimated as

$$\hat{y}^{(i)}_{k+1} \quad = \quad \mathbf{M}^{(i)}\ \mathbf{\Phi}^{(i)}_k, \tag{3.29}$$

with $\mathbf{M}^{(i)} = \left[\tilde{\mathbf{A}}^{(i)}\ \tilde{\mathbf{B}}^{(i)}\right]$ and $\mathbf{\Phi}^{(i)}_k = \left[\overline{\mathbf{y}}^{(i)}_{k|\kappa}\ \overline{\mathbf{q}}^{(i)}_{k|\kappa}\right]^{\mathsf{T}}$.

Then, $\mathbf{M}^{(i)}$ is the solution of the linear least squares problem. N samples of the measured discharges $Q^{(i)}_k$ and levels $L^{(i)}_k$ are considered in its computation:

$$\mathbf{M}^{(i)} \quad = \quad \mathbf{Y}^{(i)}\ \left(\overline{\mathbf{\Phi}}^{(i)}\right)^{\mathsf{T}}\ \left(\overline{\mathbf{\Phi}}^{(i)}\ \left(\overline{\mathbf{\Phi}}^{(i)}\right)^{\mathsf{T}}\right)^{-1}, \tag{3.30}$$

with $\mathbf{Y}^{(i)} = \left[y^{(i)}_{\chi+1}\ \cdots\ y^{(i)}_N\right]$, $\overline{\mathbf{\Phi}}^{(i)} = \left[\mathbf{\Phi}^{(i)}_{\chi}\ \cdots\ \mathbf{\Phi}^{(i)}_{N-1}\right]$, and $\chi = \max(\boldsymbol{\kappa}) + 1$, where $\max(\boldsymbol{\kappa})$ is the maximum entry of matrix $\boldsymbol{\kappa}$.

Remark 3.10. As mentioned in Appendix B, the problem of estimating the time delays from the available data is not addressed in the thesis. □

The following fit coefficients are used to determine the accuracy of the model with respect to the measurements:

— The *Pearson product-moment correlation coefficient* measures the linear dependence between two variables:

$$R^i = \frac{\sum_{k=1}^{N}\left(y^{(i)}_k - \lambda_{y^{(i)}}\right)\left(\hat{y}^{(i)}_k - \lambda_{\hat{y}^{(i)}}\right)}{\sqrt{\sum_{k=1}^{N}\left(y^{(i)}_k - \lambda_{y^{(i)}}\right)^2}\sqrt{\sum_{k=1}^{N}\left(\hat{y}^{(i)}_k - \lambda_{\hat{y}^{(i)}}\right)^2}}, \tag{3.31}$$

with $\lambda_{y^{(i)}}$ and $\lambda_{\hat{y}^{(i)}}$ the mean value of measured and estimated water levels, respectively. This coefficient is bounded between +1 (total positive linear correlation) and -1 (total negative linear correlation), and 0 means that there is no linear correlation.

— The *Nash-Sutcliffe model efficiency coefficient* is used to assess the predictive power of hydrological models [NS70]:

$$E^{(i)} = 1 - \frac{\sum_{k=1}^{N} \left(y_k^{(i)} - \hat{y}_k^{(i)}\right)^2}{\sum_{k=1}^{N} \left(y_k^{(i)} - \lambda_{y^{(i)}}\right)^2}. \tag{3.32}$$

$E^{(i)}$ can range from 1 to $-\infty$, where 1 indicates a perfect match of modeled and observed values, 0 corresponds to the case in which the model predictions are as accurate as the mean of observed data and $E^{(i)} < 0$ means that the model predictions are less accurate than the mean of observed data.

3.5 Modeling results

This section gathers the modeling results for the IDZ-based approach presented in Section 3.3 and the grey-box modeling approach described in Section 3.4. Both strategies are equally valid to design controllers, estimators and fault diagnosis approaches. However, real data are only available for part of the case study depicted in Fig. 3.7, namely reach NR_2, hereinafter referred to as the Cuinchy-Fontinettes reach, or simply the CFr. Based on this limitation, the usages of two models are described next:

— The IDZ-based approach will be used to design centralized and distributed controllers and estimators in Chapters 4 and 5, respectively. Furthermore, a model-based fault diagnosis approach considering this model will be proposed in Section 6.1. In order to be able to compare both fault diagnosis strategies, the model-based fault diagnosis approach will only focus on the CFr.

— The grey-box modeling approach will be used to design a data-driven fault diagnosis approach in Section 6.2.

Section 3.5.1 presents the complete case study that will be used throughout the thesis. Then, Section 3.5.2 gathers the results concerning individual IDZ models, its

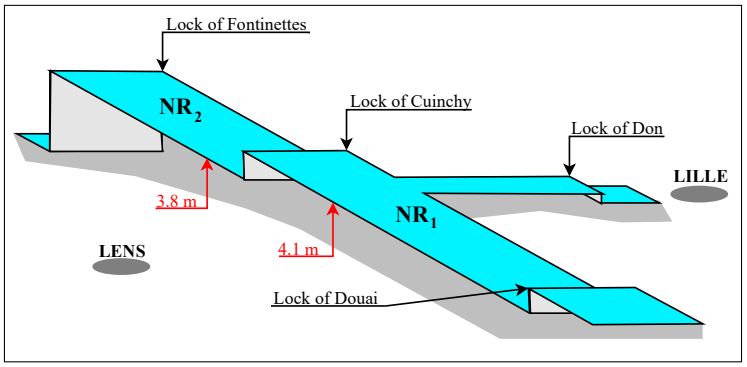

Figure 3.7: Part of the inland waterways in the north of France

validation and the building of the global state-space representation. On the other hand, the computation and validation of the identified data-based model are carried out in Section 3.5.3.

3.5.1 Description of the system

The inland waterways in the north of France is linked with the Belgian and Dutch inland waterways, and is managed by *Voies Navigables de France*[1] (VNF). Its main objective is that of guaranteeing the navigability condition, which is achieved by keeping the water levels inside the navigation rectangle defined by the LNL and the HNL, and as close as possible to the NNL.

This inland navigation network consists of more than fifty reaches that are interconnected by locks, gates and weirs. Part of it is depicted in Fig. 3.7, which shows the two reaches considered in the case study. The i-th reach is labeled as NR_i, and its setpoint (NNL) is specified in red. In addition, the locks that connect adjacent reaches are labeled in black.

The choice of the case study is motivated by the following reasons:

— It features a distributary, which branches off from NR_1 at an intermediate point and flows away, to the lock of Don. This topology is regarded as of special interest, since the mass balance at this natural bifurcation (not controlled) is not

1. http://www.vnf.fr

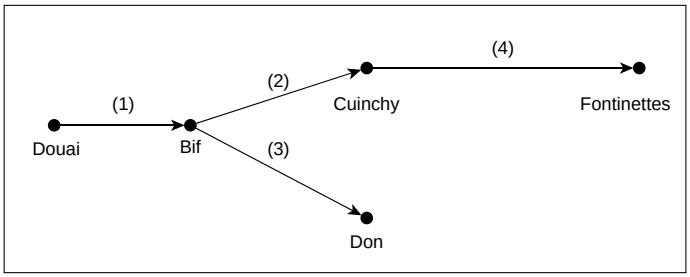

Figure 3.8: Schematic diagram of the case study

straightforward to model. Indeed, a possible approach for this situation is shown below.

— Besides, NR_2 is an important reach in this network for two reasons: its strategic location, which allows dispatching water among the three major catchments in the region; and its downstream lock in Fontinettes, which performs the largest lock operations in terms of volume, and is therefore responsible for the largest disturbances. Being able to deal with the worst-case scenario can give a feel for the magnitude of the disturbances that the control strategy attempts to reject.

3.5.2 IDZ-based state-space approach

The complete case study depicted in Fig. 3.7 is used to illustrate the approach presented in Section 3.3. A more schematic view is provided in Fig. 3.8. Since the bifurcation is of natural type (uncontrolled), this node can be eliminated, based on an estimation of the ratios of the total flow for each stream after the bifurcation. Due to the physical characteristics of the system, it can be considered that each of the flows after the bifurcation corresponds to 50% of the flow before the bifurcation. This yields the simplified, final three-reach case study scheme given in Fig. 3.9. Note that the reaches are renamed for convenience, and also the nodes for labeling purposes.

Computing and testing individual IDZ models

The physical parameters of the three reaches are summarized in Table 3.1. LNL, NNL and HNL are the relative lower, normal and higher navigation levels (with respect to the bottom of the reach), L is the length of the reach, w_r is the bottom width, m_r is

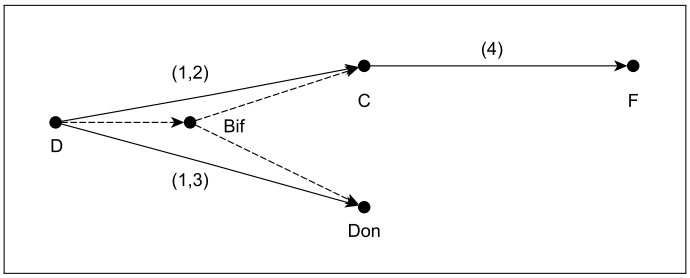

Figure 3.9: Simplified schematic diagram of the case study

Table 3.1: Parameters of the reaches

Reach nr.	LNL $[m]$	NNL $[m]$	HNL $[m]$	L $[m]$	w_r $[m]$	m_r $[m/m]$	s_b $[m/m]$	n_r $[s/m^{1/3}]$	Q_s $[m^3/s]$
(1,2)	3.95	4.1	4.25	39000	50	0	0	0.035	0.6
(1,3)	3.95	4.1	4.25	37000	50	0	0	0.035	0.6
(4)	3.65	3.8	3.95	42000	50	0	0	0.035	0.6

Table 3.2: Time delays of each reach

Reach nr.	τ_u $[s]$	τ_d $[s]$
(1,2)	6391	6384
(1,3)	6063	6057
(4)	6882	6875

the side slope ($m_r = 0$ for a rectangular cross section), s_b is the bottom slope ($s_b = 0$ for a flat reach), n_r is the Manning roughness coefficient ($n_r = 0.035$ for a stony excavated earth channel [Whi99]) and Q_s is the operating point considered when linearizing the Saint-Venant equations. Indeed, it is considered that an average flow of 1.2 m^3/s comes from upstream of Douai, and that it is divided into two equal parts after it.

Table 3.2 summarizes the time delays τ_u and τ_d for the three reaches. Note that all of them are in the interval $[6063, 6882]$ s, or equivalently $[5.05, 5.73]$ samples. Thus, a unique delay of 6 samples can be considered, according to the ceiling rule introduced in (3.22). Thus, model (3.24) can be used.

The rest of the IDZ parameters of the reaches can be computed according to the

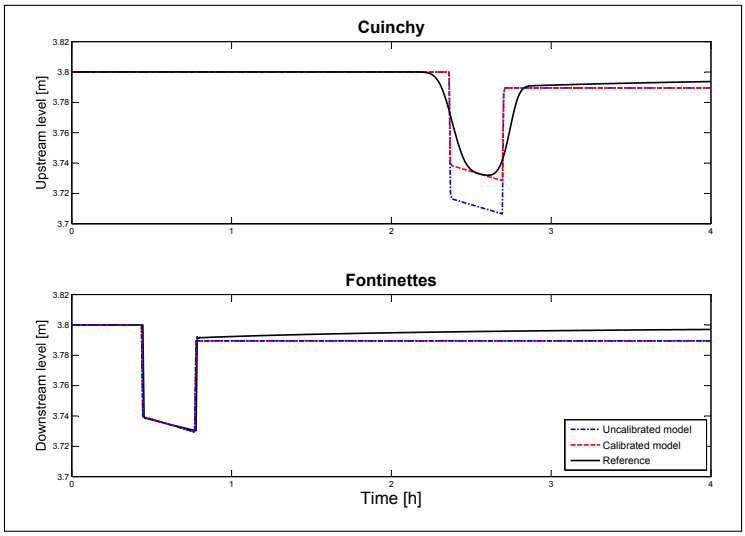

Figure 3.10: Evolution of the water levels in reach (4) for a lock operation in Fontinettes.

formulas given in [LF04b], which allows to build the partial IDZ models (3.23). However, the quality of these models needs to be tested before building the global model. To do so, the reaches are disturbed by simulating the effect of a lock operation. Then, its behavior is compared with the results obtained using the hydraulic simulator SIC^2 [2], developed at IRSTEA Montpellier [MDB14]. Since SIC^2 solves numerically the Saint-Venant equations without simplification, the results provided by this software are taken as the reference to check the performance of the computed IDZ model. The evolution of the water levels caused by a lock operation in Fontinettes are depicted in Fig. 3.10. Since the dynamics of all reaches are rather similar, the evolution of the water levels is only shown for reach (4).

The effect of the lock operation in Fontinettes is only detected at the upstream end of the reach after τ_u (defined in Section 3.1) has elapsed. Note that the resulting IDZ model is able to predict successfully the downstream water level, although it overestimates the magnitude of the upstream water level peak. This mismatch needs to be corrected by calibrating the zero of the model to ensure the correct prediction of the peak, for which the zero accounts. The water levels predicted by both the uncalibrated and the calibrated models are depicted in Fig. 3.10, proving the effectiveness of the calibration.

2. http://sic.g-eau.net

On a separate note, it might seem that the magnitude of a lock operation (around 7 cm) is not so relevant in comparison with the water depth of the reach (3.8 m). An individual lock operation, although rather large in magnitude, does not seem to have a noteworthy effect on the system, given its large dimensionality. However, the combined effect of several consecutive lock operations might cause the water levels to not remain within the navigation rectangle [LNL, HNL]. This is a requirement of the utmost importance for VNF, who might be forced to stop the navigation for safety reasons if this condition is not fulfilled. This issue justifies the need for water level regulation strategies.

Building the global state space representation

Once the models of the reaches are validated, these are stacked to build the centralized model given by:

$$\begin{bmatrix} x_{k+1}^{D(1,2)} \\ x_{k+1}^{C(1,2)} \\ x_{k+1}^{D(1,3)} \\ x_{k+1}^{Don} \\ x_{k+1}^{C(4)} \\ x_{k+1}^{F} \end{bmatrix} = \mathbf{A} \begin{bmatrix} x_{k}^{D(1,2)} \\ x_{k}^{C(1,2)} \\ x_{k}^{D(1,3)} \\ x_{k}^{Don} \\ x_{k}^{C(4)} \\ x_{k}^{F} \end{bmatrix} + \mathbf{A}_n \begin{bmatrix} x_{k-n}^{D(1,2)} \\ x_{k-n}^{C(1,2)} \\ x_{k-n}^{D(1,3)} \\ x_{k-n}^{Don} \\ x_{k-n}^{C(4)} \\ x_{k-n}^{F} \end{bmatrix} + \mathbf{B}_q \begin{bmatrix} q_k^D \\ q_k^C \\ q_k^{Don} \\ q_k^F \end{bmatrix} + \mathbf{B}_{qn} \begin{bmatrix} q_{k-n}^D \\ q_{k-n}^C \\ q_{k-n}^{Don} \\ q_{k-n}^F \end{bmatrix} + \mathbf{B}_d \begin{bmatrix} d_k^D \\ d_k^C \\ d_k^{Don} \\ d_k^F \end{bmatrix} + \mathbf{B}_{dn} \begin{bmatrix} d_{k-n}^D \\ d_{k-n}^C \\ d_{k-n}^{Don} \\ d_{k-n}^F \end{bmatrix}, \tag{3.33a}$$

$$\begin{bmatrix} y_{k}^{D(1,2)} \\ y_{k}^{C(1,2)} \\ y_{k}^{D(1,3)} \\ y_{k}^{Don} \\ y_{k}^{C(4)} \\ y_{k}^{F} \end{bmatrix} = \mathbf{C} \begin{bmatrix} x_{k}^{D(1,2)} \\ x_{k}^{C(1,2)} \\ x_{k}^{D(1,3)} \\ x_{k}^{Don} \\ x_{k}^{C(4)} \\ x_{k}^{F} \end{bmatrix} + \mathbf{C}_n \begin{bmatrix} x_{k-n}^{D(1,2)} \\ x_{k-n}^{C(1,2)} \\ x_{k-n}^{D(1,3)} \\ x_{k-n}^{Don} \\ x_{k-n}^{C(4)} \\ x_{k-n}^{F} \end{bmatrix} + \mathbf{D}_q \begin{bmatrix} q_k^D \\ q_k^C \\ q_k^{Don} \\ q_k^F \end{bmatrix} + \mathbf{D}_{qn} \begin{bmatrix} q_{k-n}^D \\ q_{k-n}^C \\ q_{k-n}^{Don} \\ q_{k-n}^F \end{bmatrix} + \mathbf{D}_d \begin{bmatrix} d_k^D \\ d_k^C \\ d_k^{Don} \\ d_k^F \end{bmatrix} + \mathbf{D}_{dn} \begin{bmatrix} d_{k-n}^D \\ d_{k-n}^C \\ d_{k-n}^{Don} \\ d_{k-n}^F \end{bmatrix}, \tag{3.33b}$$

$$\mathbf{0} = \mathbf{E}_q \begin{bmatrix} q_k^D \\ q_k^C \\ q_k^{Don} \\ q_k^F \end{bmatrix} + \mathbf{E}_{qn} \begin{bmatrix} q_{k-n}^D \\ q_{k-n}^C \\ q_{k-n}^{Don} \\ q_{k-n}^F \end{bmatrix} + \mathbf{E}_d \begin{bmatrix} d_k^D \\ d_k^C \\ d_k^{Don} \\ d_k^F \end{bmatrix} + \mathbf{E}_{dn} \begin{bmatrix} d_{k-n}^D \\ d_{k-n}^C \\ d_{k-n}^{Don} \\ d_{k-n}^F \end{bmatrix}. \tag{3.33c}$$

Remark 3.11. The superscripts of the variables in (3.33) refer to the labeling of the nodes given in Fig. 3.9. □

Next, the linearized versions of the nonlinear equations of gates and weirs (3.12) are computed, as the studied system falls under the free-flow case. To do so, the nonlinear equations are linearized around the NNL and Q_s values provided in Table 3.1. In this particular case, (3.10) is used for both gates and weirs due the free flow at the structures.

$$\text{Douai: } q_k^D = 27.5553 u_k^D, \tag{3.34a}$$

$$\text{Cuinchy: } q_k^C = 1.32 \cdot 10^{-6} x_k^{C(1,2)} - 1.8524 u_k^C, \tag{3.34b}$$

$$\text{Don: } q_k^{Don} = 1.32 \cdot 10^{-6} x_k^{Don} - 1.8524 u_k^{Don}, \tag{3.34c}$$

$$\text{Fontinettes: } q_k^F = 5.63 \cdot 10^{-8} x_k^F + 25.9037 u_k^F. \tag{3.34d}$$

Remark 3.12. q_k^D does not depend on the water level upstream of the structure. Indeed, this water level is outside of the scope of the control problem. Following the modeling approach presented in [BPB14], where a reservoir, it is considered that there is enough water upstream of Douai, and therefore this level remains constant. □

Finally, (3.34) is substituted in (3.33). Note that this substitution is performed in such a way that the mass balances, originally described by (3.33c), are embedded in the final model (3.35) to be consistent with the current implementation. This representation is equivalent to expressing the mass balances by means of equality constraints, as stated before. Therefore, the final numerical model reads as follows:

$$\begin{bmatrix} x_{k+1}^{D(1,2)} \\ x_{k+1}^{C(1,2)} \\ x_{k+1}^{D(1,3)} \\ x_{k+1}^{Don} \\ x_{k+1}^{C(4)} \\ x_{k+1}^{F} \end{bmatrix} = \begin{bmatrix} 1 & 0 & 0 & 0 & 0 & 0 \\ 0 & 0.9989 & 0 & 0 & 0 & 0 \\ 0 & 0 & 1 & 0 & 0 & 0 \\ 0 & 0 & 0 & 0.9989 & 0 & 0 \\ 0 & 0.0011 & 0 & 0 & 1 & 0 \\ 0 & 0 & 0 & 0 & 0 & 1 \end{bmatrix} \begin{bmatrix} x_k^{D(1,2)} \\ x_k^{C(1,2)} \\ x_k^{D(1,3)} \\ x_k^{Don} \\ x_k^{C(4)} \\ x_k^{F} \end{bmatrix} + \tag{3.35a}$$

$$
+10^{-5}\cdot\begin{bmatrix}0 & -112.5 & 0 & 0 & 0 & 0\\ 0 & 0 & 0 & 0 & 0 & 0\\ 0 & 0 & 0 & -115.5 & 0 & 0\\ 0 & 0 & 0 & 0 & 0 & 0\\ 0 & 0 & 0 & 0 & 0 & -4.3\\ 0 & 112.5 & 0 & 0 & 0 & 0\end{bmatrix}\begin{bmatrix}x_{k-n}^{D(1,2)}\\ x_{k-n}^{C(1,2)}\\ x_{k-n}^{D(1,3)}\\ x_{k-n}^{Don}\\ x_{k-n}^{C(4)}\\ x_{k-n}^{F}\end{bmatrix}+
$$

$$
+10^{4}\cdot\begin{bmatrix}1.6533 & 0 & 0 & 0\\ 0 & 0.2223 & 0 & 0\\ 1.6533 & 0 & 0 & 0\\ 0 & 0 & 0.2223 & 0\\ 0 & -0.2223 & 0 & 0\\ 0 & 0 & 0 & -3.1083\end{bmatrix}\begin{bmatrix}u_k^D\\ u_k^C\\ u_k^{Don}\\ u_k^F\end{bmatrix}+
$$

$$
+10^{4}\cdot\begin{bmatrix}0 & 0.2223 & 0 & 0\\ 1.6533 & 0 & 0 & 0\\ 0 & 0 & 0.2223 & 0\\ 1.6533 & 0 & 0 & 0\\ 0 & 0 & 0 & -3.1083\\ 0 & -0.2223 & 0 & 0\end{bmatrix}\begin{bmatrix}u_{k-n}^D\\ u_{k-n}^C\\ u_{k-n}^{Don}\\ u_{k-n}^F\end{bmatrix}+
$$

$$
+\begin{bmatrix}600 & 0 & 0 & 0\\ 0 & -1200 & 0 & 0\\ 600 & 0 & 0 & 0\\ 0 & 0 & -1200 & 0\\ 0 & 1200 & 0 & 0\\ 0 & 0 & 0 & -1200\end{bmatrix}\begin{bmatrix}d_k^D\\ d_k^C\\ d_k^{Don}\\ d_k^F\end{bmatrix}+
$$

$$
+\begin{bmatrix}0 & -1200 & 0 & 0\\ 600 & 0 & 0 & 0\\ 0 & 0 & -1200 & 0\\ 600 & 0 & 0 & 0\\ 0 & 0 & 0 & -1200\\ 0 & 1200 & 0 & 0\end{bmatrix}\begin{bmatrix}d_{k-n}^D\\ d_{k-n}^C\\ d_{k-n}^{Don}\\ d_{k-n}^F\end{bmatrix},
$$

$$\begin{bmatrix} y_k^{D(1,2)} \\ y_k^{C(1,2)} \\ y_k^{D(1,3)} \\ y_k^{Don} \\ y_k^{C(4)} \\ y_k^{F} \end{bmatrix} = 10^{-6} \cdot \begin{bmatrix} 0.5061 & 0 & 0 & 0 & 0 & 0 \\ 0 & 0.5061 & 0 & 0 & 0 & 0 \\ 0 & 0 & 0.5197 & 0 & 0 & 0 \\ 0 & 0 & 0 & 0.5197 & 0 & 0 \\ 0 & 1.3519 \cdot 10^{-9} & 0 & 0 & 0.4579 & 0 \\ 0 & 0 & 0 & 0 & 0 & 0.4579 \end{bmatrix} \begin{bmatrix} x_k^{D(1,2)} \\ x_k^{C(1,2)} \\ x_k^{D(1,3)} \\ x_k^{Don} \\ x_k^{C(4)} \\ x_k^{F} \end{bmatrix} + \tag{3.35b}$$

$$+ 10^{-14} \cdot \begin{bmatrix} 0 & -0.2064 & 0 & 0 & 0 & 0 \\ 0 & 0 & 0 & 0 & 0 & 0 \\ 0 & 0 & 0 & -0.2178 & 0 & 0 \\ 0 & 0 & 0 & 0 & 0 & 0 \\ 0 & 0 & 0 & 0 & 0 & -0.0072 \\ 0 & 0.1863 & 0 & 0 & 0 & 0 \end{bmatrix} \begin{bmatrix} x_{k-n}^{D(1,2)} \\ x_{k-n}^{C(1,2)} \\ x_{k-n}^{D(1,3)} \\ x_{k-n}^{Don} \\ x_{k-n}^{C(4)} \\ x_{k-n}^{F} \end{bmatrix} +$$

$$+ 10^{-7} \cdot \begin{bmatrix} 0.2196 & 0 & 0 & 0 \\ 0 & 0.0295 & 0 & 0 \\ 0.2255 & 0 & 0 & 0 \\ 0 & 0 & 0.0303 & 0 \\ 0 & -0.0267 & 0 & 0 \\ 0 & 0 & 0 & -0.3736 \end{bmatrix} \begin{bmatrix} u_k^{D} \\ u_k^{C} \\ u_k^{Don} \\ u_k^{F} \end{bmatrix} +$$

$$+ 10^{-7} \cdot \begin{bmatrix} 0 & 0.0408 & 0 & 0 \\ 0.3034 & 0 & 0 & 0 \\ 0 & 0 & 0.0419 & 0 \\ 0.3118 & 0 & 0 & 0 \\ 0 & 0 & 0 & -0.5147 \\ 0 & -0.0368 & 0 & 0 \end{bmatrix} \begin{bmatrix} u_{k-n}^{D} \\ u_{k-n}^{C} \\ u_{k-n}^{Don} \\ u_{k-n}^{F} \end{bmatrix} +$$

$$+ 10^{-8} \cdot \begin{bmatrix} 0.0797 & 0 & 0 & 0 \\ 0 & -0.1594 & 0 & 0 \\ 0.0818 & 0 & 0 & 0 \\ 0 & 0 & -0.1637 & 0 \\ 0 & 0.1442 & 0 & 0 \\ 0 & 0 & 0 & -0.1442 \end{bmatrix} \begin{bmatrix} d_k^{D} \\ d_k^{C} \\ d_k^{Don} \\ d_k^{F} \end{bmatrix} +$$

$$+10^{-8}\cdot\begin{bmatrix} 0 & -0.2202 & 0 & 0 \\ 0.1101 & 0 & 0 & 0 \\ 0 & 0 & -0.2263 & 0 \\ 0.1131 & 0 & 0 & 0 \\ 0 & 0 & 0 & -0.1987 \\ 0 & 0.1987 & 0 & 0 \end{bmatrix}\begin{bmatrix} d^D_{k-n} \\ d^C_{k-n} \\ d^{Don}_{k-n} \\ d^F_{k-n} \end{bmatrix}.$$

3.5.3 Grey-box approach

The second modeling approach lies in identifying the parameters of a grey-box model based on the available real data for the CFr, recorded from October 30, 2013 (Thursday) to November 17, 2013 (Sunday). This reach is depicted in detail in Fig. 3.11, and is equipped with two locks (in Cuinchy and Fontinettes), three sensors that allow to measure the level in Cuinchy (L^C), Aire (L^A) and Fontinettes (L^F) with a sampling time $T_s = 1\ min$, and three hydraulic devices in Cuinchy (Q^C), Aire (Q^A) and Fontinettes (Q^F) that are used to regulate the water levels. These discharges are measured each 15 min and then oversampled every minute.

Remark 3.13. The gate in Aire is only used during flood episodes to dispatch water to secondary reaches, and also to convey water from those reaches to the CFr during drought episodes. These phenomena are outside of the scope of the thesis, and it is the reason why this gate was not considered in the IDZ-based model formulation (3.33). □

The first step consists in determining the delays between each part of the CFr. These are computed according to the characteristics given in Table 3.1, which allows to determine the maximum delay in the system. Then, $\boldsymbol{\kappa}$ can be built based on this information. According to these delays, the input and output vectors $\overline{\mathbf{u}}_{k|\kappa} \in \mathbb{R}^{9\times 1}$ and $\overline{\mathbf{y}}_{k|\kappa} \in \mathbb{R}^{9\times 1}$ are built by considering the following inputs and outputs: $q^{(1)}_k = Q^C_k$ and $y^{(1)}_k = L^C_k$ for Cuinchy, $u^{(2)}_k = Q^A_k$ and $y^{(2)}_k = L^A_k$ for Aire, and $u^{(3)}_k = Q^F_k$ and $y^{(3)}_k = L^F_k$ for Fontinettes. The vectors $\overline{\mathbf{q}}_{k|\kappa}$ and $\overline{\mathbf{y}}_{k|\kappa}$ are used in the parameter identification of the model by considering a sliding window of size $N_w = 1440\ min$ (1 day).

On the other hand, matrices $\tilde{\mathbf{A}}$ and $\tilde{\mathbf{B}}$ in (3.27) are determined by considering data from the first five consecutive days. A model for each window is identified, which can then be used to estimate the levels $\hat{L}^{(i)}_k$ as outputs of the model. The real measurements $L^{(i)}_k$ and the estimated $\hat{L}^{(i)}_k$ are depicted in Fig. 3.12 in blue and dashed red lines, respectively, for each of the three level sensors. These values are relative to the NNL,

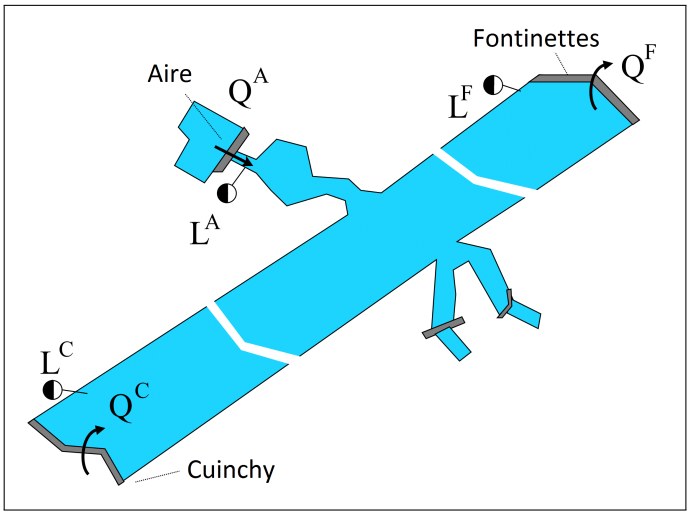

Figure 3.11: Detailed schematic representation of the CFr

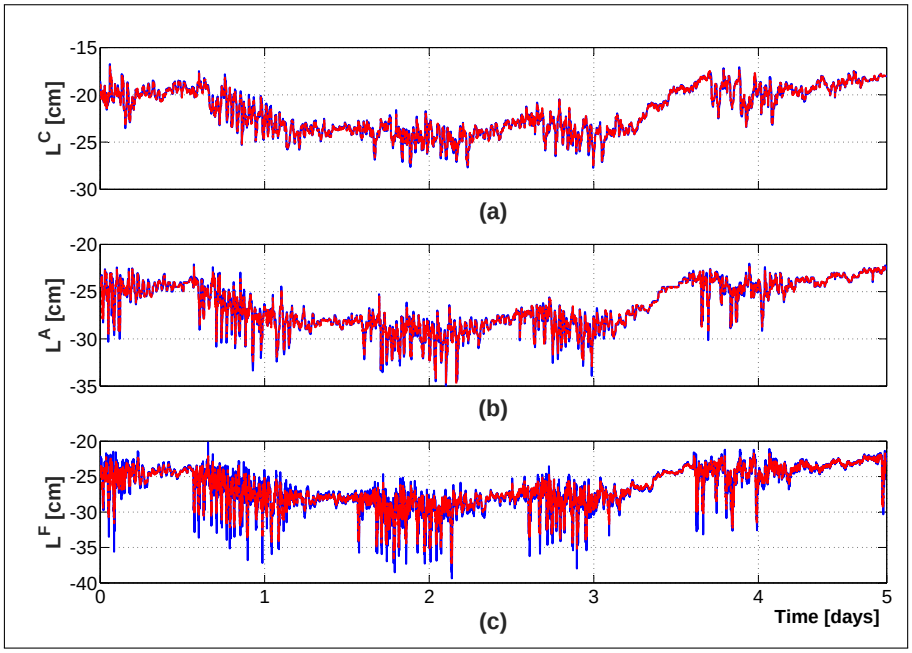

Figure 3.12: Measured (blue solid line) and estimated (red solid line) water levels in: (a) Cuinchy. (b) Aire. (c) Fontinettes.

and therefore the values $L_k^{(i)} = 0$ and $\hat{L}_k^{(i)} = 0$ correspond to the NNL.

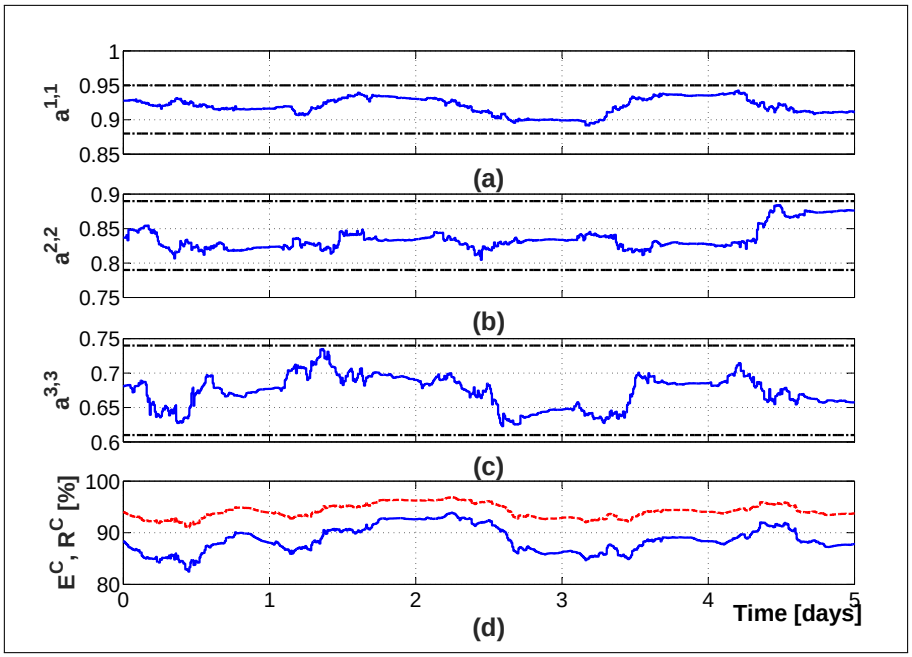

Figure 3.13: $a_k^{(i,i)}$ terms (blue solid lines) and thresholds (black dashed lines): (a) $a^{(1,1)}$. (b) $a^{(2,2)}$. (c) $a^{(3,3)}$. (d) R^C (red solid line) and E^C (blue solid line).

The grey-box parameters change for each window. Note that the *free* model case defined in Appendix B is identified, thus not forcing null coefficients in $\tilde{\mathbf{A}}^{(i)}$. However, it is precisely the $a^{(i,i)}$ terms, whose evolution is depicted in Fig. 3.13, which retain the main information in $\tilde{\mathbf{A}}^{(i)}$. Based on these data, the intervals for these terms are determined, which are depicted as black dashed lines in Fig. 3.13. These intervals will be used to detect and isolate faults in Section 6.2.

On the other hand, the Nash-Sutcliffe $\left(E^{(i)}\right)$ and correlation $\left(R^{(i)}\right)$ coefficients are also computed to verify the quality of the model. The average values of these coefficients for the three level sensors are given in Table 3.3. The closeness of these fitting indicators to the maximum theoretical values indicate that the model predictions are accurate with regard to the real data, and thus the effectiveness of the grey-box modeling approach is proved. In particular, the evolution of the coefficients for L^C are also depicted in Fig. 3.13.

Table 3.3: Average values of Nash-Sutcliffe $\left(E^{(i)}\right)$ and correlation $\left(R^{(i)}\right)$ coefficients

Water level	$E^{(i)}$ [%]	$R^{(i)}$ [%]
C	90	95
A	87	93
F	76	87

3.6 Summary

Chapter 3 has addressed the problem of obtaining accurate models for open-flow water systems, which are to be used in the following for the purposes of control, state estimation and fault diagnosis. The IDZ model, which is among the existing simplified modeling approaches presented in Section 2.1, is chosen and extended to describe the dynamics of inland waterways composed of several reaches based on the original formulation. However, it becomes apparent that the proposed approach is rather inadequate, which motivates the derivation of an equivalent state-space representation. In doing so, the connections between reaches can be easily established by means of additional constraints that represent mass balances, which describe the static part of the model. This leads to a delayed descriptor formulation, for which the appropriate control and state estimation techniques will be proposed in Chapter 4. Finally, a parameter estimation approach has also been proposed to deal with the lack of knowledge of physical parameters.

Chapter 4

Centralized control and state estimation

Chapter 3 has addressed the problem of modeling open-flow water systems, for which a new approach has been proposed. This method is particularly suitable for large inland waterways composed of many reaches. Chapter 4 builds on the derived modeling approach in order to design a CMPC that fulfills a set of operational goals linked to the system performance. The controller requires the vector of states to be known at current time to compute the set of future optimal inputs. In general, the measurements of all states are not available, and thus estimates of unmeasured states must be provided to the CMPC using observers. Although there exist many possibilities to estimate the states, a CMHE, which is considered as the dual problem of CMPC, is chosen for this purpose. Their combination is especially attractive since the MHE formulation corresponds also to an online optimization problem that can explicitly handle constraints [CH17]. The choice of MPC and MHE is motivated by the fact that standard tools for control and state estimation such as the linear quadratic regulator (LQR) and the Kalman filter need to be extended to deal with delayed descriptor systems. Moreover, they cannot deal with input and state/output constraints. Conversely, MPC and MHE can be easily adapted for this model formulation, as well as being able to deal with constraints on the states, inputs and outputs in a natural manner.

Chapter 4 is organized as follows: Section 4.1 gathers the operational goals, the multi-objective function and the set of constraints to build the CMPC. Section 4.2 is concerned with the design of the CMHE, which can be easily formulated from the CMPC. Then, some ideas on how to implement both optimization problems are presented in Section 4.3.

It is also shown how both problems are connected: indeed, the solution of the controller is used to solve the estimation problem, and *vice versa*. Finally, Section 4.4 gathers the results obtained by applying the presented techniques on the system described in Section 3.5. These contributions have been published in [SRN+18b, SRN+19b].

4.1 Control design: the MPC approach

Modern inland waterways are complex, multi-variable systems whose management requires the use of advanced control methods [vO06]. As discussed in Section 2.2.1, MPC possesses several interesting features that make it a suitable tool for the inland waterways control problem. Its main principle resides in computing a sequence of inputs that causes the predicted response of the system to move to the desired setpoint in an optimal manner while respecting the constraints. The constraints imposed by the elements that make up the model have already been defined in Section 3.3. On the other hand, the set of operational goals is defined below.

4.1.1 Operational goals and multi-objective function

One or more operational goals are expected to be achieved during the process. To this end, a certain criterion is optimized in the computation of the control signals. This criterion is usually built as the weighted sum of several terms, where each of them represents an operational goal. Note that the set of operational goals that can be taken into account is not unique. In this thesis, the following are considered:

— *Maintaining the water levels close to the setpoints:* This is the most important objective to be fulfilled. Its mathematical formulation reads as

$$J_k^1 = (\mathbf{y}_k - \mathbf{y}_r)^\intercal (\mathbf{y}_k - \mathbf{y}_r) , \tag{4.1}$$

with $\mathbf{y}_r$ the vector of NNL values.

— *Cost reduction:* This term reflects the economic costs derived from operating the available equipment. It can be formulated as

$$J_k^2 = \mathbf{c}_e \, \mathbf{u}_k^\intercal \mathbf{u}_k , \tag{4.2}$$

with $\mathbf{c}_e$ the vector of known costs associated to the equipment operation.

— *Smoothness of the control signal:* In order to avoid wear and tear, and increase the lifespan of the equipment, it is a common practice to penalize the control signal variation between consecutive time instants:

$$J_k^3 = \Delta\mathbf{u}_k^\intercal \Delta\mathbf{u}_k \ , \tag{4.3}$$

with $\Delta\mathbf{u}_k = \mathbf{u}_k - \mathbf{u}_{k-1}$.

— *Penalty in the relaxation parameter:* $\boldsymbol{\alpha}_k$, which was introduced in (3.15), is penalized to ensure that the water levels are outside the navigation interval as little as possible:

$$J_k^4 = \boldsymbol{\alpha}_k^\intercal \boldsymbol{\alpha}_k. \tag{4.4}$$

The multi-objective function J that gathers the control objectives can be described by

$$J\left(\mathbf{u}_k, \mathbf{y}_k, \boldsymbol{\alpha}_k\right) = \sum_{k=1}^{H_p} \sum_{j=1}^{4} \beta^j \, J_k^j \ , \tag{4.5}$$

where H_p is the prediction horizon and β^j are the weights of the j-th objective. Note that H_p must be chosen according not only to the system dynamics (settling time), but also to take into account the system delays. Therefore, $H_p > t_s + \max(S)$, where t_s is the settling time (in samples), and S was defined for (3.25). Moreover, the stability of the resulting MPC may be proved based on the ideas in [ON08, RA10] for time-delay systems. Finally, in order to set the weight of each objective in a multi-objective optimization problem, the procedure described in [TOML+11] can be used.

4.1.2 CMPC formulation

Gathering the control-oriented model, the system constraints and the multi-objective function, the design of the CMPC follows classical approaches [CB98, Mac02, RM09]: an optimization problem is solved over a prediction horizon, minimizing a cost function while respecting the system constraints. The first component of the vector of control inputs is extracted from the solution and is applied to the system, and the rest are disregarded. This procedure is repeated at each time instant, following a receding-horizon strategy.

The optimization problem is given by:

$$\min_{\{\mathbf{u}_{i|k}\}_{i=k}^{k+H_p-1},\, \{\mathbf{y}_{i|k}\}_{i=k}^{k+H_p-1},\, \{\boldsymbol{\alpha}_{i|k}\}_{i=k}^{k+H_p-1}} J\left(\mathbf{u}_{i|k}, \mathbf{y}_{i|k}, \boldsymbol{\alpha}_{i|k}\right) \tag{4.6a}$$

subject to:

$$\begin{aligned}
\mathbf{x}_{i+1|k} &= \mathbf{A}\mathbf{x}_{i|k} + \mathbf{A}_n\mathbf{x}_{i-n|k} + \mathbf{B}_u\mathbf{u}_{i|k} + \mathbf{B}_{un}\mathbf{u}_{i-n|k} + \\
&\quad \mathbf{B}_d\mathbf{d}_{i|k} + \mathbf{B}_{dn}\mathbf{d}_{i-n|k},\ i \in \{k, ..., k+H_p-1\}, && \text{(4.6b)}\\
\mathbf{y}_{i|k} &= \mathbf{C}\mathbf{x}_{i|k} + \mathbf{C}_n\mathbf{x}_{i-n|k} + \mathbf{D}_u\mathbf{u}_{i|k} + \mathbf{D}_{un}\mathbf{u}_{i-n|k} + \\
&\quad \mathbf{D}_d\mathbf{d}_{i|k} + \mathbf{D}_{dn}\mathbf{d}_{i-n|k},\ i \in \{k, ..., k+H_p-1\}, && \text{(4.6c)}\\
\mathbf{0} &= \mathbf{E}_u\mathbf{u}_{i|k} + \mathbf{E}_{un}\mathbf{u}_{i-n|k} + \mathbf{E}_d\mathbf{d}_{i|k} + \mathbf{E}_{dn}\mathbf{d}_{i-n|k},\ i \in \{k, ..., k+H_p-1\}, && \text{(4.6d)}\\
\underline{\mathbf{u}}^m &\leq \mathbf{u}^m_{i|k} \leq \overline{\mathbf{u}}^m,\ i \in \{k, ..., k+H_p-1\}, && \text{(4.6e)}\\
\underline{\mathbf{y}}_r - \boldsymbol{\alpha}_{i|k} &\leq \mathbf{y}_{i|k} \leq \overline{\mathbf{y}}_r + \boldsymbol{\alpha}_{i|k},\ i \in \{k, ..., k+H_p-1\}, && \text{(4.6f)}\\
\boldsymbol{\alpha}_{i|k} &\geq \mathbf{0},\ i \in \{k, ..., k+H_p-1\}, && \text{(4.6g)}\\
\mathbf{x}_{j|k} &= \hat{\mathbf{x}}_j^{MHE},\ j \in \{k-n, ..., k\}, && \text{(4.6h)}\\
\mathbf{u}_{l|k} &= \mathbf{u}_l^{MPC},\ l \in \{k-n, ..., k-1\}, && \text{(4.6i)}
\end{aligned}$$

where k is the current time instant, i is the time instant along the prediction horizon and $k+i|k$ indicates the predicted value of the variable at instant $k+i$ using information available at instant k.

Remark 4.1. j and l are used to indicate the use of past information, for which the considered time intervals are different than the one described by i. □

Equations (4.6b) and (4.6c) correspond to the model described by (3.24), (4.6d) are the mass balances given in (3.14), and (4.6e)–(4.6g) are the constraints given in (3.9), (3.15) and (3.16), respectively. Equation (4.6h) sets the values of the delayed states according to the solution provided by the CMHE (noted as $\hat{\mathbf{x}}_i^{MHE}$) in past iterations. Note that the CMHE will be introduced in the following section. These delayed values are provided to the CMPC as parameters. Similarly, the delayed control actions obtained by the CMPC (noted as $\mathbf{u}_i^{MPC}$) in previous iterations are also provided as parameters by means of (4.6i).

The optimal solution is given by the sequences $\{\mathbf{u}_{i|k}\}_{i=k}^{k+H_p-1}$, $\{\mathbf{y}_{i|k}\}_{i=k}^{k+H_p-1}$,

$\{\boldsymbol{\alpha}_{i|k}\}_{i=k}^{k+H_p-1}$ [1]. As it was stated before, only $\mathbf{u}_{k|k}$ is applied to the system, according to the receding philosophy

$$\mathbf{u}_k^{MPC} \triangleq \mathbf{u}_{k|k}. \tag{4.7}$$

4.2 State estimation: the MHE approach

The CMPC presented in Section 4.1 uses the states to compute the set of optimal control actions. The system states oftentimes are not directly measurable, and therefore they need to be estimated from the available data using a state estimator.

Thus, the problem to be solved is that of designing an observer that fully reconstructs the system states, for which a CMHE is proposed. The main principle of this technique consists in formulating the estimation problem as a quadratic program using a moving estimation window of a fixed size [ABQ+99, RRL01]. Indeed, it is assumed that only part of the available information of the system (inputs and outputs) is considered, which is shifted in time to consider the most recent information. Otherwise, the computational burden renders the full-information problem impractical to solve, as more and more data are processed with time. In this way, a truncated sequence of state estimates is computed at each time step instead of the full-state sequence to make the problem tractable [Rao00].

The formulation corresponding to the optimization problem solved by the CMHE reads as

$$\begin{aligned}\min_{\{\hat{\mathbf{x}}_{i|k}\}_{i=k-N}^{k},\,\{\boldsymbol{\gamma}_{i|k}\}_{i=k-N}^{k}} \quad & \left(\hat{\mathbf{x}}_{k-N|k}-\mathbf{x}_{k-N}\right)^{\intercal}\mathbf{P}^{-1}\left(\hat{\mathbf{x}}_{k-N|k}-\mathbf{x}_{k-N}\right)+ \\ & \sum_{i=k-N}^{k-1}\left(\mathbf{w}_{i|k}^{\intercal}\mathbf{Q}^{-1}\mathbf{w}_{i|k}+\mathbf{v}_{i|k}^{\intercal}\mathbf{R}^{-1}\mathbf{v}_{i|k}\right)+\boldsymbol{\gamma}_{i|k}^{\intercal}\boldsymbol{\gamma}_{i|k}\end{aligned} \tag{4.8a}$$

subject to:

$$\begin{aligned}\mathbf{w}_{j|k} = \hat{\mathbf{x}}_{j+1|k} - \Big(&\mathbf{A}\hat{\mathbf{x}}_{j|k}+\mathbf{A}_n\hat{\mathbf{x}}_{j-n|k}+\mathbf{B}_u\mathbf{u}_{j|k}+\mathbf{B}_{un}\mathbf{u}_{j-n|k}+ \\ &\mathbf{B}_d\mathbf{d}_{j|k}+\mathbf{B}_{dn}\mathbf{d}_{j-n|k}\Big),\ j\in\{k-N,...,k-1\},\end{aligned} \tag{4.8b}$$

$$\mathbf{v}_{j|k} = \mathbf{y}_{j|k} - \Big(\mathbf{C}\hat{\mathbf{x}}_{j|k}+\mathbf{C}_n\hat{\mathbf{x}}_{j-n|k}+\mathbf{D}_u\mathbf{u}_{j|k}+\mathbf{D}_{un}\mathbf{u}_{j-n|k}+ \tag{4.8c}$$

1. $\{\mathbf{u}_{i|k}\}_{i=k}^{k+H_p-1} \triangleq \{\mathbf{u}_{k|k},\mathbf{u}_{k+1|k},\cdots,\mathbf{u}_{k+H_p-1|k}\}$; $\mathbf{y}_{i|k}$ and $\boldsymbol{\alpha}_{i|k}$ are defined in the same manner

$$\mathbf{D}_d\mathbf{d}_{j|k} + \mathbf{D}_{dn}\mathbf{d}_{j-n|k}\Big),\ j \in \{k-N, ..., k-1\},$$

$$\mathbf{0} = \mathbf{E}_u\mathbf{u}_{j|k} + \mathbf{E}_{un}\mathbf{u}_{j-n|k} + \mathbf{E}_d\mathbf{d}_{j|k} + \mathbf{E}_{dn}\mathbf{d}_{j-n|k},\ j \in \{k-N, ..., k-1\}, \tag{4.8d}$$

$$\underline{\mathbf{x}}_r \leq \hat{\mathbf{x}}_{i|k} \leq \overline{\mathbf{x}}_r,\ i \in \{k-N, ..., k\}, \tag{4.8e}$$

$$-\boldsymbol{\gamma}_{i|k} \leq \hat{\mathbf{x}}_{i|k}^{D(1,2)} - \hat{\mathbf{x}}_{i|k}^{D(1,3)} \leq \boldsymbol{\gamma}_{i|k},\ i \in \{k-N, ..., k\}, \tag{4.8f}$$

$$\boldsymbol{\gamma}_{i|k} \geq \mathbf{0},\ i \in \{k-N, ..., k\}, \tag{4.8g}$$

$$\hat{\mathbf{x}}_{l|k} = \hat{\mathbf{x}}_l^{MHE},\ l \in \{k-N-n, ..., k-N-1\}, \tag{4.8h}$$

$$\mathbf{u}_{m|k} = \mathbf{u}_m^{MPC},\ m \in \{k-N-n, ..., k-1\}, \tag{4.8i}$$

$$\mathbf{y}_{o|k} = \mathbf{y}_o,\ o \in \{k-N, ..., k-1\}, \tag{4.8j}$$

with (4.8b) accounting for the system disturbances and (4.8c) for the measurement noise. Additionally, (4.8d) describes the static part of the model, (4.8e) defines the valid interval of the state variables, (4.8f) establishes a link between two of the states in (3.33), (4.8g) imposes the non-negativity of the relaxing parameter $\boldsymbol{\gamma}_k$, and (4.8h), (4.8i) and (4.8j) set the values of the delayed states, inputs and outputs, respectively, following the same ideas as in (4.6). Additional insight on the CMHE formulation is given below:

— The value $\mathbf{x}_{k-N}$ in (4.8a) corresponds to the most likely initial state vector, and is chosen based on the available knowledge of the system, whereas $\hat{\mathbf{x}}_{k-N|k}$ is the first value of the optimal state sequence computed by the CMHE at time instant k. The error in this initial guess, given by $\left(\hat{\mathbf{x}}_{k-N|k} - \mathbf{x}_{k-N}\right)$, is weighted by means of the matrix $\mathbf{P}^{-1}$, which indicates the confidence into the initial state, and its tuning allows to guarantee the boundedness of the estimation, as discussed in [RRM03]. On the other hand, $\mathbf{Q}^{-1}$ and $\mathbf{R}^{-1}$ are the weighting matrices inverses of suitable dimensions linked to the confidence in the quality of the model and the measurements, respectively. The larger these matrices are, the lesser the confidence in the associated term is, as the matrices are inverted. These inverses are directly related to the covariance matrices only in the case of linear systems with zero-mean uncorrelated random variables for unknown disturbances [Boe14]. In any other situation, e.g., constrained states, this connection is only an approximation.

— On the other hand, the need for (4.8f) and (4.8g) comes from the mass balance at the bifurcation node, which requires to impose an additional relationship between the state variables immediately after the bifurcation. Indeed, note that the states can be interpreted in terms of water volumes, which can be deduced by inspecting

matrix $\mathbf{C}$ in (3.23). Therefore, $\hat{\mathbf{x}}_k^{D(1,2)}/\hat{\mathbf{x}}_k^{D(1,3)} = \boldsymbol{\psi}_k$, where $\boldsymbol{\psi}_k$ is the existing proportionality between the two variables and is equal to the ratio of the flows after the bifurcation. Since it was considered in Section 3.5 that both flows are of equal magnitude, $\boldsymbol{\psi}_k = 1$ and thus the values of the states must be equal to one another. Note that this equality is relaxed by means of $\boldsymbol{\gamma}_k$ to avoid possible numerical infeasibility during the simulation.

— Finally, note that the cost function (4.8a) is extended with an additional term, given by $\boldsymbol{\gamma}_{i|k}^{\mathsf{T}}\boldsymbol{\gamma}_{i|k}$, to penalize large differences in the estimates. Indeed, a quadratic penalty is set on the relaxation parameter $\boldsymbol{\gamma}_{i|k}$, which must be monitored to ensure that large differences between the estimates $\hat{\mathbf{x}}_{i|k}^{D(1,2)}$ and $\hat{\mathbf{x}}_{i|k}^{D(1,3)}$ are not permitted.

The CMHE problem (4.8) is formulated as follows: at the current time instant k, N input-output pairs $[(\mathbf{u}_{k-N}, \mathbf{y}_{k-N}) : (\mathbf{u}_{k-1}, \mathbf{y}_{k-1})]$ shall be available. Therefore, N is the length of the moving estimation window, which bounds the size of the problem. The resulting least-squares problem is solved, yielding the optimal sequences $\{\hat{\mathbf{x}}_{i|k}\}_{i=k-N}^{k}$, $\{\boldsymbol{\gamma}_{i|k}\}_{i=k-N}^{k}$ [2]. However, as is the case in the CMPC problem, only one value in the sequence of state estimates is considered, and the rest are discarded. In the CMHE problem, this corresponds to the last value, that is, $\hat{\mathbf{x}}_{k|k}$. Therefore,

$$\hat{\mathbf{x}}_k^{MHE} \triangleq \hat{\mathbf{x}}_{k|k}. \tag{4.9}$$

In the next iteration ($k' = k + 1$), the truncated data sequence is updated and becomes $[(\mathbf{u}_{k'-N}, \mathbf{y}_{k'-N} : (\mathbf{u}_{k'-1}, \mathbf{y}_{k'-1})]$, which is equivalent to $[(\mathbf{u}_{k-N+1}, \mathbf{y}_{k-N+1}) : (\mathbf{u}_k, \mathbf{y}_k)]$. Note that the oldest measurement pair $(\mathbf{u}_{k-N}, \mathbf{y}_{k-N})$ is dropped, and the newest measurement pair $(\mathbf{u}_k, \mathbf{y}_k)$ is incorporated, following the moving horizon philosophy.

4.3 Implementation of the CMPC and the CMHE

Once the CMPC and the CMHE are designed, they must be integrated in the simulation loop. Algorithm 4.1, coded in MATLAB® using YALMIP [Löf04] as parser, illustrates how the solution provided by the controller is used by the estimator, and *vice versa*. Note that the simulation is designed in such a way that the estimator is called

2. $\{\hat{\mathbf{x}}_{i|k}\}_{i=k-N}^{k} \triangleq \{\hat{\mathbf{x}}_{k-N|k}, \hat{\mathbf{x}}_{k-N+1|k}, \cdots, \hat{\mathbf{x}}_{k|k}\}$; $\boldsymbol{\gamma}_{i|k}$ is defined in the same manner

Algorithm 4.1 Integration of the CMPC and CMHE in the simulation loop

Require: $\mathbf{y}_i, \mathbf{u}_i \; \forall i \in [k-N, k-1]$ and parameters in (4.6) and (4.8)

1: Estimate the initial state $\hat{\mathbf{x}}_{k=1}$ by solving (4.8) using $[(\mathbf{u}_{k-N}, \mathbf{y}_{k-N}) : (\mathbf{u}_{k-1}, \mathbf{y}_{k-1})]$
2: $\hat{\mathbf{x}}_k^{MHE} \triangleq \hat{\mathbf{x}}_{k=1}$
3: **for** $k = 1 : t_{sim}$ **do**
4: Solve the control problem (4.6) using $\hat{\mathbf{x}}_k^{MHE}$
5: $\mathbf{u}_k^{MPC} \triangleq \mathbf{u}_{k|k}$
6: Apply $\mathbf{u}_k^{MPC}$ to the system
7: Measure $\mathbf{y}_k$
8: Update the sequence of data as $\left[(\mathbf{u}_{k-N+1}, \mathbf{y}_{k-N+1}) : (\mathbf{u}_k^{MPC}, \mathbf{y}_k)\right]$
9: Solve the estimation problem (4.8) using the sequence of data defined in step 8
10: $\hat{\mathbf{x}}_k^{MHE} \triangleq \hat{\mathbf{x}}_{k+1|k+1}$
11: **end for**

first, which allows to initialize the system. The initial state is used as the starting point by the controller to compute the set of optimal inputs. The first element in the sequence is applied to the system, which allows to measure the outputs at current time. This information is then used by the estimator to provide the state estimates for the next time instant (with a slight abuse of notation to preserve the same variable name), which prepares the simulation for the next iteration.

Real systems are usually equipped with sensors that provide measurements, which are necessary to estimate the unmeasurable states. If these measurements were not available (as was the case at this stage), they would need to be generated in simulation, using the output equation. The effect of this limitation is that the estimator cannot be used for the first time at $k = 1$, but at $k = N + 1$. Indeed, an input-measurement pair $(\mathbf{u}_k, \mathbf{y}_k)$ is generated at each time instant k, using the solution of the controller. Thus, the necessary data to compute the state estimates is not available until N samples elapsed. Furthermore, the initial state $\hat{\mathbf{x}}_{k=1}$ has to be selected as any feasible state.

Finally, note that, at time k, the CMPC yields the sequence $\{\mathbf{u}_{i|k}\}_{i=k}^{k+H_p-1}$. It is therefore necessary to know the disturbances until, at least, the instant $k + H_p - 1$. By contrast, the CMHE sets its starting point N samples in the past, and reconstructs the optimal sequence of state estimates until the current time instant k. This requirement in terms of available information is fulfilled based on the policy introduced in Chapter 3, which allows to anticipate future lock operations.

Table 4.1: Lock operations

Lock	Dispatched water volume $[m^3]$	Duration $[min]$
Douai	18000	20
Cuinchy	12000	20
Don	12000	20
Fontinettes	30000	20

4.4 Simulation results for the CMPC and CMHE

The last section illustrates the performance of the CMPC and the CMHE by means of the realistic case study system depicted in Fig. 3.9. Its numerical model was obtained in Section 3.5 and is given by (3.35). The lock operations that take place in Douai, Don, Cuinchy and Fontinettes disturb the system, and their average magnitudes and durations are given in Table 4.1. The magnitudes of the lock operations are rather large compared to the operating points given in Table 3.1, which might temporarily cause the system dynamics to be far from those predicted by the linearized model. As it will be discussed in Chapter 7, a possible solution might be to resort to LPV or nonlinear modeling strategies. However, the use of a controller is expected to minimize the effect of such mismatch.

A realistic 24-hour scenario, depicted in Fig. 4.1, is designed by considering a lock operation time-series model for a typical navigation profile. Additionally, the following management restrictions must be taken into account:

— A day is divided in two periods: navigation and stoppage. Boats are only allowed to navigate during the navigation period, which starts each day at 6 a.m. and finishes after fourteen hours, at 8 p.m. The navigation is interrupted until the next day at 6 a.m.

— The current policy allows a maximum of two lock operations per hour.

Besides, the scenario does not consider changes in the setpoints, thus assuming that the navigation conditions do not change during the simulation. Such modifications typically occur due to changes in the weather condition, e.g., flood and drought episodes, which might require to readjust the LNL, NNL and HNL values.

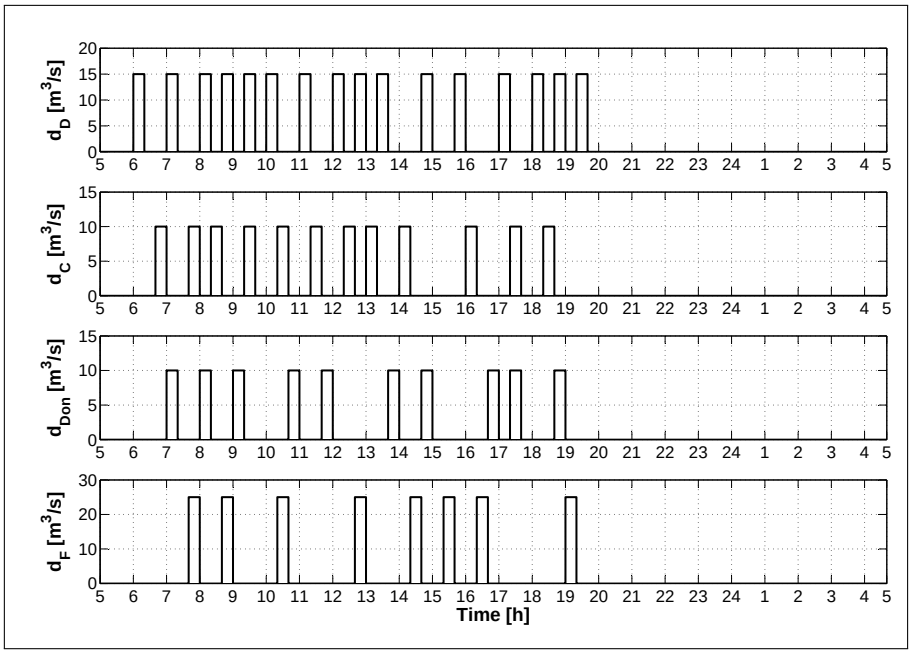

Figure 4.1: The considered lock operation profile

On the other hand, the same four nodes are equipped with controlled devices which allow to dispatch water to fulfill the control objectives. In particular, Douai and Fontinettes are equipped with undershot gates, whereas Don and Cuinchy are equipped with weirs. It is considered that all gates and weirs can deliver a maximum flow of 10 m^3/s, which will have to be converted into maximum gate openings and sill elevations, respectively. Their nonlinear expressions, as well as their linearized equations, are given by (3.12) and (3.34), respectively.

The simulation is carried out in MATLAB®, using a processor Intel® Core™ i5-3230M CPU 2.60GHz and 4 GB of RAM. Figure 4.2 depicts, for each discrete-time instant, the computation times spent in solving the CMPC plus the CMHE. Note that the CPU times include YALMIPs overhead to convert the problem to solver-specific format, and not only the solver times. Although some coding effort could be made to reduce computation times, the current design is satisfactory and could be implemented in real time, given the considered sampling time. Furthermore, the total simulation time is 22.12 s.

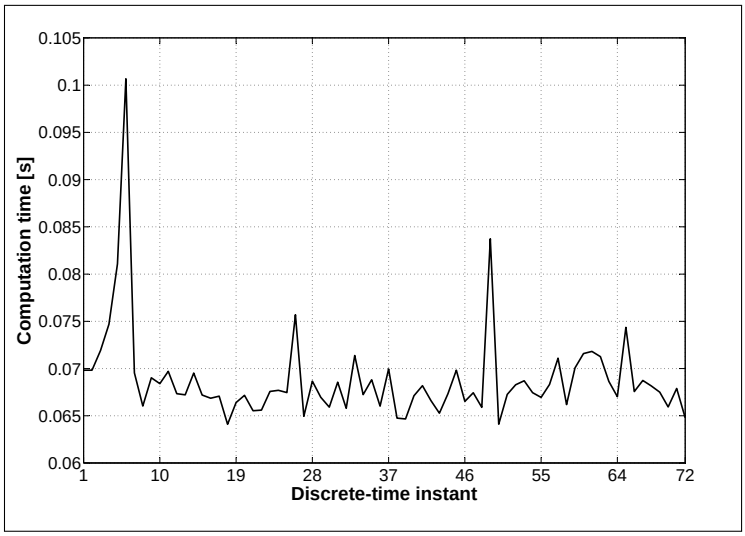

Figure 4.2: CMPC+CMHE computation time

4.4.1 CMHE

In order to estimate the states, the measurements of the system are needed. Depending on the structure of the problem, e.g., the topology of the network or the connections between reaches, not all measurements are required. This statement can be realized by inspecting matrix $\mathbf{C}$, which links the states and the measurements. In the present case, it is not necessary to consider the measurement $y_k^{C(1,2)}$, since the associated state has an effect on the downstream level $y_k^{C(4)}$, given by the off-diagonal, nonzero entry in the fourth row of $\mathbf{C}$. Hence, in order to show the effectiveness of the approach, the six states are reconstructed with only five measurements, i.e., assuming that the water level $y_k^{C(1,2)}$ is not available. Thus, this value is obtained from the state estimates.

The comparison between the optimal estimated states given by the CMHE and the real states obtained in simulation are depicted in Figure 4.3. As mentioned in Section 3.5, real data are only available in this thesis for a small part of the system, and thus the output equation is used to compute the water levels. On the other hand, the CMHE is fed with the corresponding sequence of N input-measurement pairs at each time instant, which are used to compute the optimal sequence of states. The following weights are used in the definition of the CMHE: $\mathbf{P}^{-1} = \mathbb{I}_{n_x} = \mathbb{I}_6$, $\mathbf{Q}^{-1} = \mathbb{I}_{n_y-1} = \mathbb{I}_5$ and $\mathbf{R}^{-1} = \mathbb{I}_{n_x} = \mathbb{I}_6$.

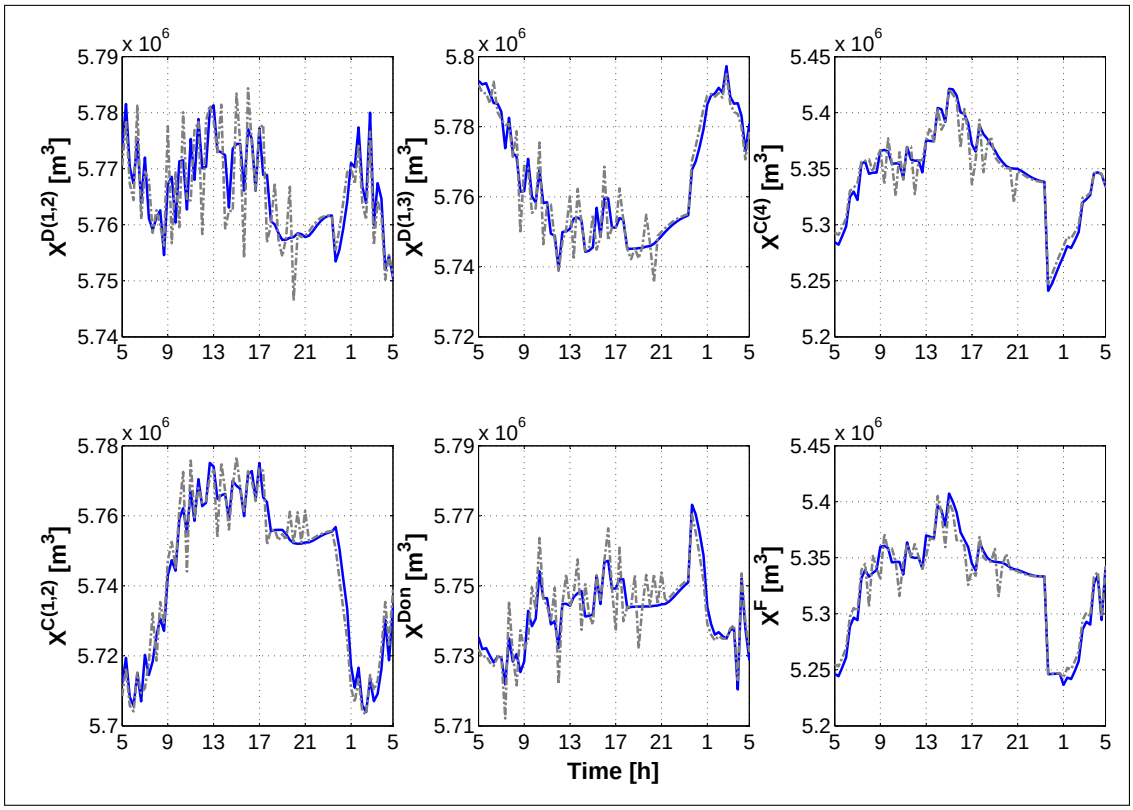

Figure 4.3: State estimates (blue solid lines) and computed states (dash-dot gray lines)

In general, the values provided by the estimator match the real states with no significant error. In addition, the real states are noisier than the estimated states. This behavior is in line with the nature of the observer, which acts as a filter, smoothing the predictions. Furthermore, the constraints on the state bounds are satisfied. Such bounds are not even depicted in Fig. 4.3 for the benefit of a better visualization of the results, as the states are far from the bounds.

On the other hand, recall the relationship between $\hat{\mathbf{x}}^{D(1,2)}$ and $\hat{\mathbf{x}}^{D(1,3)}$ given by (4.8f). According to what was stated in Section 4.2, although these two variables must be equal to one another, this condition was relaxed in order to avoid possible numerical infeasibility. It can be seen how the two state estimates are not exactly the same, for which the relaxation parameter $\boldsymbol{\gamma}$ accounts. However, the differences are rather small, being the largest relative difference equal to 0.5%.

Table 4.2: Correlation coefficients for the CMHE

D (1,2)	C (1,2)	D (1,3)	Don	C (4)	F
0.8389	0.8856	0.8841	0.9276	0.9654	0.9403

In order to ensure a quantitative comparison between the real and the estimated states, the similarity of both signals is quantified by means of the correlation coefficient. Given a pair of signals (m_t, n_t) with M observations each, the correlation coefficient is defined as

$$\rho_{m,n} = \frac{1}{M-1} \sum_{i=1}^{M} \left(\frac{m_i - \mu_m}{\sigma_m} \right) \left(\frac{n_i - \mu_n}{\sigma_n} \right), \tag{4.10}$$

where μ_m and σ_m are the mean and standard deviation of m_t, respectively, and μ_n and σ_n are the mean and standard deviation of n_t. This coefficient is bounded between 1 and -1: the closer this coefficient is to 1 (respectively -1), the stronger the positive (respectively negative) correlation between the pair of signals is. The correlation coefficients between the real and the estimated states are summarized in Table 4.2.

It can be stated that the performance of the CMHE is satisfactory, since all the correlation coefficients are very close to 1, which indicates a strong, positive correlation. Indeed, the main goal of the estimator is that of reconstructing an accurate state sequence that is not directly measurable. This procedure is used to achieve the final goal, which consists in fulfilling the control objectives, so that the desired system performance is attained. Therefore, state estimation is regarded as a tool employed by the controller in pursuit of the final goal.

4.4.2 CMPC

The estimated states are used by the controller in order to compute the sequence of future optimal inputs, applying only its first component. It must be recalled that the real system measurements are not available at this stage, and thus they must be obtained using the output equation.

Based on the control objectives defined before, two main results are looked at: the water levels and the control signals, depicted in Figs. 4.4 and 4.5, respectively. The following weights are used in the definition of the CMPC: $\beta^1 = 20$, $\beta^2 = 2$, $\beta^3 = 5$ and

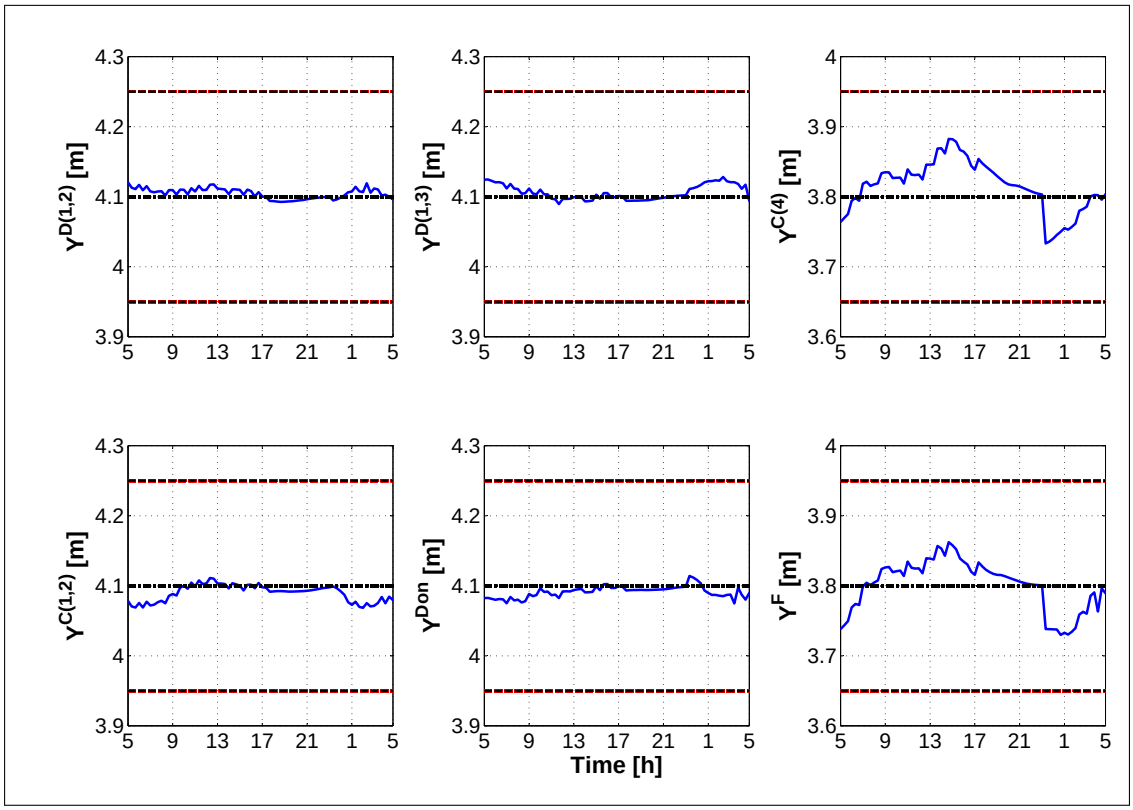

Figure 4.4: Water levels (blue solid lines) and LNL, NNL and HNL (black dashed lines)

$\beta^4 = 1$.

The modeling simplification introduced in Fig. 3.9 led to considering three reaches, where their upstream and downstream water levels are arranged by columns in Fig. 4.4. Recall that $y_k^{C(1,2)}$ is not measured, but computed from the state estimates.

Regarding the control objectives linked to the water levels, it can be stated that the CMPC is able to keep the levels very close to the setpoints despite of the disturbances. To quantify the performance of the controller, consider the indices given by:

$$TP = 1 - \frac{1}{H_p}\sqrt{\sum_{k=1}^{H_p}\left(\frac{\mathbf{y}_k - \mathbf{y}_r}{\frac{1}{2}\left(\overline{\mathbf{y}}_r - \underline{\mathbf{y}}_r\right)}\right)^2}, \tag{4.11}$$

with H_p the prediction horizon as defined in (4.5). Equation (4.11) was introduced in

Table 4.3: Tracking performances for the CMPC

D (1,2)	C (1,2)	D (1,3)	Don	C (4)	F
0.9930	0.9877	0.9904	0.9907	0.9693	0.9717

[SRN+18b] as a modification of the standard root relative squared error. These tracking performance indices are defined as the relative error between the predicted levels $\mathbf{y}_k$ and the setpoints $\mathbf{y}_r$ (NNL values). The denominator, given by $\frac{1}{2}\left(\overline{\mathbf{y}}_r - \underline{\mathbf{y}}_r\right)$, equals the semi-amplitude of the symmetric [LNL, HNL] interval, which is the maximum allowed variation from $\mathbf{y}_r$. The squaring emphasizes larger differences, which is of interest in this case, since it focuses on the water levels $\mathbf{y}_k$ that are far from the setpoints $\mathbf{y}_r$.

The numerical values of the indices for each water level are summarized in Table 4.3. Note that TP is bounded between 0 and 1, where 1 corresponds to the perfect tracking performance. Therefore, it can be stated that the CMPC provides satisfactory results in terms of keeping the water levels close to the setpoints. Moreover, Fig. 4.4 shows that the levels are never outside of the navigation rectangle, and therefore the penalty on this behavior, represented by $\boldsymbol{\alpha}_k$ in (4.4), equals 0.

On the other hand, the control objectives (4.2) and (4.3) are linked to the control signals, depicted in Fig. 4.5. The undershot gates in Douai and Fontinettes allow maximum flow for a maximal gate opening, and zero flow for a null gate opening. Conversely, the weirs in Cuinchy and Don allow maximum flow for null sill elevation, and zero flow for a maximal sill elevation. This fact can be realized by the minus sign in the linearized weir equations (3.34). The controller regulates the openings and elevations so that there is neither a deficit nor an excess of water in the reaches. Indeed, while the gate openings in Douai and Fontinettes are minimal (no flow), the sill elevations in Don and Cuinchy are maximal (no flow), and *vice versa*. Of course, the transport delays need to be taken into account for the sake of a complete explanation.

On the other hand, minimum flows, i.e., minimal gate openings and maximal sill elevations, are expected to be delivered by the actuators when the water levels reach the setpoints. However, rejecting disturbances results in continuously operating the actuators, as these disturbances go against the control objectives. Therefore, it can be seen how the actuators work close to their maximum capacity only during short periods of time, and always within the equipment design range. During most of the simulation,

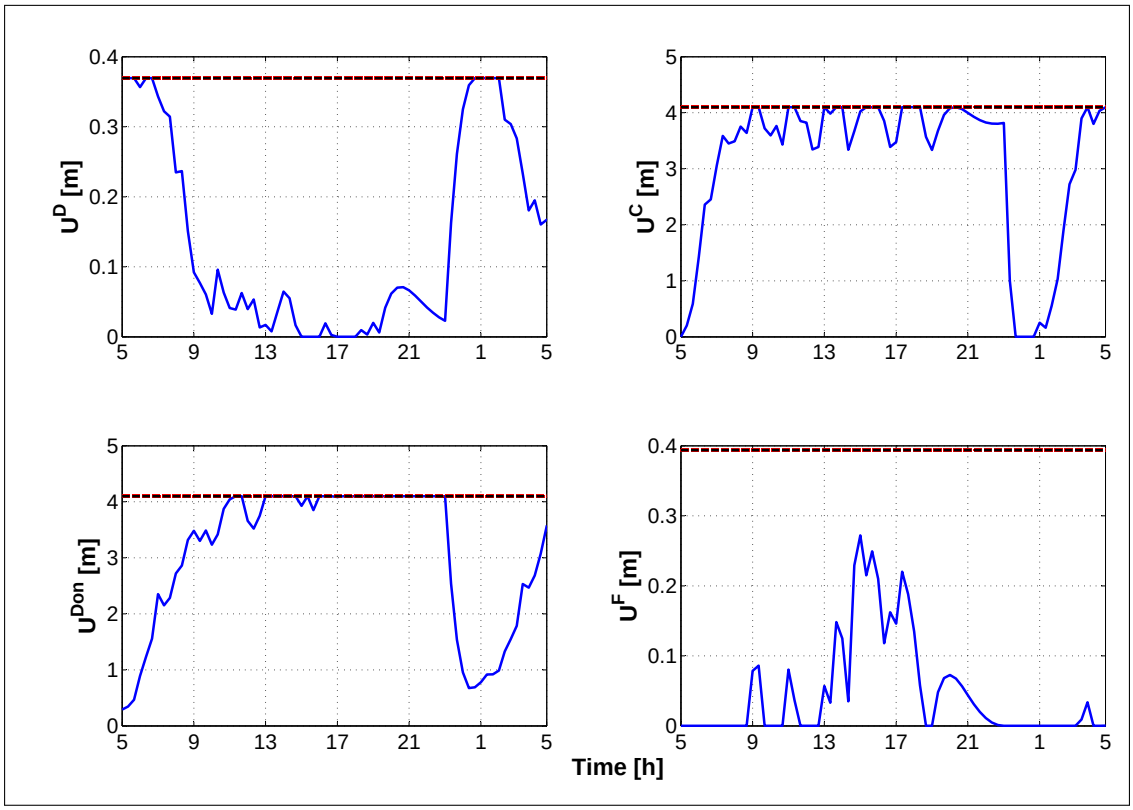

Figure 4.5: Gate openings and sill elevations (blue solid lines) and physical limits (dash-dot black lines)

the inputs are far from the limits of the actuators, thus taking into account the cost reduction objective (4.2).

Regarding the smoothness of the control signals given by the operational goal (4.3), the control actions present some peaks. However, there are no large variations between consecutive control actions, especially compared with the design range of the actuators. This behavior should result in a long lifespan of the equipment. Although the weight of this objective could be increased, this would probably interfere with the rest of objectives.

4.5 Summary

Chapter 4 has approached the issue of designing a controller and an observer using the centralized approach. Given the model formulation proposed in Chapter 3, MPC and

MHE have been chosen due to their adequacy to deal with delayed descriptor systems in a natural manner, as well as their suitability to take into account multiple objectives and physical and operational constraints. In particular, MPC aims at guaranteeing that the water levels are kept within the navigation interval and minimizing the control effort, with an additional term that penalizes non-smooth control actions. This strategy requires the vector of states to be known at current time, which can be estimated by the MHE based on available data. This observer considers the most recent data to solve an optimization problem with a structure that is closely linked to the MPC problem. Both approaches are tested in simulation in the last part of the chapter, and their performances are discussed and validated with regard to the design goals. However, a centralized implementation might not be the most efficient option for large-scale systems such as inland waterways. In this regard, the next chapter discusses its adequacy and explores non-centralized implementation alternatives.

Chapter 5

Distributed control and state estimation

Centralized control and state estimation approaches for large-scale systems such as those presented in Chapter 4 might lead to implementation problems due to the spatial distribution, multi-time scales and non-scalability. Indeed, the large dimensionality of the centralized model often renders such representation impractical to reconfigure when part of the network needs to be disregarded because of maintenance or malfunctioning [OMBPB12]. Furthermore, the centralization of decisions in a single controller might compromise the network reliability [GOMP17b] or be affected by bandwidth limitations [Sca09]. Non-centralized approaches, on the other hand, provide more flexibility and allow to build the controller in an incremental manner, i.e., adding new parts to an existing control scheme.

In this regard, many non-centralized control strategies have been proposed in the last years. One of the possibilities consists in partitioning the systemwide plant into subsystems with local agents in charge of meeting the local objectives. The notion of agent was defined in Section 2.3 as a computing system within an environment that is capable of performing certain actions, aiming at attaining its objectives. In general, the system partitioning leads to a set of smaller subsystems, each of them defining a subproblem. These subsystems are usually not completely decoupled from one another, i.e., one or more variables appear in more than one subproblem. Therefore, a distributed approach is usually preferable over a decentralized one.

Chapter 5 is organized as follows: an existing partitioning approach based on a reorganization of the interconnection (or adjacency) matrix is presented in Section 5.1. The first step is concerned with the derivation of the adjacency matrix associated to Fig. 3.9. Then, this matrix is reordered based on a row-and-column permutation methodology, and its final structure determines the number of subsystems in which the overall system decomposes, as well as the couplings between subsystems. The resulting partitioning allows to perform distributed control and state estimation, and thus the distributed performance can be compared with the centralized results presented in Chapter 4. Section 5.2 regards the coordination of the subproblems based on a communication protocol, where the coupled variables are optimized for each subsystem and then shared with the rest of subsystems. Then, the solution for each coupled variable at each time instant is assumed to be found only when the values computed by all agents match with no significant error and the convergence between consecutive iterations is guaranteed. The implementation of the DMPC and DMHE is provided in Section 5.3, following the ideas used in the design of Algorithm 4.1. Finally, Section 5.4 performs the partitioning of the centralized model given in Chapter 4, and gathers and discusses the results obtained using the distributed approach. The content featured in this chapter has been published in [SRN+18a] and submitted for publication in [SRN+19a, SRN+].

5.1 System partitioning

This section regards the partitioning of large-scale systems. The proposed approach consists in two steps: first, the adjacency matrix is defined. Then, it is manipulated based on row-and-column permutation operations, which allows to identify possible subsystems into which the overall system can be decomposed.

5.1.1 Building the adjacency matrix

The adjacency matrix of a system defines its structural properties in a compact manner. The same information can be retrieved from the graph representation, where each variable is assigned to a vertex of the graph, and an edge connects a pair of variables whenever the corresponding coefficient in the system matrix is different from zero. This matrix can be built as follows [Sil11]:

$$\mathbf{E} = \begin{bmatrix} \bar{\mathbf{A}} & \bar{\mathbf{B}} & \mathbf{0} \\ \mathbf{0} & \mathbf{0} & \mathbf{0} \\ \bar{\mathbf{C}} & \mathbf{0} & \mathbf{0} \end{bmatrix}, \tag{5.1}$$

where the matrices $\bar{\mathbf{A}} = (\bar{a}_{ij}) \in \mathbb{R}^{n_x \times n_x}$, $\bar{\mathbf{B}} = \left(\bar{b}_{ij}\right) \in \mathbb{R}^{n_x \times n_u}$ and $\bar{\mathbf{C}} = (\bar{c}_{ij}) \in \mathbb{R}^{n_y \times n_x}$ are defined as

$$\bar{a}_{ij} = \begin{cases} 1, \ a_{ij} \neq 0, \\ 0, \ a_{ij} = 0, \end{cases} \qquad \bar{b}_{ij} = \begin{cases} 1, \ b_{ij} \neq 0, \\ 0, \ b_{ij} = 0, \end{cases} \qquad \bar{c}_{ij} = \begin{cases} 1, \ c_{ij} \neq 0, \\ 0, \ c_{ij} = 0, \end{cases} \tag{5.2}$$

and the dimensions of the several $\mathbf{0}$ blocks are as given in [Sil11] so that $\mathbf{E}$ is a square matrix.

However, note that (5.1) needs to be adapted in order to deal with the centralized model (3.35). Indeed, its current formulation does not represent systems with a nonzero feedforward matrix $\mathbf{D}$. Furthermore, the delayed matrices $\mathbf{A}_n$, $\mathbf{B}_{un}$, $\mathbf{C}_n$ and $\mathbf{D}_{un}$ must be also included in $\mathbf{E}$, as they provide additional links between variables. To do so, the delays can be dropped when building the adjacency matrix as it was done in (3.19). Indeed, removing the delays does not affect the structural properties of the system. Therefore, and following the notation introduced in (3.24), the modified version of the adjacency matrix $\mathbf{E}$ reads as

$$\tilde{\mathbf{E}} = \begin{bmatrix} \tilde{\mathbf{A}} & \tilde{\mathbf{B}} & \mathbf{0} \\ \mathbf{0} & \mathbf{0} & \mathbf{0} \\ \tilde{\mathbf{C}} & \tilde{\mathbf{D}} & \mathbf{0} \end{bmatrix}, \tag{5.3}$$

where $\tilde{\mathbf{A}} = (\tilde{a}_{ij})$, $\tilde{\mathbf{B}} = \left(\tilde{b}_{ij}\right)$, $\tilde{\mathbf{C}} = (\tilde{c}_{ij})$ and $\tilde{\mathbf{D}} = \left(\tilde{d}_{ij}\right)$ are given by

$$\begin{aligned} \tilde{a}_{ij} &= \begin{cases} 1, \ a_{ij} \neq 0 \vee a_{n_{ij}} \neq 0, \\ 0, \ \text{otherwise}, \end{cases} & \tilde{b}_{ij} &= \begin{cases} 1, \ b_{u_{ij}} \neq 0 \vee b_{un_{ij}} \neq 0, \\ 0, \ \text{otherwise}, \end{cases} \\ \tilde{c}_{ij} &= \begin{cases} 1, \ c_{ij} \neq 0 \vee c_{n_{ij}} \neq 0, \\ 0, \ \text{otherwise}, \end{cases} & \tilde{d}_{ij} &= \begin{cases} 1, \ d_{u_{ij}} \neq 0 \vee d_{un_{ij}} \neq 0, \\ 0, \ \text{otherwise}. \end{cases} \end{aligned} \tag{5.4}$$

Remark 5.1. The structural approach followed in this work does not take into account

quantitative information, i.e., the degree of coupling. A future extension of the system partitioning method could include additional criteria that takes into account the magnitude of the couplings. □

5.1.2 The reordering Cuthill-McKee algorithm

Once the adjacency matrix has been obtained, the next step consists in determining possible *configurations* for the subsystems. The definition of configuration in this framework is that of a set of groups of variables and model equations, where each group defines a subproblem. The chosen approach consists in manipulating $\tilde{\mathbf{E}}$ such that a block-diagonal structure is attained. A number of methods can be employed, although not all of them are well suited for this task. For instance, some approaches compromise the coupling information due to the elimination of some matrix coefficients. Hence, the Cuthill-McKee ordering algorithm [GL81] is chosen here, and consists in performing row and column permutations on both symmetric and asymmetric matrices to yield a reordered matrix with all its nonzero entries closer to the diagonal. This algorithm is implemented in MATLAB®: the command `symrcm` returns the permutation vector $order$, so that the block-diagonal matrix $\tilde{\mathbf{E}}_{blk}$ can be obtained as $\tilde{\mathbf{E}}(order, order)$. Then, each of the identified blocks can be regarded as a subsystem, and the coupled variables are those

5.2 Coordinating multiple optimization problems: a communication-based strategy

Once the system partitioning has been performed, the next problem to be solved is that of synthesizing the controllers and estimators for the identified subsystems, as well as their coordination. In this regard, the proposed approach consists in solving the subproblems in combination with a communication strategy that allows each local agent to compare its optimal solution with the solution obtained by the other agents [CJKT02, RS08]. The proposed strategy considers that a local controller and a local estimator are available for each subsystem, which exchange information with the rest of controllers and estimators involved in the computation of the same coupled inputs and states, respectively.

This procedure is repeated until two conditions are met. First, the differences among the local solutions must not exceed a given threshold. Moreover, the convergence of the solutions between consecutive iterations must be ensured. Only when these conditions are verified, the receding philosophy given by (4.7) and (4.9) is followed in a distributed manner.

5.2.1 DMPC formulation

The distributed control problems can be obtained from the original centralized formulation (4.6). Note that the local control problems solved by each agent have the same structure. Assuming that the overall system can be decomposed into M subsystems, the problem solved by the controller assigned to subsystem Σ_a reads as follows:

$$\min_{\left\{\mathbf{u}_{i|k}^{(\Sigma_a)}\right\}_{i=k}^{k+H_p-1},\left\{\mathbf{y}_{i|k}^{(\Sigma_a)}\right\}_{i=k}^{k+H_p-1},\left\{\boldsymbol{\alpha}_{i|k}^{(\Sigma_a)}\right\}_{i=k}^{k+H_p-1},\left\{\boldsymbol{\epsilon}_{i|k}^{(\Sigma_a)}\right\}_{i=k}^{k+H_p-1}} J^{(\Sigma_a)}\left(\mathbf{u}_{i|k}^{(\Sigma_a)},\mathbf{y}_{i|k}^{(\Sigma_a)},\boldsymbol{\alpha}_{i|k}^{(\Sigma_a)},\boldsymbol{\epsilon}_{i|k}^{(\Sigma_a)}\right) \tag{5.5a}$$

subject to:

$$\begin{aligned}
\mathbf{x}_{i+1|k}^{(\Sigma_a)} &= \mathbf{A}^{(\Sigma_a)}\mathbf{x}_{i|k}^{(\Sigma_a)} + \mathbf{A}_n^{(\Sigma_a)}\mathbf{x}_{i-n|k}^{(\Sigma_a)} + \mathbf{B}_u^{(\Sigma_a)}\mathbf{u}_{i|k}^{(\Sigma_a)} + \mathbf{B}_{un}^{(\Sigma_a)}\mathbf{u}_{i-n|k}^{(\Sigma_a)} + \\
&\quad \mathbf{B}_d^{(\Sigma_a)}\mathbf{d}_{i|k}^{(\Sigma_a)} + \mathbf{B}_{dn}^{(\Sigma_a)}\mathbf{d}_{i-n|k}^{(\Sigma_a)},\ i \in \{k,...,k+H_p-1\}, && \text{(5.5b)}\\
\mathbf{y}_{i|k}^{(\Sigma_a)} &= \mathbf{C}^{(\Sigma_a)}\mathbf{x}_{i|k}^{(\Sigma_a)} + \mathbf{C}_n^{(\Sigma_a)}\mathbf{x}_{i-n|k}^{(\Sigma_a)} + \mathbf{D}_u^{(\Sigma_a)}\mathbf{u}_{i|k}^{(\Sigma_a)} + \mathbf{D}_{un}^{(\Sigma_a)}\mathbf{u}_{i-n|k}^{(\Sigma_a)} + \\
&\quad \mathbf{D}_d^{(\Sigma_a)}\mathbf{d}_{i|k}^{(\Sigma_a)} + \mathbf{D}_{dn}^{(\Sigma_a)}\mathbf{d}_{i-n|k}^{(\Sigma_a)},\ i \in \{k,...,k+H_p-1\}, && \text{(5.5c)}\\
\mathbf{0} &= \mathbf{E}_u^{(\Sigma_a)}\mathbf{u}_{i|k}^{(\Sigma_a)} + \mathbf{E}_{un}^{(\Sigma_a)}\mathbf{u}_{i-n|k}^{(\Sigma_a)} + \mathbf{E}_d^{(\Sigma_a)}\mathbf{d}_{i|k}^{(\Sigma_a)} + \mathbf{E}_{dn}^{(\Sigma_a)}\mathbf{d}_{i-n|k}^{(\Sigma_a)}, && \text{(5.5d)}\\
&\quad i \in \{k,...,k+H_p-1\},\\
\underline{\mathbf{u}}^{(\Sigma_a)} &\leq \mathbf{u}_{i|k}^{(\Sigma_a)} \leq \overline{\mathbf{u}}^{(\Sigma_a)},\ i \in \{k,...,k+H_p-1\}, && \text{(5.5e)}\\
\underline{\mathbf{y}}_r^{(\Sigma_a)} - \boldsymbol{\alpha}_{i|k}^{(\Sigma_a)} &\leq \mathbf{y}_{i|k}^{(\Sigma_a)} \leq \overline{\mathbf{y}}_r^{(\Sigma_a)} + \boldsymbol{\alpha}_{i|k}^{(\Sigma_a)},\ i \in \{k,...,k+H_p-1\}, && \text{(5.5f)}\\
\boldsymbol{\alpha}_{i|k}^{(\Sigma_a)} &\geq \mathbf{0},\ i \in \{k,...,k+H_p-1\}, && \text{(5.5g)}\\
\mathbf{x}_{j|k}^{(\Sigma_a)} &= \hat{\mathbf{x}}_j^{MHE\,(\Sigma_a)},\ j \in \{k-n,...,k\}, && \text{(5.5h)}\\
\mathbf{u}_{l|k}^{(\Sigma_a)} &= \mathbf{u}_l^{MPC\,(\Sigma_a)},\ l \in \{k-n,...,k-1\}, && \text{(5.5i)}\\
-\boldsymbol{\epsilon}_{i|k}^{(\Sigma_a)} &\leq \mathbf{u}_{i|k}^{(\Sigma_a)} - \mathbf{u}_i^{(\Sigma_b)} \leq \boldsymbol{\epsilon}_{i|k}^{(\Sigma_a)},\ i \in \{k,...,k+H_p-1\}, && \text{(5.5j)}\\
\forall b &\mid \mathbf{u}^{(\Sigma_a)} \cap \mathbf{u}^{(\Sigma_b)} \neq \varnothing,
\end{aligned}$$

$$\boldsymbol{\epsilon}_{i|k}^{(\Sigma_a)} \geq 0,\ i \in \{k, ..., k + H_p - 1\}. \tag{5.5k}$$

Additional insight on the DMPC formulation is provided below:

— The superscripts (Σ_a) and (Σ_b) indicate that the corresponding parameters and variables are linked to the a-th and b-th subsystems, respectively. Moreover, Σ_b regards all subsystems with a coupled input with Σ_a, and not just a single subsystem, as stated in (5.5j).

— Constraints (5.5j) and (5.5k) are added to the original centralized formulation to guarantee that the differences between the solutions provided by subsystems Σ_a and Σ_b remain within the specified bounds $[-\boldsymbol{\epsilon}^{(\Sigma_a)}, \boldsymbol{\epsilon}^{(\Sigma_a)}]$. Although these bounds can be determined offline based on some desirable performance, they are defined here as decision variables to avoid possible infeasibility problems in the first steps of the iteration. In this case, these values must be monitored to ensure that significant differences for the coupled inputs are not permitted.

— Furthermore, the term $\mathbf{u}_i^{(\Sigma_b)}$ in (5.5j) is not a decision variable, but a parameter that corresponds to the solution obtained for the subsystem Σ_b. This constraint accounts for the communication between agents. Moreover, note that (5.5j) regards not only the first value of the optimal input sequence $\left\{\mathbf{u}_{i|k}^{(\Sigma_a)}\right\}_{i=k}^{k+H_p-1}$, but the sequence for the whole prediction horizon. Indeed, the whole sequence is transmitted to other agents, and not only its first component.

— An additional term must be added to the local objective function (5.5a) with respect to the original global objective function (4.6a) to penalize large values of $\boldsymbol{\epsilon}^{(\Sigma_a)}$, which can be simply formulated as $\left(\boldsymbol{\epsilon}_k^{(\Sigma_a)}\right)^{\mathsf{T}} \boldsymbol{\epsilon}_k^{(\Sigma_a)}$. An analogous formulation could be that of a reward or *bonus*, aiming at promoting cooperation among local agents.

5.2.2 DMHE formulation

Following the same ideas as in Section 5.2.1, the DMHE problem solved for by the estimator assigned to subsystem Σ_a reads as follows:

$$\min_{\substack{\left\{\hat{\mathbf{x}}_{i|k}^{(\Sigma_a)}\right\}_{i=k-N}^{k} \\ \left\{\boldsymbol{\gamma}_{i|k}^{(\Sigma_a)}\right\}_{i=k-N}^{k}}} \left(\hat{\mathbf{x}}_{k-N|k}^{(\Sigma_a)} - \mathbf{x}_{k-N}^{(\Sigma_a)}\right)^{\intercal} \left(\mathbf{P}^{(\Sigma_a)}\right)^{-1} \left(\hat{\mathbf{x}}_{k-N|k}^{(\Sigma_a)} - \mathbf{x}_{k-N}^{(\Sigma_a)}\right) + \tag{5.6a}$$

$$\sum_{i=k-N}^{k-1} \left(\left(\mathbf{w}_{i|k}^{(\Sigma_a)}\right)^{\intercal} \left(\mathbf{Q}^{(\Sigma_a)}\right)^{-1} \mathbf{w}_{i|k}^{(\Sigma_a)} + \left(\mathbf{v}_{i|k}^{(\Sigma_a)}\right)^{\intercal} \left(\mathbf{R}^{(\Sigma_a)}\right)^{-1} \mathbf{v}_{i|k}^{(\Sigma_a)}\right) + \left(\boldsymbol{\gamma}_{i|k}^{(\Sigma_a)}\right)^{\intercal} \boldsymbol{\gamma}_{i|k}^{(\Sigma_a)}$$

subject to:

$$\mathbf{w}_{j|k}^{(\Sigma_a)} = \hat{\mathbf{x}}_{j+1|k}^{(\Sigma_a)} - \left(\mathbf{A}^{(\Sigma_a)} \hat{\mathbf{x}}_{j|k}^{(\Sigma_a)} + \mathbf{A}_n^{(\Sigma_a)} \hat{\mathbf{x}}_{j-n|k}^{(\Sigma_a)} + \mathbf{B}_u^{(\Sigma_a)} \mathbf{u}_{j|k}^{(\Sigma_a)} + \mathbf{B}_{un}^{(\Sigma_a)} \mathbf{u}_{j-n|k}^{(\Sigma_a)} + \mathbf{B}_d^{(\Sigma_a)} \mathbf{d}_{j|k}^{(\Sigma_a)} + \mathbf{B}_{dn}^{(\Sigma_a)} \mathbf{d}_{j-n|k}^{(\Sigma_a)}\right), \; j \in \{k-N, ..., k-1\}, \tag{5.6b}$$

$$\mathbf{v}_{j|k}^{(\Sigma_a)} = \mathbf{y}_{j|k}^{(\Sigma_a)} - \left(\mathbf{C}^{(\Sigma_a)} \hat{\mathbf{x}}_{j|k}^{(\Sigma_a)} + \mathbf{C}_n^{(\Sigma_a)} \hat{\mathbf{x}}_{j-n|k}^{(\Sigma_a)} + \mathbf{D}_u^{(\Sigma_a)} \mathbf{u}_{j|k}^{(\Sigma_a)} + \mathbf{D}_{un}^{(\Sigma_a)} \mathbf{u}_{j-n|k}^{(\Sigma_a)} + \mathbf{D}_d^{(\Sigma_a)} \mathbf{d}_{j|k}^{(\Sigma_a)} + \mathbf{D}_{dn}^{(\Sigma_a)} \mathbf{d}_{j-n|k}^{(\Sigma_a)}\right), \; j \in \{k-N, ..., k-1\}, \tag{5.6c}$$

$$\mathbf{0} = \mathbf{E}_u^{(\Sigma_a)} \mathbf{u}_{j|k}^{(\Sigma_a)} + \mathbf{E}_{un}^{(\Sigma_a)} \mathbf{u}_{j-n|k}^{(\Sigma_a)} + \mathbf{E}_d^{(\Sigma_a)} \mathbf{d}_{j|k}^{(\Sigma_a)} + \mathbf{E}_{dn}^{(\Sigma_a)} \mathbf{d}_{j-n|k}^{(\Sigma_a)}, \quad j \in \{k-N, ..., k-1\}, \tag{5.6d}$$

$$\underline{\mathbf{x}}_r^{(\Sigma_a)} \leq \hat{\mathbf{x}}_{i|k}^{(\Sigma_a)} \leq \overline{\mathbf{x}}_r^{(\Sigma_a)}, \; i \in \{k-N, ..., k\}, \tag{5.6e}$$

$$-\boldsymbol{\gamma}_{i|k}^{(\Sigma_a)} \leq \hat{\mathbf{x}}_{i|k}^{(\Sigma_a)} - \hat{\mathbf{x}}_i^{(\Sigma_b)} \leq \boldsymbol{\gamma}_{i|k}^{(\Sigma_a)}, \; i \in \{k-N, ..., k\}, \tag{5.6f}$$

$$\forall b \mid \hat{\mathbf{x}}^{(\Sigma_a)} \cap \hat{\mathbf{x}}^{(\Sigma_b)} \neq \varnothing,$$

$$\boldsymbol{\gamma}_{i|k}^{(\Sigma_a)} \geq 0, \; i \in \{k-N, ..., k\}. \tag{5.6g}$$

$$\hat{\mathbf{x}}_{l|k}^{(\Sigma_a)} = \hat{\mathbf{x}}_l^{MHE\,(\Sigma_a)}, \; l \in \{k-N-n, ..., k-N-1\}, \tag{5.6h}$$

$$\mathbf{u}_{m|k}^{(\Sigma_a)} = \mathbf{u}_m^{MPC\,(\Sigma_a)}, \; m \in \{k-N-n, ..., k-1\}, \tag{5.6i}$$

$$\mathbf{y}_{o|k}^{(\Sigma_a)} = \mathbf{y}_o^{(\Sigma_a)}, \; o \in \{k-N, ..., k-1\}. \tag{5.6j}$$

In the case of the DMHE, Σ_b refers to all subsystems with a coupled state with Σ_a, as stated in (5.6f).

Algorithm 5.1 Integration of the DMPC and DMHE in the simulation loop

Require: $\mathbf{y}_i^{(l)}, \mathbf{u}_i^{(l)}\ \forall i \in [k-N, k-1]$ and $\forall l = \{1, 2, ..., N\}$, and all parameters in (5.5) and (5.6)

1: Define the initial states $\hat{\mathbf{x}}_k^{MHE\,(l)}$ based on the centralized solution
2: $\hat{\mathbf{x}}_k^{MHE\,(l)} \triangleq \hat{\mathbf{x}}_{k=1}^{(l)}$
3: **for** $k = 1 : t_{sim}$ **do**
4: Solve the control subproblems (5.5) using $\hat{\mathbf{x}}_k^{MHE\,(l)}$
5: **while** any difference between local solutions exceeds the threshold *or* any local solution does not converge **do**
6: Update the transmitted information as: $\mathbf{u}_i^{(l)} = \mathbf{u}_{i|k}^{(l)}$
7: Repeat step 4
8: **end while**
9: $\mathbf{u}_k^{MPC\,(l)} \triangleq \mathbf{u}_{k|k}^{(l)}$
10: Apply $\mathbf{u}_k^{MPC\,(l)}$
11: Measure $\mathbf{y}_k^{(l)}$
12: Update the sequences of data as: $\left[(\mathbf{u}_{k-N+1}^{(l)}, \mathbf{y}_{k-N+1}^{(l)}) : (\mathbf{u}_k^{MPC\,(l)}, \mathbf{y}_k^{(l)})\right]$
13: Solve the estimation subproblems (4.8) using the sequences defined in step 12
14: **while** any difference between local solutions exceeds the threshold *or* any local solution does not converge **do**
15: Update the transmitted information as: $\hat{\mathbf{x}}_i^{D\,(l)} = \hat{\mathbf{x}}_{i|k}^{D\,(l)}$
16: Repeat step 13
17: **end while**
18: $\hat{\mathbf{x}}_k^{MHE\,(l)} \triangleq \hat{\mathbf{x}}_{k+1|k+1}^{(l)}$
19: **end for**

5.3 Implementation of the DMPC and the DMHE

This section is concerned with the integration of the DMPC and the DMHE in the simulation loop, which follows the main ideas in the design of Algorithm 4.1. However, the existing differences between the centralized and the distributed implementation need to be stressed. In the centralized approach, the optimal inputs and state estimates are computed only once at every time instant k, and then the simulation moves on to $k+1$, where the same steps are performed. By contrast, the distributed problems are not solved by a unique agent, but by a set of local agents. Hence, an iterative procedure of coordination and exchange of information is implemented in Algorithm 5.1, thus being necessary to define secondary loops inside the main simulation loop. The simulation only moves on to the next time instant when the differences between the local solutions remain within the allowed bounds and the convergence of the solutions is guaranteed.

Algorithm 5.1 is initialized based on the centralized solution, which is assumed to

be available. Another alternative could be to perform the estimation of these values following the steps defined in the second *while* loop (lines 14-17). Regarding the iterative nature of the approach, note that it is only necessary to perform the *while* subroutines provided that the solution obtained in the first iteration does not comply with the design specifications in terms of convergence and accuracy of the local solutions. When all the local solutions converge from one iteration to the next one and the values of the coupled variables computed by all the agents involved are similar enough, the simulation can move on.

Finally, the attention is drawn towards lines 7 and 16, in which the control and state estimation iterations are performed, respectively. Note that the only difference between iterations lies in the information transmitted to the other agents, which is updated in order to provide the last computed values. The current states and the data sequences used by the controllers and the estimators, respectively, remain the same until the simulation moves on to the next time instant.

5.4 Simulation results for the DMPC and DMHE

The scenario described in Section 4.4 is considered to test the distributed control and state estimation approaches presented in Section 5.2. First, the partitioning of the centralized model (3.35) is carried out, analyzing several possibilities. Then, the analysis of the results obtained using the distributed approach follows guidelines similar to those presented for the centralized approaches in Section 4.4.

The computation times are reported in Fig. 5.1 for each time instant, in order to ensure a quantitative comparison with the centralized implementation, depicted in Fig. 4.2. Since several iterations are required at each time instant in order to find a solution that satisfies all local agents, the computation times are higher in the distributed case (103.87 s) than in the centralized case (22.12 s, given in Section 4.4). Note that the case study considered in this thesis might tarnish the advantages offered by the distributed approach, as the simulation results seem to indicate that a centralized approach is more advantageous than the distributed counterpart. However, a real implementation would most likely need to be carried out in a non-centralized manner, given the dimensionality of the system.

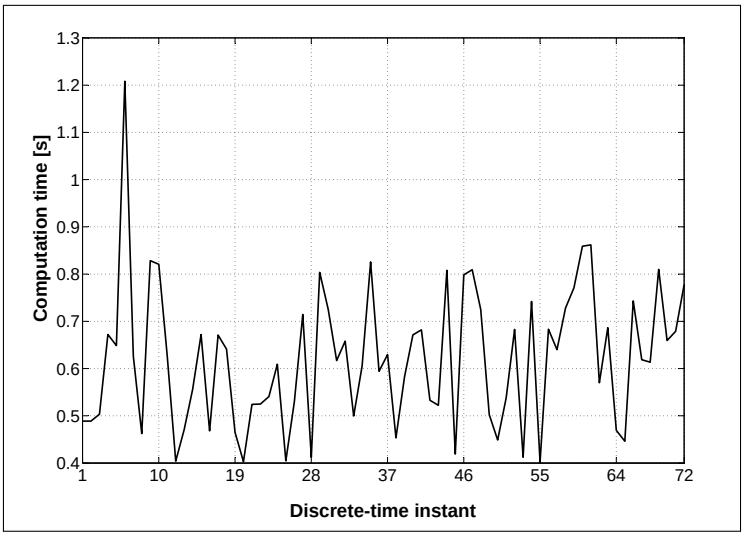

Figure 5.1: DMPC+DMHE computation time

5.4.1 Partitioning of the centralized model

The criteria introduced in (5.4) are used to build the $\tilde{\mathbf{E}}$, given below:

$$
\begin{array}{c}
\begin{array}{cccccccccc}
x^{D(1,2)} & x^{C(1,2)} & x^{D(1,3)} & x^{Don} & x^{C(4)} & x^{F} & u^{D} & u^{C} & u^{Don} & u^{F}
\end{array} \\
\left[\begin{array}{cccccc|cccc|cccccc|c}
1 & 1 & 0 & 0 & 0 & 0 & 1 & 1 & 0 & 0 & 0 & 0 & 0 & 0 & 0 & 0 & x^{1}_{(1,2)} \\
0 & 1 & 0 & 0 & 0 & 0 & 1 & 1 & 0 & 0 & 0 & 0 & 0 & 0 & 0 & 0 & x^{2}_{(1,2)} \\
0 & 0 & 1 & 1 & 0 & 0 & 1 & 0 & 1 & 0 & 0 & 0 & 0 & 0 & 0 & 0 & x^{1}_{(1,3)} \\
0 & 0 & 0 & 1 & 0 & 0 & 1 & 0 & 1 & 0 & 0 & 0 & 0 & 0 & 0 & 0 & x^{2}_{(1,3)} \\
0 & 1 & 0 & 0 & 1 & 1 & 0 & 1 & 0 & 1 & 0 & 0 & 0 & 0 & 0 & 0 & x^{1}_{(4)} \\
0 & 1 & 0 & 0 & 0 & 1 & 0 & 1 & 0 & 1 & 0 & 0 & 0 & 0 & 0 & 0 & x^{2}_{(4)} \\
\hline
0 & 0 & 0 & 0 & 0 & 0 & 0 & 0 & 0 & 0 & 0 & 0 & 0 & 0 & 0 & 0 & \\
0 & 0 & 0 & 0 & 0 & 0 & 0 & 0 & 0 & 0 & 0 & 0 & 0 & 0 & 0 & 0 & \\
0 & 0 & 0 & 0 & 0 & 0 & 0 & 0 & 0 & 0 & 0 & 0 & 0 & 0 & 0 & 0 & \\
0 & 0 & 0 & 0 & 0 & 0 & 0 & 0 & 0 & 0 & 0 & 0 & 0 & 0 & 0 & 0 & \\
\hline
1 & 1 & 0 & 0 & 0 & 0 & 1 & 1 & 0 & 0 & 0 & 0 & 0 & 0 & 0 & 0 & y^{1}_{(1,2)} \\
0 & 1 & 0 & 0 & 0 & 0 & 1 & 1 & 0 & 0 & 0 & 0 & 0 & 0 & 0 & 0 & y^{2}_{(1,2)} \\
0 & 0 & 1 & 1 & 0 & 0 & 1 & 0 & 1 & 0 & 0 & 0 & 0 & 0 & 0 & 0 & y^{1}_{(1,3)} \\
0 & 0 & 0 & 1 & 0 & 0 & 1 & 0 & 1 & 0 & 0 & 0 & 0 & 0 & 0 & 0 & y^{2}_{(1,3)} \\
0 & 1 & 0 & 0 & 1 & 1 & 0 & 1 & 0 & 1 & 0 & 0 & 0 & 0 & 0 & 0 & y^{1}_{(4)} \\
0 & 1 & 0 & 0 & 0 & 1 & 0 & 1 & 0 & 1 & 0 & 0 & 0 & 0 & 0 & 0 & y^{2}_{(4)}
\end{array}\right]
\end{array}
\tag{5.7}
$$

Note that the columns represent the variables (states and inputs), whereas the rows represent each of the state and output equations. The labeling of the rows indicates whether it corresponds to a state (x) or an output equation (y), the subscript denotes the reach numbering according to the notation introduced in Fig. 3.9 and the superscripts 1 and 2 indicate whether it corresponds to the upstream or the downstream equation, respectively.

Then, $\tilde{\mathbf{E}}$ is provided to the Cuthill-McKee algorithm, yielding

$$order = [10 \;\; 6 \;\; 15 \;\; 5 \;\; 16 \;\; 8 \;\; 2 \;\; 11 \;\; 1 \;\; 12 \;\; 7 \;\; 4 \;\; 13 \;\; 3 \;\; 14 \;\; 9], \tag{5.8}$$

and consequently $\tilde{\mathbf{E}}_{blk} = \tilde{\mathbf{E}}(order, order)$ reads as follows:

$$\begin{array}{c}
\begin{array}{cccccccccccccccc}
u^F & x^F & & x^{C(4)} & & u^C & x^{C(1,2)} & & x^{D(1,2)} & & u^D & x^{Don} & & x^{D(1,3)} & & u^{Don}
\end{array} \\
\left[\begin{array}{cccccccccccccccc}
0 & 0 & 0 & 0 & 0 & 0 & 0 & 0 & 0 & 0 & 0 & 0 & 0 & 0 & 0 & 0 \\
1 & 1 & 0 & 0 & 0 & 1 & 1 & 0 & 0 & 0 & 0 & 0 & 0 & 0 & 0 & 0 \\
1 & 1 & 0 & 1 & 0 & 1 & 1 & 0 & 0 & 0 & 0 & 0 & 0 & 0 & 0 & 0 \\
1 & 1 & 0 & 1 & 0 & 1 & 1 & 0 & 0 & 0 & 0 & 0 & 0 & 0 & 0 & 0 \\
1 & 1 & 0 & 0 & 0 & 1 & 1 & 0 & 0 & 0 & 0 & 0 & 0 & 0 & 0 & 0 \\
0 & 0 & 0 & 0 & 0 & 0 & 0 & 0 & 0 & 0 & 0 & 0 & 0 & 0 & 0 & 0 \\
0 & 0 & 0 & 0 & 0 & 1 & 1 & 0 & 0 & 0 & 1 & 0 & 0 & 0 & 0 & 0 \\
0 & 0 & 0 & 0 & 0 & 1 & 1 & 0 & 1 & 0 & 1 & 0 & 0 & 0 & 0 & 0 \\
0 & 0 & 0 & 0 & 0 & 1 & 1 & 0 & 1 & 0 & 1 & 0 & 0 & 0 & 0 & 0 \\
0 & 0 & 0 & 0 & 0 & 1 & 1 & 0 & 0 & 0 & 1 & 0 & 0 & 0 & 0 & 0 \\
0 & 0 & 0 & 0 & 0 & 0 & 0 & 0 & 0 & 0 & 0 & 0 & 0 & 0 & 0 & 0 \\
0 & 0 & 0 & 0 & 0 & 0 & 0 & 0 & 0 & 0 & 1 & 1 & 0 & 0 & 0 & 1 \\
0 & 0 & 0 & 0 & 0 & 0 & 0 & 0 & 0 & 0 & 1 & 1 & 0 & 1 & 0 & 1 \\
0 & 0 & 0 & 0 & 0 & 0 & 0 & 0 & 0 & 0 & 1 & 1 & 0 & 1 & 0 & 1 \\
0 & 0 & 0 & 0 & 0 & 0 & 0 & 0 & 0 & 0 & 1 & 1 & 0 & 0 & 0 & 1 \\
0 & 0 & 0 & 0 & 0 & 0 & 0 & 0 & 0 & 0 & 0 & 0 & 0 & 0 & 0 & 0
\end{array}\right]
\begin{array}{l}
\\
x^2_{(4)} \\
y^1_{(4)} \\
x^1_{(4)} \\
y^2_{(4)} \\
\\
x^2_{(1,2)} \\
y^1_{(1,2)} \\
x^1_{(1,2)} \\
y^2_{(1,2)} \\
\\
x^2_{(1,3)} \\
y^1_{(1,3)} \\
x^1_{(1,3)} \\
y^2_{(1,3)} \\
\\
\end{array}
\end{array} \tag{5.9}$$

The final partitioning depends on the goal that is to be achieved. The most common approach consists in identifying blocks that are minimally coupled to reduce the communication costs between subsystems. However, another possibility might be to determine blocks with similar sizes, so that the subsystems have similar dimensions. Furthermore, the partitioning needs to respect the physical nature of the system, which means that variables that belong to the same reach should be part of the same subproblem. For instance, there is little sense in considering the discharge and the water level for a given node in different subproblems.

Based on these considerations, two different partitionings can be proposed. Note that they are defined by means of two sets: the first set indicates the variables, whereas the second one indicates the model equations.

— Partitioning (a) considers three subsystems:

$$\begin{aligned}
\text{SS1}^{(a)} &= \left\{ \left\{ u^F,\ x^F,\ x^{C(4)},\ u^C,\ x^{C(1,2)} \right\},\ \left\{ x^2_{(4)},\ y^1_{(4)},\ x^1_{(4)},\ y^2_{(4)} \right\} \right\}, \\
\text{SS2}^{(a)} &= \left\{ \left\{ u^C,\ x^{C(1,2)},\ x^{D(1,2)},\ u^D \right\},\ \left\{ x^2_{(1,2)},\ y^1_{(1,2)},\ x^1_{(1,2)},\ y^2_{(1,2)} \right\} \right\}, \\
\text{SS3}^{(a)} &= \left\{ \left\{ u^D,\ x^{Don},\ x^{D(1,3)},\ u^{Don} \right\},\ \left\{ x^2_{(1,3)},\ y^1_{(1,3)},\ x^1_{(1,3)},\ y^2_{(1,3)} \right\} \right\}.
\end{aligned}$$

— Partitioning (b) considers two subsystems:

$$\begin{aligned}
\text{SS1}^{(b)} &= \Big\{ \left\{ u^F,\ x^F,\ x^{C(4)},\ u^C,\ x^{C(1,2)},\ x^{D(1,2)},\ u^D \right\}, \\
&\qquad \left\{ x^2_{(4)},\ y^1_{(4)},\ x^1_{(4)},\ y^2_{(4)},\ x^2_{(1,2)},\ y^1_{(1,2)},\ x^1_{(1,2)},\ y^2_{(1,2)} \right\} \Big\}, \\
\text{SS2}^{(b)} &= \left\{ \left\{ u^D,\ x^{Don},\ x^{D(1,3)},\ u^{Don} \right\},\ \left\{ x^2_{(1,3)},\ y^1_{(1,3)},\ x^1_{(1,3)},\ y^2_{(1,3)} \right\} \right\}.
\end{aligned}$$

Note that both partitionings respect the physical nature of the system, grouping the variables that are physically linked in the same subsystem. On the one hand, partitioning (a) yields three subsystems with almost the same size in terms of variables and model equations involved, but at the cost of more coupled variables than the second partitioning. Note that this possibility basically regards each of the three reaches as a subsystem. On the other hand, the second option proposes two subsystems, being one of them the combination of reaches (1,2) and (4). This results in a lower number of variable couplings, as u^D is the only common variable between $\text{SS1}^{(b)}$ and $\text{SS2}^{(b)}$. However, the relationship between $x^{D(1,2)}$ and $x^{D(1,3)}$ introduced in Section 4.2 forces an additional coupling between both subsystems. Indeed, $x^{D(1,2)}$ belongs to $\text{SS1}^{(b)}$, whereas $x^{D(1,3)}$ belongs to $\text{SS2}^{(b)}$, which requires to introduce also a communication protocol between the estimators.

With all this in mind, partitioning (b) is chosen over partitioning (a) in order to have minimal coupled variables, and thus minimal communication costs. The strategies presented in Section 5.2 are illustrated next by considering two DMPC and two DMHE.

5.4.2 DMHE

The comparison between the optimal estimated states given by the DMHE and the real states obtained in simulation are depicted in Fig. 5.2. The corresponding sequence

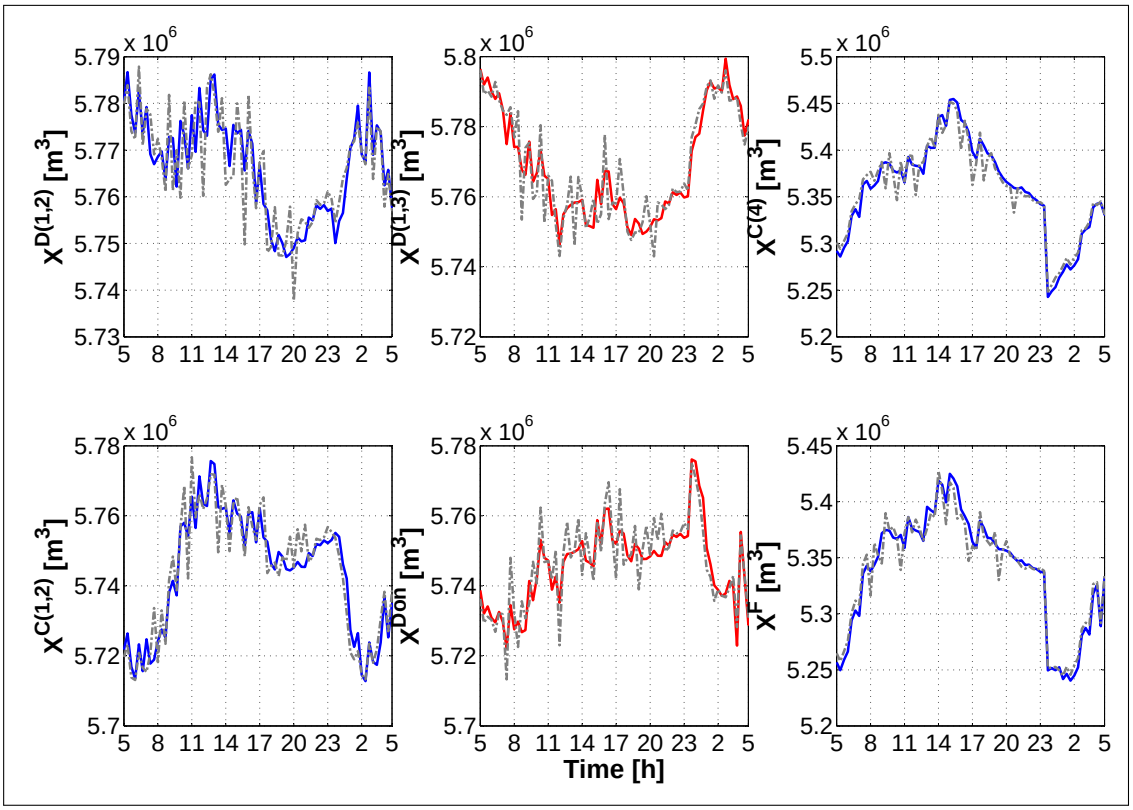

Figure 5.2: State estimates (SS1: blue solid lines; SS2: red solid lines) and computed states (dash-dot gray lines)

of N input-measurement pairs is provided to the DMHE at each time instant, which are used to estimate the optimal state sequence.

It can be observed that the state estimates provided by the DMHE match the real states with no significant error while respecting the constraints on the state bounds. Note that these are not depicted in Fig. 5.2, as the states are kept far from the bounds. On the other hand, the distributed estimation approach proves to perform well when the states $\hat{\mathbf{x}}^{D(1,2)}$ and $\hat{\mathbf{x}}^{D(1,3)}$ are compared. Indeed, constraint (5.6f) restricts the difference between these two states by penalizing its difference, defined as a decision variable, in the objective function. As in the case of the CMHE, the DMHE does not provide the exact same values for both states, although its maximum difference amounts to 1.5% (slightly larger than in the case of the CMHE), for which the relaxation parameter accounts.

The correlation coefficients given by (4.10) are computed also in the case of the

Table 5.1: Correlation coefficients for the DMHE

D (1,2)	C (1,2)	D (1,3)	Don	C (4)	F
0.8157	0.8703	0.8801	0.9113	0.9517	0.9375

Table 5.2: Correlation coefficients differences (CMHE vs DMHE)

D (1,2)	C (1,2)	D (1,3)	Don	C (4)	F
0.0232	0.0153	0.0040	0.0163	0.0137	0.0028

DMHE, aiming at measuring not only the similarity of the real and the estimated states, but also at providing additional quantitative information that allows to compare the performance of the CMHE and DMHE. These values are summarized in Table 5.1. The performance of the DMHE can also be deemed satisfactory, since all the correlation coefficients are very close to 1. The differences between the centralized and the distributed correlation coefficients, obtained by subtracting the values in Table 5.1 from those in Table 4.2, are given in Table 5.2. The positive differences indicate a slightly superior performance of the centralized approach over the distributed approach.

5.4.3 DMPC

The water levels and the control signals obtained using the DMPC are presented and analyzed in Figs. 5.3 and 5.4, respectively. It can be stated that the DMPC succeeds at keeping the water levels close to the setpoints by rejecting the disturbances reported in Fig. 4.1. The tracking indices defined in (4.11) are used again to quantify the performance of the DMPC, and are summarized in Table 5.3. These indices are bounded between 0 and 1, where 1 corresponds to the perfect tracking performance.

Again, the centralized and the distributed approaches are compared by computing the differences in terms of tracking performances, summarized in Table 5.4. In the light of the results, the DMPC provides satisfactory results, although it is slightly outperformed by the CMPC.

On the other hand, the control signals computed by the DMPC are depicted in Fig.

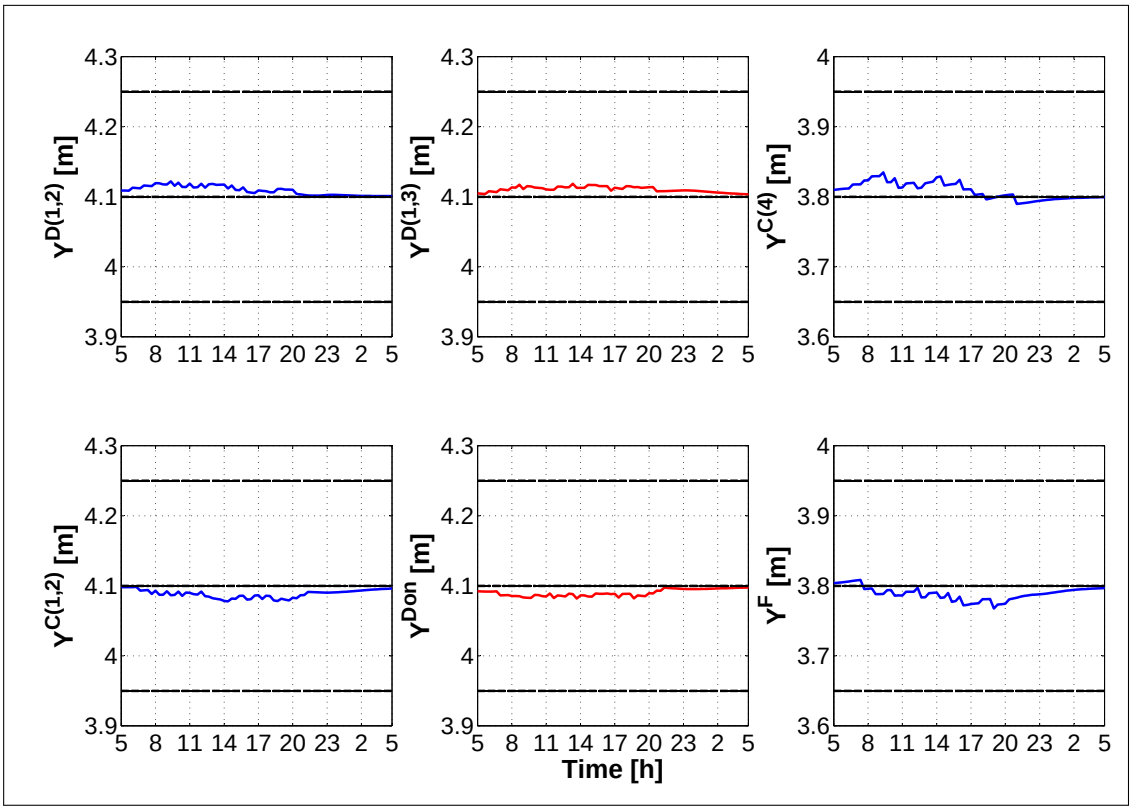

Figure 5.3: Water levels (SS1: blue solid lines; SS2: red solid lines) and LNL, NNL and HNL (black dashed lines)

Table 5.3: Tracking performances for the DMPC

D (1,2)	C (1,2)	D (1,3)	Don	C (4)	F
0.9656	0.9622	0.9672	0.9666	0.9597	0.9705

Table 5.4: Tracking performance differences (CMPC vs DMPC)

D (1,2)	C (1,2)	D (1,3)	Don	C (4)	F
0.0274	0.0255	0.0232	0.0241	0.0096	0.0012

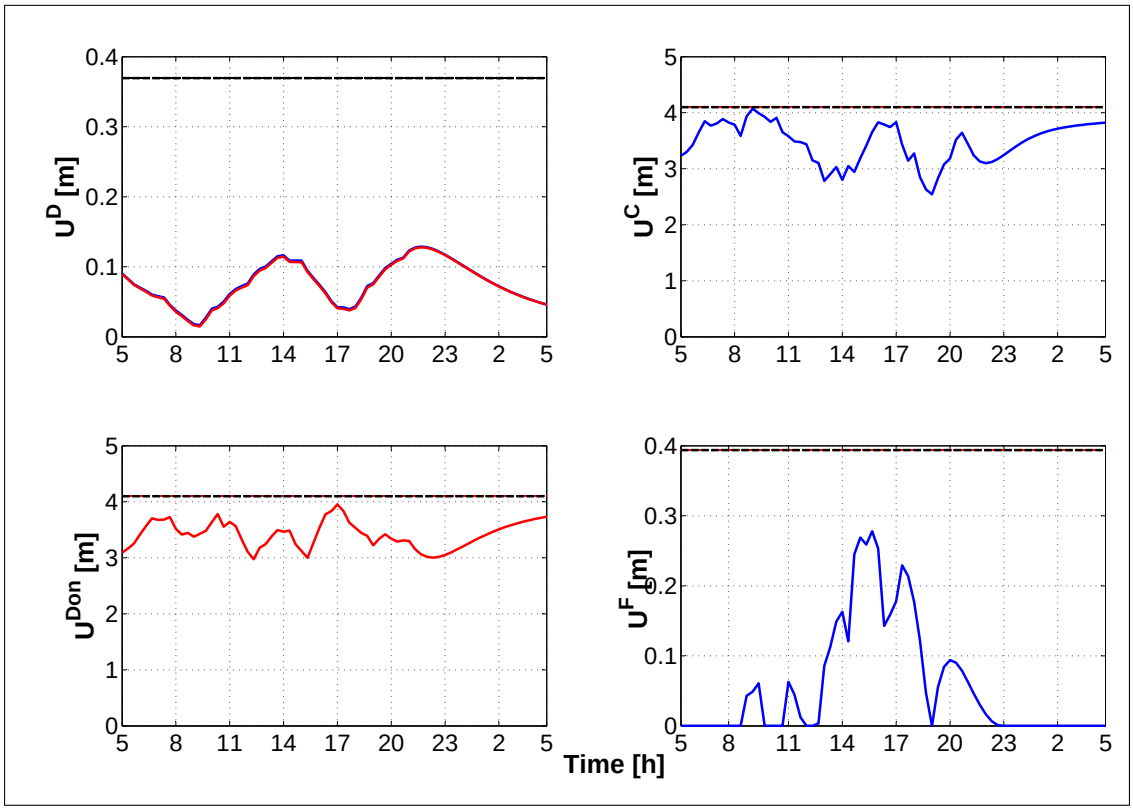

Figure 5.4: Gate openings and sill elevations (SS1: blue solid lines; SS2: red solid lines) and physical limits (black dash-dot lines)

5.4. Note that the coupled input is depicted for both subsystems in the top left-hand subplot of Fig. 5.3. It can be concluded that the communication-based DMPC is able to provide solutions that match with no significant error, as the solutions computed for $\mathbf{u}^D$ by both subsystems are almost identical. Furthermore, the DMPC computes a set of control actions that are far from the operational limits during most of the simulation. It can also be realized that, while the CMPC signals span the whole design range of the actuators, the DMPC signals are bounded in a much narrower interval. Nevertheless, it is not easy to assess which of the two approaches provides a smoother solution.

An analysis similar to the one in Section 4.4.2 can be conducted for the DMPC, which regulates the openings and elevations so that there is the optimal amount of water in each reach. Hence, when the gates in Douai and Fontinettes are closed (no flow), the weirs in Don and Cuinchy are lifted to the maximal height (no flow), and *vice versa*.

Again, the effect of the transport delays should be taken into account in the analysis of the results.

5.5 Summary

The centralized control and state estimation approaches designed in Chapter 4 constitute the starting point of Chapter 5. The main limitations of such implementation are discussed, concluding that it is often advantageous to explore non-centralized alternatives when dealing with large-scale systems. Such strategies are often based in partitioning the overall system in a set of subsystems, each of them governed by a local agent. The proposed approach performs this decomposition by identifying subsystems that minimize the interactions (the number of coupled variables) among them. The aim is to minimize the communication among subsystems without ignoring the interactions, since those strategies that take interactions into account often yield better performances than those that ignore them. Once the subsystems have been identified, DMPC and DMHE are designed based on the centralized counterparts, including a communication protocol that accounts for the interactions. The same case study is used to assess the performance of the distributed strategy with respect to the centralized approach, which allows to validate the obtained results.

Chapter 6

Fault diagnosis

Centralized and distributed control and state estimation approaches have been proposed in Chapters 4 and 5, respectively, in order to accommodate the navigation in inland waterways. As stated before, the main objective consists in maintaining the water levels within the LNL and the HNL, and as close as possible to the NNL, so that the vessels can travel safely. However, the use of these strategies requires the acquisition of reliable data. Furthermore, the control actions can only be applied correctly if the actuators are not impacted by faults. Indeed, any error caused by a water level sensor or an actuator can lead to an inefficient management of the system.

Chapter 6 is concerned with the design of supervisory strategies that allow to detect and isolate faults in inland waterways. More specifically, two diagnosis approaches are designed in order to assess the occurrence of faults. Given the fact that a substantial modeling effort has been made in Chapter 3, it seems natural to use the derived model structure for the purpose of fault diagnosis. However, while the first strategy directly computes the parameters based on the procedure described in [LF09], the second only assumes its structure and estimates the model parameters using available data. This difference in terms of obtaining the model parameters leads to referring to the former strategy as a model-based approach, whereas the latter is referred to as a data-based approach.

In order to compare both strategies, real data is required to estimate a model for the data-based approach. Given the limitations in terms of available data mentioned in Section 3.5, both approaches are tested on the CFr, depicted in Fig. 3.11, in order to be comparable.

The present chapter is structured as follows: Section 6.1 presents the model-based approach, which is based on the comparison of the faultless system dynamics with the measured inputs and outputs, which are obtained using SIC^2. The presence of a fault can be proved when the water levels predicted by the model of the faultless system are not consistent with the measurements provided by SIC^2. These contributions have been published in [SRD+17, SBH+18]. On the other hand, Section 6.2 describes the data-based approach. Contrary to the first approach, the proposed strategy consists in monitoring the evolution of the grey-box model coefficients. Indeed, it is shown how faults can be correctly detected and isolated when a coefficient crosses one of the bounds of the interval depicted in Fig. 3.12. This approach is designed to diagnose intermittent faults, thus extending the results in [DRBC13], whose strategy was well suited to detect abrupt and incipient faults. The contributions regarding the data-based fault diagnosis approach have been collected in [SBD+18a, SBD+18b].

6.1 The model-based approach

6.1.1 Fault detection

Fault detection is based on checking the consistency between the measured inputs and outputs and the behavior described by a model of the faultless system. The presence of a fault is detected when the model of the faultless system is not consistent with the available measurements. The model of the system should describe the behavior of the system in any non-faulty scenario, and also in faulty scenarios where the fault can be modeled by a change of model parameters or variables.

In the case of the use of qualitative models, i.e., mathematical models that can be described in time or frequency domain, fault diagnosis is usually based on the evaluation of a residual (or analytical redundancy) $r(k)$[Ger98, BKLS06, Ise06], which is computed as the difference between the real observed behavior of a system $y(k)$ provided by sensors and the value $\hat{y}(k)$ predicted by the model as

$$r(k) = y(k) - \hat{y}(k). \tag{6.1}$$

In an ideal case, residuals should only be different from zero when the system is affected by a fault. However, due to modeling errors, sensor noises and disturbances,

the residuals can be different from zero in non-faulty scenarios. Therefore, residual-based fault detection methods should be robust in order to avoid false alarms.

A passive robust fault detection method can be implemented by computing the maximum positive and negative deviations (bounds $\overline{\sigma}$ and $\underline{\sigma}$) of the residual $r(k)$ in the time domain from zero in a non-faulty scenario. Therefore, the values of the bounds are directly linked to the accuracy of the model. The fault detection test can be formulated as:

$$\phi(k) = \begin{cases} 0 \text{ if } r(k) \in [\underline{\sigma}, \overline{\sigma}] \Rightarrow \text{ no fault,} \\ 1 \text{ otherwise.} \end{cases} \tag{6.2}$$

The main drawback of the fault detection test defined by (6.2) is that some faults whose effect in the residual is not large enough to reach the threshold are not detected (undetected faults). This means that a minimum fault magnitude is necessary to guarantee its detection. This minimum detectable fault ensures that the residual reaches its threshold (*triggering limit*) despite model uncertainties [Ger98].

6.1.2 Fault isolation

Fault isolation usually requires the evaluation of a set of residuals $r_1, \ldots, r_{n_r}$, which derives a set of fault signals $\phi_1, \ldots, \phi_{n_r}$ computed, for instance, by means of (6.2). The proposed strategy follows the ideas in [MPE10, PB13] and is depicted in Fig. 6.1.

First, a memory component updates cyclically the fault occurrence signal provided by the fault detection algorithm. When a fault is detected, the information of the different fault signals are stored in a table. This information consists in the first activation instant k_o of the fault signal, the activation instant k_i of the other signals that are activated in the time window $k \in [k_o,\ k_o + k_w]$, where k_w is a prefixed waiting time, and the maximum activation value $\phi_{i,\max}$ for every fault signal ϕ_i in this time window $(i = 1, ..., n_r)$, which is computed as

$$\phi_{i,\max}(k) = \max_{l \in [k_o, k]} |\phi_i(l)|, \tag{6.3}$$

with $k \leq k_o + k_w$, and where k_w must be chosen as the largest transient time response k_{lt}

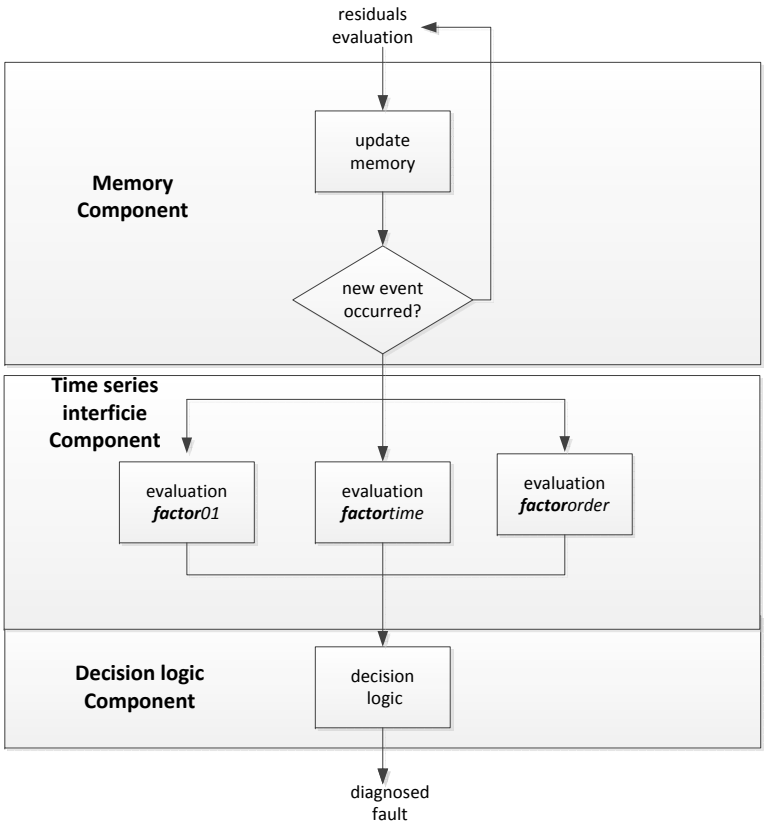

Figure 6.1: Fault isolation components (taken from [MPE10])

from a fault-free scenario to any faulty scenario. The advantage of using maximum activation values $\phi_{i,\max}(k)$ computed by (6.3) instead of temporal fault signals $\phi_i(k)$ is that the undesirable effect of non-persistent fault indicators, sensor noises and disturbances is minimized.

Once a new event has been detected in the memory component, different time-series analysis are carried out to compare the observed fault behavior with the different considered fault patterns. In the fault isolation module depicted in Fig. 6.1, three different analysis are considered. One is the standard static Boolean analysis, denoted as $\boldsymbol{factor}01(k)$, where the Boolean fault signal activation matrix $\mathbf{FSM}01$ that contains information about the incidence or no incidence of faults (columns) on residuals (rows) is used to determine which is the most probable fault. The probability of a fault is determined by the match between the columns of the $\mathbf{FSM}01$ matrix and a vector

whose components are $\phi_{i,\max}$ $i = 1, ..., n_r$. $\boldsymbol{factor}01_j$ is calculated for all the fault hypotheses $j = 1, ..., n_f$ in the following manner:

$$\boldsymbol{factor}01_j(k) = \frac{\sum_{i=1}^{n_r} \phi_{i,\max}(k)\ \mathbf{FSM}01_{ij}}{\sum_{i=1}^{n_r} \mathbf{FSM}01_{ij}} \boldsymbol{zvf}_j(k), \tag{6.4}$$

where $\boldsymbol{zvf}_j$ is a zero-violation-factor defined as

$$\boldsymbol{zvf}_j(k) = \begin{cases} 0 & \text{if } \exists i \in \{1, ..., n_r\}, \text{with } \mathbf{FSM}01_{\mathrm{ij}} = 0 \\ & \qquad \text{and } \phi_{\mathrm{i,max}}(\mathrm{k}) = 1, \\ 1 & \text{otherwise.} \end{cases} \tag{6.5}$$

The fault signal occurrence order analysis, denoted as $\boldsymbol{factor}order$, compares the order of activation of the different fault signals with the expected order for all the considered faults stored in $\mathbf{FSM}order$. $\boldsymbol{factor}order_j$ is calculated for all the fault hypotheses $j = 1, ..., n_f$ as follows:

$$\boldsymbol{factor}order_j(k) = \frac{\sum_{i=1}^{n_r} \left(order\left(\phi_{i,\max}(t), \mathbf{FSM}order_{ij}\right)\right)}{\sum_{i=1}^{n_r} boolean(\mathbf{FSM}order_{ij})} \boldsymbol{zvf}order_j(k), \tag{6.6}$$

where

$$order(\phi_{i,\max}(k), \mathbf{FSM}order_{ij}) = \begin{cases} 0 & \text{if } order(\phi_{i,\max}(k)) \neq \mathbf{FSM}order_{ij}, \\ 1 & \text{if } order(\phi_{i,\max}(k)) = \mathbf{FSM}order_{ij}, \end{cases} \tag{6.7}$$

and $\boldsymbol{zvf}order_j(k)$ is defined as $\boldsymbol{zvf}_j(k)$ in (6.5), but excluding those fault hypotheses that do not coincide in the order.

The time occurrence analysis, denoted as $\boldsymbol{factor}time$, checks the consistency of the delay between the different fault activation signals and the time of the first fault signal activation time t_o and the expected one stored in the matrix $\mathbf{FSM}time$, whose components are computed as follows:

$$\mathbf{FSM}time_{ij} = \begin{cases} [\underline{\kappa}_{ij}, \bar{\kappa}_{ij}] & \text{if } \mathbf{FSM}_{ij} = 1, \\ [-1, -1] & \text{if } \mathbf{FSM}_{ij} = 0, \end{cases} \tag{6.8}$$

where $[\underline{\kappa}_{ij}, \bar{\kappa}_{ij}]$ is the time interval in which the fault signal ϕ_i caused by fault f_j is expected to appear. $\boldsymbol{factor}time_j$ is calculated for all the fault hypotheses $j = 1, ..., n_f$ in the following manner:

$$\boldsymbol{factor}time_j(k) = \frac{\sum_{i=1}^{nr} \left(checktime\left(k_{\phi i}, k_{ref}, \mathbf{FSM}time_{ij}\right)\right)}{\sum_{i=1}^{nr} boolean(\mathbf{FSM}time_{ij})} \boldsymbol{zvf}order_j(k), \tag{6.9}$$

where k_{ϕ_i} is the apparition time instant of the fault signal $\phi_i(k)$, k_{ref} is the apparition time instant of the first observed fault signal, $checktime\left(k_{\phi_i}, k_{ref}, \mathbf{FSM}time_{ij}\right)$ is defined as

$$checktime\left(k_{\phi_i}, k_{ref}, \mathbf{FSM}time_{ij}\right) = \begin{cases} 0 & \text{if } (k_{\phi_i} - k_{ref}) \notin \mathbf{FSM}time_{ij}, \\ 1 & \text{if } (k_{\phi_i} - k_{ref}) \in \mathbf{FSM}time_{ij}, \end{cases} \tag{6.10}$$

and $boolean(\mathbf{FSM}time_{ij})$ is defined as

$$boolean(\mathbf{FSM}time_{ij}) = \begin{cases} 0 & \text{if } \mathbf{FSM}time_{ij} = [-1, -1], \\ 1 & \text{if } \mathbf{FSM}time_{ij} \neq [-1, -1], \end{cases} \tag{6.11}$$

where [-1,-1] denotes no influence of a fault in a residual [PB13].

Finally, the most probable fault among all the possible candidates is selected by means of a decision logic block, considering the result of the different time-series analysis. A $\boldsymbol{factor}total_j$ is calculated for all the fault hypotheses $j = 1, ..., n_f$ as follows:

$$\boldsymbol{factor}total_j(k) = \boldsymbol{factor}01_j(k) + \boldsymbol{factor}order_j(k) + \boldsymbol{factor}time_j(k). \tag{6.12}$$

Then, the most probable fault can be computed as

$$\hat{f}(k) = \underset{\forall j=1,...,n_f}{\arg\max}\ \boldsymbol{factor}total_j(k). \tag{6.13}$$

The isolation decision must be made in a time not greater than the waiting time k_w, i.e., $k \leq k_o + k_w$, which can be computed as

$$k_w = \max_{\forall i,j}(\overline{\kappa}_{ij}). \tag{6.14}$$

During this period of time, a likelihood index $P_j(k)$ for every fault hypothesis $j = 1, ..., n_f$ can be defined as follows:

$$P_j(k) = \frac{\boldsymbol{factor}total_j(k)}{\sum_{i=1}^{n_f} \boldsymbol{factor}total_i(k)}. \tag{6.15}$$

6.1.3 Model-based fault diagnosis in the CFr

The model-based fault diagnosis approach is applied to the CFr to compare its performance to the data-based approach, which can only be applied to the CFr due to the limitation in terms of data availability. Recall that the water level and discharge in Aire do not appear in model (3.33), and thus faults in Aire are not considered in the model-based approach. Thus, two different residuals $r_C(k)$ and $r_F(k)$ are generated from the difference between the available level measurements in Cuinchy and Fontinettes, $y^C(k)$ and $y^F(k)$, and the level estimations, $\hat{y}^C(k)$ and $\hat{y}^F(k)$. Furthermore, $q^C(k)$ and $q^F(k)$ are the total flows in Cuinchy and Fontinettes, respectively, which are computed as the sum of the flows through the hydraulic equipment. As stated in Section 4.4, Cuinchy is equipped with a controlled weir with the known input $u^C(k)$ and a lock with a known operation profile $q^C_{lock}(k)$. On the other hand, Fontinettes is equipped with a controlled gate with the known input $u^F(k)$ and a lock with a known operation profile $q^F_{lock}(k)$.

The possible faults that can impact the CFr are sensor and actuator faults in both Cuinchy and Fontinettes sensors. The effects of the considered faults in the different variables involved in the two residual computations are:

$$y^C(k) = y^C_0(k) + f_{y^C}(k), \tag{6.16a}$$
$$y^F(k) = y^F_0(k) + f_{y^F}(k), \tag{6.16b}$$
$$q^C(k) = q^C_{lock}(k) + u^C(k) = q^C_{lock}(k) + u^C_0(k) + f_{u^C}(k), \tag{6.16c}$$
$$q^F(k) = q^F_{lock}(k) + u^C(k) = q^F_{lock}(k) + u^F_0(k) + f_{u^F}(k), \tag{6.16d}$$

	f_{y^C}	f_{y^F}	f_{u^C}	f_{u^F}
r_C	1	0	1	1
r_F	0	1	1	1

Table 6.1: **FSM**01 matrix for the CFr

	f_{y^C}	f_{y^F}	f_{u^C}	f_{u^F}
r_C	1	0	1	2
r_F	0	1	2	1

Table 6.2: **FSM***order* matrix for the CFr

	f_{y^C}	f_{y^F}	f_{u^C}	f_{u^F}
r_C	0	[-1,-1]	0	$[\underline{\kappa}_{1,4}, \overline{\kappa}_{1,4}]$
r_F	[-1,-1]	0	$[\underline{\kappa}_{2,3}, \overline{\kappa}_{2,3}]$	0

Table 6.3: **FSM***time* matrix for the CFr

where y_0^C, y_0^F, u_0^C and u_0^F denote faultless levels and controls, whereas f_{y^C}, f_{u^C}, f_{y^F} and f_{u^F} denote sensor and actuator faults.

Then, considering the effect of the three faults in the two residuals, matrices **FSM**01 (Table 6.1), **FSM***order* (Table 6.2) and **FSM***time* (Table 6.3) can be obtained. The sensor faults f_{y^C} and f_{y^F} only affect the associated level residual. Thus, the **FSM**order matrix does not provide any additional information to the **FSM**01 matrix, and neither does the **FSM***time* matrix. On the other hand, f_{u^C} affects the two level residuals, first r_C and later r_F . The time values $\underline{\kappa}_{2,3}$ and $\overline{\kappa}_{2,3}$ denote the minimum and maximum delays from the activation of the fault signal in r_C to the activation of r_F in the presence of an actuator fault in Cuinchy given by f_{u^C}, and are around the delay of the transfer function $p_{12}(s)$ as in (3.2). Note that $\kappa_{2,3}$ links the second residual (r_F) with the third fault candidate (f_{u^C}). Therefore, when the fault signal associated to the Cuinchy level residual is activated, a waiting time $k_w = \overline{\kappa}_{2,3}$ has to be considered in (6.3) to distinguish between a fault in the Cuinchy level sensor (f_{y^C}) and an actuator fault in the Cuinchy control gate (f_{u^C}). An equivalent analysis is valid for the other actuator fault, i.e., f_{u^F}.

	Directly		Applying $\Delta\tau$	
	$\underline{\sigma}$	$\overline{\sigma}$	$\underline{\sigma}$	$\overline{\sigma}$
$r_C\ [m]$	-0.062	0.052	-0.05	0.042
$r_F\ [m]$	-0.096	0.096	-0.032	0.013

Table 6.4: Residual thresholds

6.1.4 Simulation results for the model-based approach

The IDZ model (3.2) that allows to derive the equivalent state-space representation in Section 3.5 is used to diagnose sensor and actuator faults. On the other hand, in order to cope with errors due to uncertainty in transport delays that are present in open-flow canal systems, the residual has been computed following the ideas in [BPB10] as

$$r(k) = y(k) - \hat{y}(k - \Delta\kappa^0), \tag{6.17}$$

where

$$\Delta\kappa^0 = \arg \min_{\Delta\kappa \in [-\lambda_\kappa, \lambda_\kappa]} |y(k) - \hat{y}(k - \Delta\kappa)|, \tag{6.18}$$

with λ_κ the maximum deviation from the nominal time delay.

Uncertainties in time delays lead to important instantaneous errors in level estimations. Figure 6.2 shows the evolution of residuals computed directly with (6.1) and applying (6.17) in a realistic scenario. Maximum and minimum residual values in fault-free scenarios have been chosen as residual bounds $\underline{\sigma}$ and $\overline{\sigma}$ used in the fault detection procedure (6.2). The residual bounds for the two residuals computed directly and applying (6.17) are summarized in Table 6.4.

Two realistic scenarios where faults can impact the system have been generated to study the performance of the proposed fault diagnosis method considering Tables 6.1, 6.2 and 6.3, with $\underline{\tau}_{2,3} = \underline{\tau}_{1,4} = 5900\ s$ and $\overline{\tau}_{2,3} = \overline{\tau}_{1,4} = 7900\ s$. Note that these delays must be converted to samples in order to implement the presented approach. However, the simulation results are given in minutes as their interpretation is more natural.

Furthermore, and although there are four possible faulty scenarios (a sensor and an actuator fault at each end of the reach), only one sensor and one actuator fault scenarios are included, as the analysis for the two remaining situations are analogous.

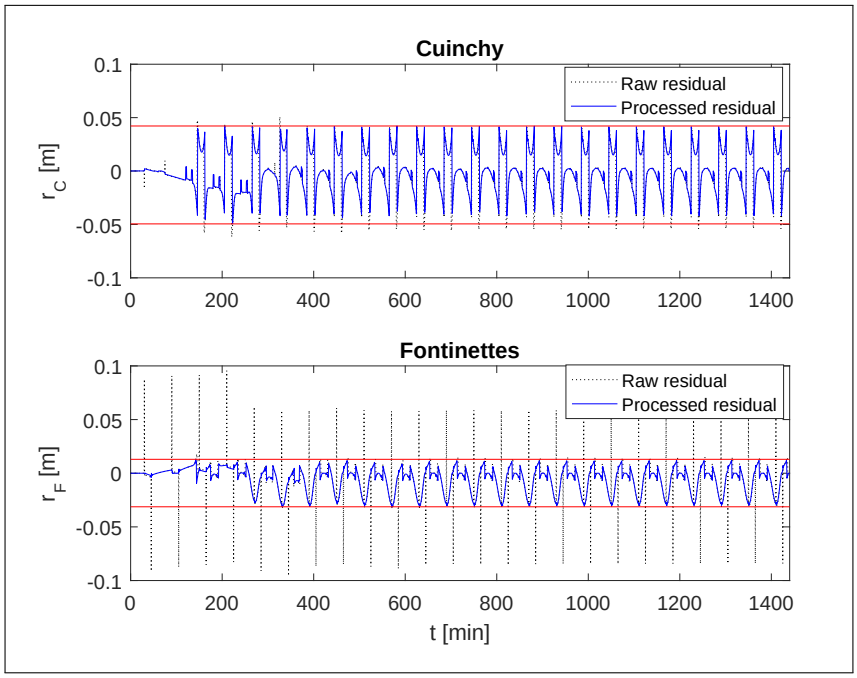

Figure 6.2: Level residuals $r_C(k)$ and $r_F(k)$ in a 24-hour fault-free scenario.

Finally, and with the purpose of avoiding that uncertainty and modeling errors compensate the fault effects, when a fault is detected using (6.2), the residual is computed using (6.17) by considering $\Delta\kappa^0$ computed with (6.18), but changing *min* by *max*. In the following, the results of these faulty scenarios are explained in detail.

Sensor fault in Fontinettes

An additive fault of 6 *cm* is simulated at the Fontinettes level sensor at $t \geq 500$ *min*, which emulates a fall of 6 *cm* of an ultrasonic sensor from its support arm. Figure 6.3 shows the evolution of the two residuals: r_F is activated when the fault is produced (at $t = 500$ *min*). Then, applying (6.12) and considering Tables 6.1, 6.2 and 6.3, the Cuinchy sensor and actuator fault hypotheses ($j = 1$ and $j = 3$, respectively) provide a $\boldsymbol{factor}total_j$ equal to zero, $j = \{1, 3\}$. On the other hand, the Fontinettes sensor and actuator fault hypotheses ($j = 2$ and $j = 4$, respectively) provide $\boldsymbol{factor}total_2 = 3$ and $\boldsymbol{factor}total_4 = 1.5$, respectively. Therefore, the most probable hypothesis is a sensor fault in Cuinchy, with a likelihood index (6.15) of $P_2 = 0.67$, whereas the likelihood of

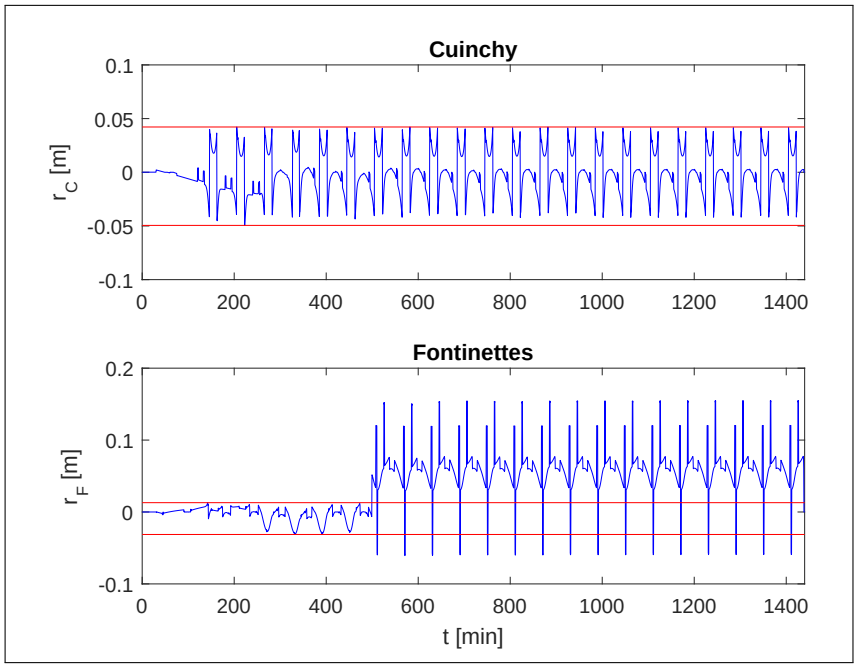

Figure 6.3: Level residuals r_C and r_F for a sensor fault scenario in Fontinettes, with $f_{y^F} = 6\ cm$ at $t \geq 500\ min$

an actuator fault in Cuinchy is equal to $P_4 = 0.33$. This hypothesis is confirmed after the waiting time $T_w = 7900\ s$, with no more activated signals, and thus $P_2 = 1$ and $P_4 = 0$, which allows to isolate the sensor fault correctly.

Actuator fault in Cuinchy

An additive fault of $-4\ m^3/s$ is simulated at the Cuinchy control weir at $t \geq 300$ min, which emulates a partial obstruction. Figures 6.4 and 6.5 show the residuals and the evolution of the fault signals, respectively. The first fault signal ϕ_C is activated at $t = 342\ min$, 42 min after the gate is partially blocked. Later, at $t = 442\ min$, the fault signal ϕ_F is activated. Then, during 100 min, from $t = 342\ min$ to $t = 442$ min, there are two fault candidates, according to Tables 6.1, 6.2 and 6.3: f_{y^C} and f_{u^C}, with $\boldsymbol{factor}total_1 = 1.5$ and $\boldsymbol{factor}total_3 = 3$ and likelihood indices $P_1 = 0.67$ and $P_3 = 0.33$, respectively. However, after the activation of ϕ_F, only f_{u^C} is consistent with the observed fault signals, with $\boldsymbol{factor}total_3$ different from zero. The fault diagnosis strategy does work despite the intermittent activation of the fault signals, thanks to the

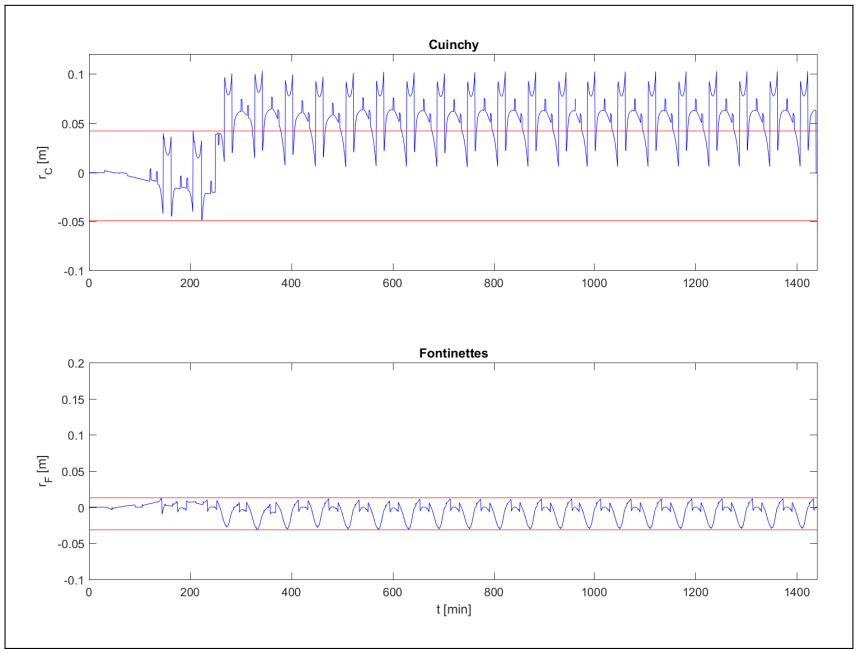

Figure 6.4: Level residuals r_C and r_F for an actuator fault scenario in Cuinchy, with $f_{uC} = -4\ m^3/s$ at $t \geq 300\ min$

memory component (6.3) and Table 6.3.

6.2 The data-based approach

As discussed before, the IDZ model used in the previous section is a simplified model, thus not taking into account real features of the system, e.g., different cross section profiles, variable time delays, uncertainties and unknown inflows and outflows. A possible alternative consists in using models computed from real data, such as the one proposed in Section 3.4. These models are particularly well suited to diagnose intermittent faults, as these faults modify the dynamics of the estimated system, thus leading to their detection and isolation. This section presents a methodology that aims at diagnosing faults using a model whose parameters are estimated using real data.

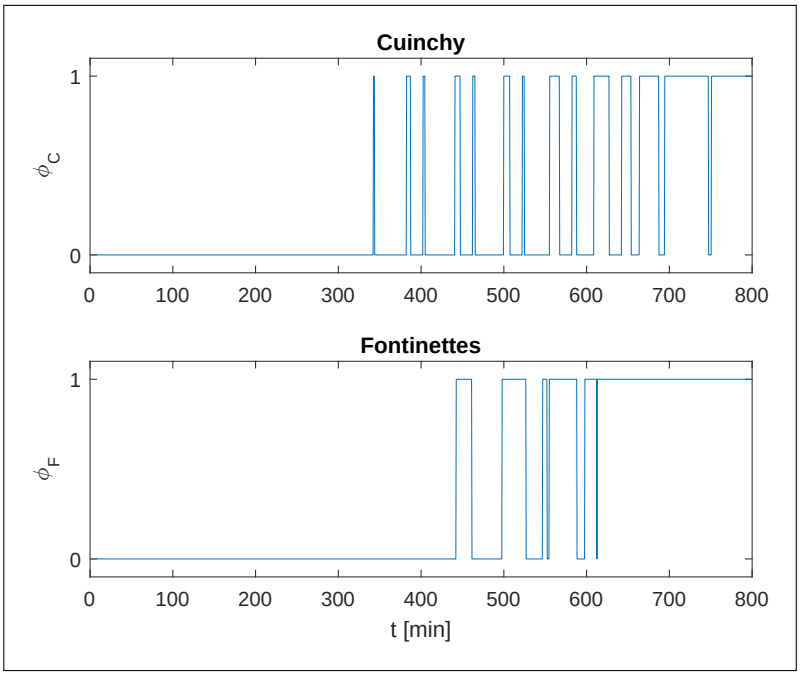

Figure 6.5: Instantaneous activation signals ϕ_C and ϕ_F for an actuator fault scenario in Cuinchy

6.2.1 Fault detection and isolation

The data-based diagnosis approach focuses on sensor level faults:

$$L_k^{(i)} = L_k^{(i,0)} + \Delta_k^{(i)}, \quad \forall i = 1, ..., l \tag{6.19}$$

where $L_k^{(i,0)}$ denotes the i-th level and $\Delta_k^{(i)}$ the fault at time k.

As model (3.27) provides the level estimations $\hat{\mathbf{y}}_{k+1}$, the most straightforward fault detection method consists in evaluating the difference between the level sensor measurements and the estimations:

$$r_k^{(i)} = y_k^{(i)} - \hat{y}_k^{(i)}, \quad \forall i = 1, ..., l, \tag{6.20}$$

where $r_k^{(i)}$ is the temporal residual of the i-th level sensor. The fault detection test can

be formulated as follows:

$$\phi_k^{r^{(i)}} = \begin{cases} 0 \text{ if } r_k^{(i)} \in [\underline{\sigma}^{(i)}, \overline{\sigma}^{(i)}] \Rightarrow \text{ no fault,} \\ 1 \text{ otherwise,} \end{cases} \tag{6.21}$$

where bounds $\underline{\sigma}^{(i)}$ and $\overline{\sigma}^{(i)}$ are the maximum positive and negative deviations of the residual $r_k^{(i)}$ in a fault-free scenario, respectively.

Another possibility consists in considering the evolution of the grey-box parameters. To do so, the determination of $\mathbf{M}^{(i)}$ given in (3.30) is performed by considering a time window of size N_w. Hence, a temporal matrix $\mathbf{M}_k^i$ is computed at every instant k:

$$\mathbf{M}_k^{(i)} = \mathbf{Y}_k^{(i)} \left(\overline{\mathbf{\Phi}}_k^{(i)}\right)^\intercal \left(\overline{\mathbf{\Phi}}_k^{(i)} \left(\overline{\mathbf{\Phi}}_k^{(i)}\right)^\intercal\right)^{-1}, \tag{6.22}$$

with $\mathbf{Y}_k^{(i)} = [y_{k+\chi+1-N_w}^{(i)} \cdots y_k^{(i)}]$ and $\overline{\mathbf{\Phi}}_k^{(i)} = [\mathbf{\Phi}_{k+\chi-N_w}^{(i)} \cdots \mathbf{\Phi}_{k-1}^{(i)}]$.

The parameters $a_k^{(j,i)}$ and $b_k^{(j,i)}$ $\forall i, j = 1, ..., l$ are obtained from $\mathbf{M}_k^{(i)} = \left[\tilde{\mathbf{A}}_k^{(i)} \ \tilde{\mathbf{B}}_k^i\right]$. The next step consists in comparing these parameters with their bounds $\left[\underline{a}^{(j,i)}, \overline{a}^{(j,i)}\right]$ and $\left[\underline{b}^{(j,i)}, \overline{b}^{(j,i)}\right]$ obtained in a fault-free scenario which is representative enough and validated by means of the fitting indicators (3.31) and (3.32). Finally, the parameter fault signals $\phi_k^{a^{(j,i)}}$ and $\phi_k^{b^{(j,i)}}$ can be generated in a similar way as $\phi_{r_k^{(i)}}$ in (6.21):

$$\phi_k^{a^{(j,i)}} = \begin{cases} 0 \text{ if } a_k^{(j,i)} \in [\underline{a}^{(j,i)}, \overline{a}^{(j,i)}] \Rightarrow \text{ no fault,} \\ 1 \text{ otherwise.} \end{cases} \tag{6.23}$$

$\phi_k^{b^{(j,i)}}$ is computed as $\phi_k^{a^{(j,i)}}$ but considering the parameter estimations $b_k^{(j,i)}$ and the bounds $\left[\underline{b}^{(j,i)}, \overline{b}^{(j,i)}\right]$ in (6.23). The main drawback of the fault detection test defined in (6.23) is that a non-persistent excitation in the inputs when applying (6.22) can lead to false alarms due to parameter estimation errors. To overcome this issue, the parameter fault signals $\phi_k^{a^{(j,i)}}$ and $\phi_k^{b^{(j,i)}}$ should be computed only when the input persistent exciting order is enough to guarantee an accurate parameter estimation [Lju99].

A fault is detected when at least one fault signal $\phi_k^{r^{(i)}}$, $\phi_k^{a^{(j,i)}}$ or $\phi_k^{b^{(j,i)}}$ is activated, i.e., its value equals 1. Once the fault is detected, it should be isolated with the information of the different fault signals. The main problem of isolating level faults defined in (6.19) considering model (B.14) is that, since every level is present in all level estimations, every

Table 6.5: Considered faults

Fault	Mag. [*cm*]	Occurrence (dd:hh:mm)	Duration [*min*]
f_1	-8	01:16:44	200
f_2	1.5	03:07:04	540
f_3	5	00:01:24	300

level fault potentially affects all the fault signals (residual fault signals and parameter fault signals). This means that it is not possible to isolate faults by means of the standard Boolean fault signature matrix [Ger98]. However, as the effect of a level fault in the limnimeter $L^{(i)}$ $\left(\Delta_k^{(i)}\right)$ in the estimation of the level in the limnimeter $L^{(j)}$ $\left(\hat{y}_k^{(j)}\right)$ is delayed, $\boldsymbol{\kappa}$ can be used to isolate faults considering the fault signature occurrence and delay as proposed in [PB13]. For instance, when a fault $\Delta_k^{(i)}$ occurs, the temporal residual fault signal $\phi_k^{r^{(i)}}$ and the parametric fault signals $\phi_k^{a^{(j,i)}}$ and $\phi_k^{b^{(j,i)}}$ $\forall i = 1, \cdots, l$ should be activated in the first place. In the case of parametric fault signals, the effect of the fault $\Delta_k^{(i)}$ is more direct in the estimation of parameter $a_k^{(i,i)}$. Due to the use of a time window of length N_w, an extra delay between the fault appearance and the effect in the fault signals can be present. Next, the effect of the fault will be propagated to the nearest measurement point j, which will affect the estimation of the level and the parameters. As the effect of the fault $\Delta_k^{(i)}$ is attenuated in the propagation, it might be observed only in the nearest measurement points.

6.2.2 Data-based fault diagnosis in the CFr: simulation results

The measurements corresponding to five consecutive days starting from November 12, 2013 (Tuesday) have been considered. Additionally, a sliding window of size N_w = 1440 *min* (1 day) has been considered, which allows to take into account the CFr dynamics during night and day, thus guaranteeing the input persistent exciting order condition.

Then, three faulty scenarios have been created by adding three faults to the real measurements. Fault f_1 corresponds to a constant fault of -8 *cm* on the level L^C. Fault f_2 consists in an intermittent fault with a magnitude of 1.5 *cm* on the level L^A. Fault f_3 is also an intermittent fault with a magnitude of 5 *cm* on the level L^F. The features of the three faults are summarized in Table 6.5.

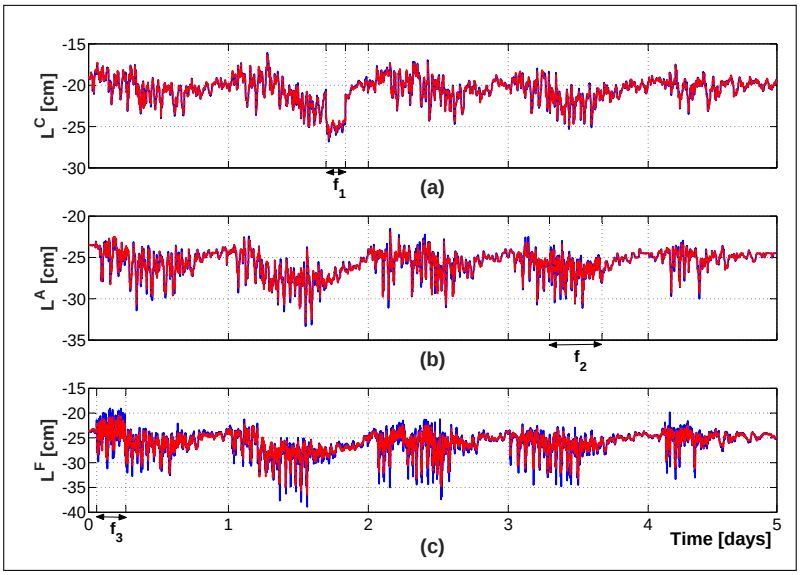

Figure 6.6: Measured faulty levels (blue solid line) and estimated levels (red solid line) in: (a) Cuinchy. (b) Aire-sur-la-Lys. (c) Fontinettes.

The three measured levels and their estimations are depicted in Fig. 6.6 for the three level sensors. The time occurrence and the duration of the faults are indicated with black arrows. Due to the dynamics of the CFr and the occurrence of lock operations, the detection of the faults is not obvious.

The level residuals have also been computed and are depicted in Fig. 6.7. It is not possible to detect fault f_1, except for two peaks in r^C that appear when the constant fault occurs and disappears. Moreover, the magnitude of these two peaks is not higher than other peaks in the residual r^C. By considering f_2 and residual r^A, an increase in the frequency of peaks with a similar magnitude can be observed during the occurrence of the fault, but their magnitude is not big enough. A similar behavior is obtained for f_3 and residual r^F.

Therefore, the proposed approach is performed according to the identified grey-box parameters by considering the $a_k^{(i,i)}$ terms and the predefined thresholds given in Fig. 6.7. These terms change during the simulation, as it is shown in Fig. 6.8. The parameter $a^{(1,1)}$ crosses the upper threshold after the occurrence of the fault f_1, which allows to detect the occurrence of one fault. The isolation task is carried out by considering which parameter is affected by the fault. Here, the fault f_1 is isolated because the

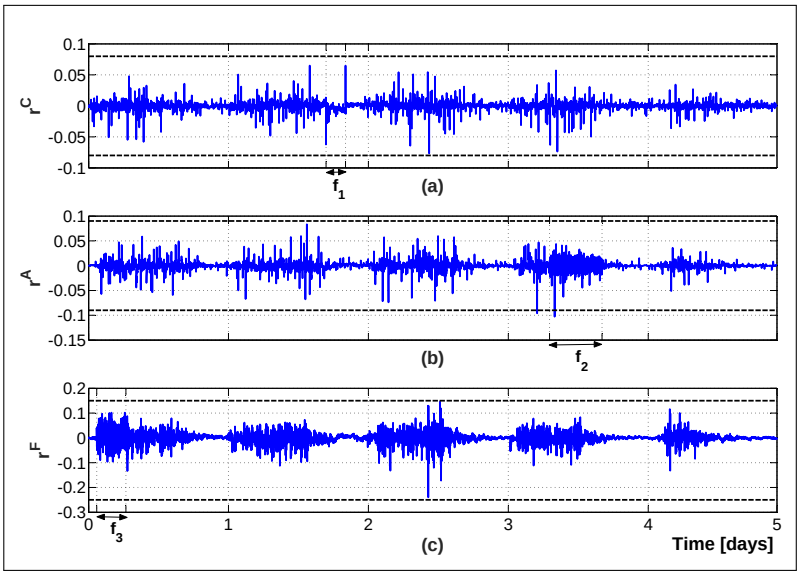

Figure 6.7: Level residuals (blue solid line) and thresholds (black dashed lines) for: (a) Cuinchy. (b) Aire-sur-la-Lys. (c) Fontinettes.

sensor level L^C is impacted. The detection and isolation of faults f_2 and f_3 is achieved by considering the parameters $a^{(2,2)}$ and $a^{(3,3)}$, respectively. The faults are detected when these parameters cross one of the predefined interval bounds. It can be observed that all faults can be detected after 4 h in average, and only the parameter residual fault signals $\phi_k^{a^{(j,i)}}$ are activated. The detection delays, given in Table 6.6, are due to the size of the sliding window. However, the magnitude of the considered faults is very small: larger faults should be detected faster and activate more fault signals.

It is shown that the detection and isolation of constant and intermittent faults can be performed by dealing with the grey-box model parameters. The dynamics of the system are modified in each scenario, but only one parameter moves away from its nominal value. Thus, this approach seems well suited to diagnose these kinds of faults.

6.3 Summary

Chapter 6 has addressed the design of fault diagnosis strategies that allow to detect and isolate sensor and actuator faults that might occur in inland waterways. Indeed, the

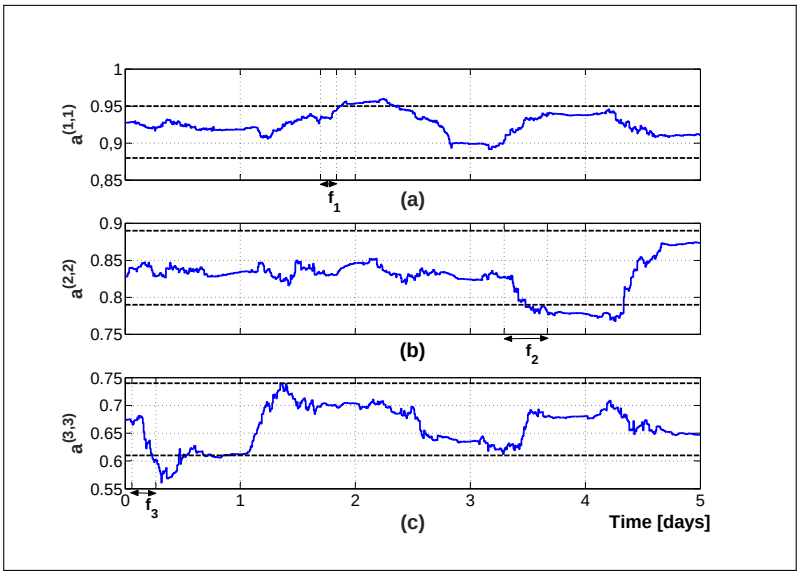

Figure 6.8: Evolution of the $a_k^{i,i}$ parameters (blue solid line) and determined thresholds (black dashed lines) in the faulty case: (a) $a^{1,1}$, (b) $a^{2,2}$, (c) $a^{3,3}$.

Table 6.6: Detection delay of each fault

Fault	Detection delay $[min]$
f_1	241
f_2	261
f_3	239

centralized and distributed control and state estimation techniques designed in previous chapters will only be effective provided that the acquired data is reliable and the actuators apply the correct control signals. To this end, two possible strategies are discussed and tested, based on the general model formulation derived in Chapter 3. However, the main difference lies in the approach that is followed to compute the parameters of the model. Indeed, the first one uses physical principles in the parameter computation (model-based approach), whereas the second one estimates them using available data (data-based approach). Given the fact that data are only available for part of the case study used throughout the thesis, both approaches are tested for the same part of the network in order to be comparable.

Part III

Concluding remarks

Chapter 7

Conclusions and future work

7.1 Conclusions

This thesis has proposed some contributions to the management of inland waterways from a control theory perspective, aiming at guaranteeing the navigability condition of the system, as well as other secondary operational goals. This chapter summarizes the work that has been carried out, which allows to draw conclusions and identify possible future works related to topics that were left out of the scope of the thesis.

— Chapter 3 has addressed the problem of modeling inland navigation networks, a challenging task due to the complex dynamics, large time delays and negligible bottom slopes that characterize such systems. Although the Saint-Venant equations represent the most accurate manner to describe their dynamics, these are not well suited for control purposes. As a first step, the IDZ model is employed in its original formulation to model systems consisting in only one reach. Owing to the importance of the backwater effect in inland waterways, caused by the negligible slope, the full model is considered, and not only the downstream equation. However, it can be realized that this formulation is not adequate when dealing with larger systems composed of interconnected reaches. Therefore, a more convenient state-space formulation is derived, which provides flexibility and allows to coordinate current and delayed information in a systematic manner. Additionally, mass balances at the junctions of the reaches can be incorporated into the model formulation (static part) by means of equality constraints. These features cause

the proposed model description to fall under the family of delayed descriptor models. Moreover, a parameter estimation approach for the state-space formulation is proposed, which can be used when the any physical parameter is not available, but system measurements are. These two approaches are tested using a realistic case study based on the inland waterways in the north of France. In the first scenario, all physical parameters are known, and thus the formulas for the IDZ parameters can be used. The obtained results show that a correct prediction is obtained for the downstream levels of the reaches, whereas the upstream levels deviate slightly from those computed using an hydraulic simulator, which requires some calibration. On the other hand, available data for part of the same inland waterways is used to adjust a gray-box model, whose predictive power is then assessed by means of different data. Fitting indicators between measured and predicted water levels are computed, demonstrating the effectiveness of the grey-box model.

— Chapter 4 has approached the issue of designing control and state estimation strategies that are able to cope with the proposed model formulation. It is argued that standard tools such as the LQR and the Kalman filter might need to be extended to deal with such models, concluding that MPC and MHE are suitable alternatives. Additionally, physical and operational constraints can be easily dealt with. This chapter regards their centralized design and implementation: first, the multi-objective function and the constraints are formulated in order to define the MPC. Then, after discussing the need to provide the vector of states to the MPC, the MHE is built using the MPC problem, as they are rather analogous. Some hints about the implementation and coding of both problems are provided by means of an algorithm, and their performance is tested by considering a realistic scenario. Both approaches perform as expected, succeeding at fulfilling the design goals in each case.

— Chapter 5 has discussed the adequacy of a centralized implementation for the MPC and MHE designed in the previous chapter. Indeed, a number of limitations such as the computational burden, the reliability and the scalability are pointed out, giving rise to non-centralized approaches, which are based on partitioning the overall system in subsystems and distributing the computational burden among the local agents, each of them in charge of meeting the objectives of a subsystem. Based on the existing available options, a distributed approach is preferred in the context of inland waterways due to their strongly connected nature. Then, the problem can be divided in two steps: first, the overall system is partitioned based on an existing

method that minimizes the number of couplings among the resulting subsystems. Next, DMPC and DMHE are designed for each local agent based on the centralized versions designed in the previous chapter. A communication protocol that allows them to communicate with the rest of subsystems is implemented, following the distributed philosophy. Results are obtained for the same scenario considered in the centralized approach, which allows to compare both results. Again, the results demonstrate the effectiveness of the DMPC and DMHE.

— Chapter 6 has addressed the occurrence of sensors and actuator faults in inland waterways, a topic that was not taken into account in the design of centralized and distributed control and state estimation approaches. Their solutions will only have the expected effect provided that sensors and actuators are not impacted by faults. In this regard, two different strategies, each of them using one of the approaches presented in Chapter 3 but both of them based on the computation of residuals. The first diagnosis strategy is of model-based type, and uses the water level predictions (given by the model) and the measurements (obtained using an hydraulic simulator) to compute water level residuals, which are used to assess the occurrence of faults. On the other hand, the second strategy is a data-based approach, as it uses real data. Another difference comes from the fact that the occurrence of faults is not deduced from water level residuals, but from the variation of the grey-box parameters, as real water levels are affected by unmodeled phenomena that complicates the fault diagnosis task. In any case, both approaches demonstrate their effectiveness by diagnosing correctly faulty events that were artificially injected into the system.

7.2 Directions for future research

Despite the efforts made in the context of this thesis to propose a solution for the inland waterways management problem, there are still many open issues that need to be addressed. The following list outlines open problems that were not considered within the scope of the thesis, thus establishing some directions for future research:

— In the context of modeling open-flow water systems, this thesis assumes that the system works always close to the same operating point, and thus that the use of only one linear model is enough to describe the dynamics of the system during

the whole simulation. Although this statement can be justified from the fact that the average flows do not deviate too much from the operating point, the nonlinear behavior can be retained, for instance, by considering LPV models. The extension to such formulation could be obtained using the results in [BP16].

— The derived state-space model formulation could be applied to other open-flow water systems such as irrigation and drainage canals and sewage systems, which are modeled using the same physical principles.

— Moreover, the general delayed descriptor model formulation could be employed to model any kind of system characterized by the transportation of mass, energy or information. Of course, the model parameters would need to be computed using different physical principles, but the backbone of the modeling approach remains the same.

— From the proposed approach, it has been shown that the MPC is able to reject the disturbances that are caused by the lock operations, using the state estimates provided by the MHE. These disturbances are assumed to be known in this thesis, but this seldom happens in real applications. Thus, strategies to estimate the effect of unknown disturbances, such as the unknown input observer (UIO), could be considered. This class of observer assumes no *a priori* knowledge about such inputs, which is an interesting feature to be exploited for fault diagnosis purposes.

— The system partitioning approach used in this thesis was rather qualitative, i.e., the relative importance of the couplings was not taken into account in order to define the partitioning. Future works might take into account this aspect to refine the approach.

— In Chapter 5, an iterative procedure of synchronous nature that allows the agents to reach a consensus was proposed. However, possible future works might consider asynchronous communication protocols. In this regard, an existing approach that could be investigated is that of allowing only one agent at a time to perform local computations and send information to the next agent [NDSH08]. Furthermore, communication reliability and decrease of performance due to loss of information are other issues that could also be examined in order to make the protocol more robust.

— Another possible improvement linked to control and state estimation could be to integrate the fault diagnosis module and the control and state estimation approaches in a fault-tolerant control (FTC) strategy, aiming at ensuring that the

navigability condition is met even when the system is in faulty condition. In this way, each time a fault was detected, the faulty component could be isolated. Then, a reconfiguration mechanism could modify the structure of the control and state estimation problems, aiming at providing the optimal (degraded) performance.

— It was stated that centralized approaches are often impractical to reconfigure for maintenance or malfunctioning purposes. Therefore, it seems natural to consider the distributed approach for the purpose of FTC.

— Finally, the fault diagnosis approaches are tested by considering the occurrence of only one fault at a time. This methodology could be tested in the case of simultaneous fault occurrences.

Part IV

Appendices

Appendix A

Derivation of the distributary model

The first step consists in finding model (3.1) for each reach, which reads as

$$\begin{aligned} y_1^{(\kappa)} &= p_{11}^{(\kappa)}(s)q_1^{(\kappa)} + p_{12}^{(\kappa)}(s)q_2^{(\kappa)}, \\ y_2^{(\kappa)} &= p_{21}^{(\kappa)}(s)q_1^{(\kappa)} + p_{22}^{(\kappa)}(s)q_2^{(\kappa)}, \end{aligned} \tag{A.1}$$

with $\kappa \in \{1, 2, 3\}$. Based on Remark 5.1, (A.1) can be rewritten as

$$\begin{aligned} y_1^{(\kappa)} &= p_{11}^{(\kappa)}(s)q_1^{(\kappa)} - p_{12}^{(\kappa)}(s)q_2^{(\kappa)}, \\ y_2^{(\kappa)} &= p_{21}^{(\kappa)}(s)q_1^{(\kappa)} - p_{22}^{(\kappa)}(s)q_2^{(\kappa)}. \end{aligned} \tag{A.2}$$

Then, the following conditions need to be imposed at the central node:

$$y_2^{(1)} = y_1^{(2)} = y_1^{(3)}, \tag{A.3a}$$
$$q_1^{(2)} = \lambda q_2^{(1)}, \tag{A.3b}$$
$$q_1^{(3)} = (1-\lambda) q_2^{(1)}, \tag{A.3c}$$

where (A.3a) ensures that no sudden jump in the water levels occurs, while $\lambda \in (0, 1)$ indicates that the flow is divided between the two streams after the node.

Imposing $y_2^{(1)} = y_1^{(2)}$ as given in (A.3a) leads to

$$p_{21}^{(1)} q_1^{(1)} - p_{22}^{(1)} q_2^{(1)} = p_{11}^{(2)} q_1^{(2)} - p_{12}^{(2)} q_2^{(2)}, \tag{A.4}$$

and substituting (A.3b) into (A.4) and reordering yields

$$q_2^{(1)} = \frac{p_{21}^{(1)}}{\lambda p_{11}^{(2)} + p_{22}^{(1)}} + \frac{p_{12}^{(2)}}{\lambda p_{11}^{(2)} + p_{22}^{(1)}}. \tag{A.5}$$

On the other hand, imposing the other equality $y_2^{(1)} = y_1^{(3)}$ given in (A.3a) leads to

$$p_{21}^{(1)} q_1^{(1)} - p_{22}^{(1)} q_2^{(1)} = p_{11}^{(3)} q_1^{(3)} - p_{12}^{(3)} q_2^{(3)}, \tag{A.6}$$

and substituting (A.3c) into (A.6) and reordering yields

$$q_2^{(1)} = \frac{p_{21}^{(1)}}{(1-\lambda)\, p_{11}^{(3)} + p_{22}^{(1)}} + \frac{p_{12}^{(3)}}{(1-\lambda)\, p_{11}^{(3)} + p_{22}^{(1)}}. \tag{A.7}$$

The linear combination $\lambda\cdot$(A.5) + $(1-\lambda)\cdot$(A.7), where the terms are given by

$$\lambda q_2^{(1)} = \frac{\lambda p_{21}^{(1)}}{\lambda p_{11}^{(2)} + p_{22}^{(1)}} q_1^{(1)} + \frac{\lambda p_{12}^{(2)}}{\lambda p_{11}^{(2)} + p_{22}^{(1)}} q_2^{(2)}, \tag{A.8a}$$

$$(1-\lambda)\, q_2^{(1)} = \frac{(1-\lambda)\, p_{21}^{(1)}}{(1-\lambda)\, p_{11}^{(3)} + p_{22}^{(1)}} q_1^{(1)} + \frac{(1-\lambda)\, p_{12}^{(3)}}{(1-\lambda)\, p_{11}^{(3)} + p_{22}^{(1)}} q_2^{(3)}, \tag{A.8b}$$

is computed and reads as follows:

$$\begin{aligned} q_2^{(1)} = &\left(\frac{\lambda p_{21}^{(1)}}{\lambda p_{11}^{(2)} + p_{22}^{(1)}} + \frac{(1-\lambda)\, p_{21}^{(1)}}{(1-\lambda)\, p_{11}^{(3)} + p_{22}^{(1)}} \right) q_1^{(1)} \\ &+ \frac{\lambda p_{12}^{(2)}}{\lambda p_{11}^{(2)} + p_{22}^{(1)}} q_2^{(2)} + \frac{(1-\lambda)\, p_{12}^{(3)}}{(1-\lambda)\, p_{11}^{(3)} + p_{22}^{(1)}} q_2^{(3)}. \end{aligned} \tag{A.9}$$

Equation (A.9) is then substituted into $y_1^{(1)}$, $y_2^{(2)}$ and $y_2^{(3)}$, whose expressions are given by (A.1), yielding the final model (3.7):

$$y_1^{(1)} = p_{11}^{(1)} q_1^{(1)} + p_{12}^{(1)} q_2^{(1)} = \tag{A.10a}$$
$$= p_{11}^{(1)} q_1^{(1)} + p_{12}^{(1)} \left[\left(\frac{\lambda p_{21}^{(1)}}{\lambda p_{11}^{(2)} + p_{22}^{(1)}} + \frac{(1-\lambda)\, p_{21}^{(1)}}{(1-\lambda)\, p_{11}^{(3)} + p_{22}^{(1)}} \right) q_1^{(1)} + \right.$$
$$\left. + \frac{\lambda p_{12}^{(2)}}{\lambda p_{11}^{(2)} + p_{22}^{(1)}} q_2^{(2)} + \frac{(1-\lambda)\, p_{12}^{(3)}}{(1-\lambda)\, p_{11}^{(3)} + p_{22}^{(1)}} q_2^{(3)} \right] =$$
$$= \left[p_{11}^{(1)} + p_{12}^{(1)} p_{21}^{(1)} \left(\frac{\lambda}{\lambda p_{11}^{(2)} - p_{22}^{(1)}} + \frac{1-\lambda}{(1-\lambda) p_{11}^{(3)} - p_{22}^{(1)}} \right) \right] q_1^{(1)} +$$
$$+ \left(\frac{\lambda p_{12}^{(1)} p_{12}^{(2)}}{\lambda p_{11}^{(2)} + p_{22}^{(1)}} \right) q_2^{(2)} + \left(\frac{(1-\lambda)\, p_{12}^{(1)} p_{12}^{(3)}}{(1-\lambda)\, p_{11}^{(3)} + p_{22}^{(1)}} \right) q_2^{(3)},$$

$$y_2^{(2)} = p_{21}^{(2)} q_1^{(2)} + p_{22}^{(2)} q_2^{(2)} = p_{21}^{(2)} \lambda q_2^{(1)} + p_{22}^{(1)} q_2^{(2)} = \tag{A.10b}$$
$$= p_{21}^{(2)} \lambda \left[\left(\frac{\lambda p_{21}^{(1)}}{\lambda p_{11}^{(2)} + p_{22}^{(1)}} + \frac{(1-\lambda)\, p_{21}^{(1)}}{(1-\lambda)\, p_{11}^{(3)} + p_{22}^{(1)}} \right) q_1^{(1)} + \right.$$
$$\left. + \frac{\lambda p_{12}^{(2)}}{\lambda p_{11}^{(2)} + p_{22}^{(1)}} q_2^{(2)} + \frac{(1-\lambda)\, p_{12}^{(3)}}{(1-\lambda)\, p_{11}^{(3)} + p_{22}^{(1)}} q_2^{(3)} \right] + p_{22}^{(1)} q_2^{(2)} =$$
$$= \lambda p_{21}^{(1)} p_{21}^{(2)} \left(\frac{\lambda}{\lambda p_{11}^{(2)} + p_{22}^{(1)}} + \frac{1-\lambda}{(1-\lambda) p_{11}^{(3)} + p_{22}^{(1)}} \right) q_1^{(1)} +$$
$$+ \left(p_{22}^{(2)} + \frac{\lambda^2 p_{12}^{(2)} p_{21}^{(2)}}{\lambda p_{11}^{(2)} + p_{22}^{(1)}} \right) q_2^{(2)} + \frac{\lambda(1-\lambda) p_{21}^{(2)} p_{12}^{(3)}}{(1-\lambda) p_{11}^{(3)} + p_{22}^{(1)}} q_2^{(3)},$$

$$y_2^{(3)} = p_{21}^{(3)} q_1^{(3)} + p_{22}^{(3)} q_2^{(3)} = p_{21}^{(3)} (1-\lambda)\, q_2^{(1)} + p_{22}^{(3)} q_2^{(3)} = \tag{A.10c}$$
$$= p_{21}^{(3)} (1-\lambda) \left[\left(\frac{\lambda p_{21}^{(1)}}{\lambda p_{11}^{(2)} + p_{22}^{(1)}} + \frac{(1-\lambda)\, p_{21}^{(1)}}{(1-\lambda)\, p_{11}^{(3)} + p_{22}^{(1)}} \right) q_1^{(1)} + \right.$$
$$\left. + \frac{\lambda p_{12}^{(2)}}{\lambda p_{11}^{(2)} + p_{22}^{(1)}} q_2^{(2)} + \frac{(1-\lambda)\, p_{12}^{(3)}}{(1-\lambda)\, p_{11}^{(3)} + p_{22}^{(1)}} q_2^{(3)} \right] + p_{22}^{(3)} q_2^{(3)} =$$
$$= (1-\lambda) p_{21}^{(1)} p_{21}^{(3)} \left(\frac{\lambda}{\lambda p_{11}^{(2)} + p_{22}^{(1)}} + \frac{1-\lambda}{(1-\lambda) p_{11}^{(3)} + p_{22}^{(1)}} \right) q_1^{(1)} +$$
$$+ \frac{\lambda(1-\lambda) p_{12}^{(2)} p_{21}^{(3)}}{\lambda p_{11}^{(2)} + p_{22}^{(1)}} q_2^{(2)} + \left(p_{22}^{(3)} + \frac{(1-\lambda)^2 p_{12}^{(3)} p_{21}^{(3)}}{(1-\lambda) p_{11}^{(3)} + p_{22}^{(1)}} \right) q_2^{(3)}.$$

Appendix B

A grey-box model for inland waterways

B.1 The autoregressive exogenous model

An AutoRegressive eXogenous (ARX) model is chosen for the purpose of time-series modeling. Hence, it is assumed that the current value of the series of interest (output) depends not only on past output values, but also on past values of the exogenous series (inputs)[JWH05].

The general formulation for this class of models is as follows:

$$y_k = -a_1 y_{k-1} - a_2 y_{k-2} - ... - a_{n_a} y_{k-n_a} + b_1 u_{k-1} + b_2 u_{k-2} + ... + b_{n_b} u_{k-n_b} + e_k, \quad \text{(B.1)}$$

where n_a and n_b are the model orders, a_i and b_j are the model coefficients, for $i = 1, ..., n_a$ and $j = 1, ..., n_b$, and e_k is a white noise process.

A more compact representation of (B.1) is given below:

$$\tilde{A}(q^{-1}) y_k = \tilde{B}(q^{-1}) u_k + e_k, \quad \text{(B.2)}$$

with

$$\tilde{A}(q^{-1}) = 1 + a_1 q^{-1} + a_2 q^{-2} + ... + a_{n_a} q^{-n_a} \quad \text{(B.3)}$$

and

$$\tilde{B}(q^{-1}) = b_1 q^{-1} + b_2 q^{-2} + ... + b_{n_b} q^{-n_b}, \tag{B.4}$$

where q^{-1} is the delay operator.

Remark B.1. The tilde in $\tilde{A}$ and $\tilde{B}$ is used to avoid confusion with the state-space matrices $\mathbf{A}$ and $\mathbf{B}$. □

Based on the available data, the output can be estimated at each time instant as follows:

$$\hat{y}_k = \left(1 - \tilde{A}(q^{-1})\right) y_k + \tilde{B}(q^{-1}) u_k + e_k. \tag{B.5}$$

B.2 Model derivation

A grey-box model structure, similar to (B.5), can be derived from the continuous-time state-space representation of the IDZ model:

$$\dot{\mathbf{x}}(t) = \mathbf{A}\mathbf{x}(t) + \mathbf{B}_q \mathbf{q}(t) + \mathbf{B}_{qn} \mathbf{q}(t-\tau), \tag{B.6a}$$

$$\mathbf{y}(t) = \mathbf{C}\mathbf{x}(t) + \mathbf{D}_q \mathbf{q}(t) + \mathbf{D}_{qn} \mathbf{q}(t-\tau). \tag{B.6b}$$

Note that (B.6) describes any system that can be represented by the matrices $\mathbf{A}$, $\mathbf{B}_q$, $\mathbf{B}_{qn}$, $\mathbf{C}$, $\mathbf{D}_q$, and $\mathbf{D}_{qn}$, e.g., one-reach systems and larger portions of inland waterways.

Then, the variable $\mathbf{x}(t)$ is isolated from (B.6b) as

$$\mathbf{x}(t) = \mathbf{C}^{-1}\mathbf{y}(t) - \mathbf{C}^{-1}\mathbf{D}_q \mathbf{q}(t) - \mathbf{C}^{-1}\mathbf{D}_{qn} \mathbf{q}(t-\tau). \tag{B.7}$$

Then, (B.7) is derived, which leads to

$$\dot{\mathbf{x}}(t) = \mathbf{C}^{-1}\dot{\mathbf{y}}(t) - \mathbf{C}^{-1}\mathbf{D}_q \dot{\mathbf{q}}(t) - \mathbf{C}^{-1}\mathbf{D}_{qn} \dot{\mathbf{q}}(t-\tau). \tag{B.8}$$

The right-hand side terms of (B.6a) and (B.8) are equated:

$$\mathbf{A}\mathbf{x}(t) + \mathbf{B}_q \mathbf{q}(t) + \mathbf{B}_{qn} \mathbf{q}(t-\tau) = \mathbf{C}^{-1}\dot{\mathbf{y}}(t) - \mathbf{C}^{-1}\mathbf{D}_q \dot{\mathbf{q}}(t) - \mathbf{C}^{-1}\mathbf{D}_{qn} \dot{\mathbf{q}}(t-\tau). \tag{B.9}$$

Note that $\mathbf{A} = \mathbf{0}$ as stated in (3.20), and thus (B.9) can be simplified as

$$\mathbf{B}_q\mathbf{q}(t) + \mathbf{B}_{qn}\mathbf{q}(t-\tau) = \mathbf{C}^{-1}\dot{\mathbf{y}}(t) - \mathbf{C}^{-1}\mathbf{D}_q\dot{\mathbf{q}}(t) - \mathbf{C}^{-1}\mathbf{D}_{qn}\dot{\mathbf{q}}(t-\tau). \tag{B.10}$$

The discretization of (B.10) is performed in such a way that the continuous current time instant t corresponds to the discrete time instant k:

$$\begin{aligned}\mathbf{B}_q\mathbf{q}_{k-1} + \mathbf{B}_{qn}\mathbf{q}_{k-n-1} = \\ \mathbf{C}^{-1}\frac{\mathbf{y}_k - \mathbf{y}_{k-1}}{T_s} - \mathbf{C}^{-1}\mathbf{D}_q\frac{\mathbf{q}_k - \mathbf{q}_{k-1}}{T_s} - \mathbf{C}^{-1}\mathbf{D}_{qn}\frac{\mathbf{q}_{k-n} - \mathbf{q}_{k-n-1}}{T_s},\end{aligned} \tag{B.11}$$

with T_s the sampling time and $n = \lceil \tau/T_s \rceil$ as in (3.23).

Rearranging terms in (B.11) leads to

$$\mathbf{y}_k = \mathbf{y}_{k-1} + \mathbf{D}_q\mathbf{q}_k + \underbrace{(T_s\mathbf{C}\mathbf{B}_q - \mathbf{D}_q)}_{\mathbf{B}_1}\mathbf{q}_{k-1} + \mathbf{D}_{qn}\mathbf{q}_{k-n} + \underbrace{(T_s\mathbf{C}\mathbf{B}_{qn} - \mathbf{D}_{qn})}_{\mathbf{B}_2}\mathbf{q}_{k-n-1}, \tag{B.12}$$

which can be expressed in a more compact form as

$$\hat{\mathbf{y}}_{k+1} = \tilde{\mathbf{A}}\overline{\mathbf{y}}_{k|\kappa} + \tilde{\mathbf{B}}\overline{\mathbf{q}}_{k|\kappa}, \tag{B.13}$$

with $\tilde{\mathbf{A}} \in \mathbb{R}^{n_y \times (n_y \times n_\kappa)}$, $\tilde{\mathbf{B}} \in \mathbb{R}^{n_y \times (n_u \times n_\kappa)}$, $\overline{\mathbf{y}}_{k|\kappa} \in \mathbb{R}^{(n_y \times n_\kappa)\times 1}$ and $\overline{\mathbf{q}}_{k|\kappa} \in \mathbb{R}^{(n_u \times n_\kappa)\times 1}$. Moreover, n_u is the number of actuators, n_y is the number of sensors and n_κ is the total delay in the system. On the other hand, $\tilde{\mathbf{B}}$ can be built by adequately placing the elements of $\mathbf{D}_q$, $\mathbf{B}_1$, $\mathbf{D}_{qn}$ and $\mathbf{B}_2$, taking into account the corresponding delay of each term. A schematic view of a general system that can be described by (B.13) is reported in Fig. B.1.

Further insight on the grey-box model formulation is provided below:

— Equation (B.13) assumes that the i-th water level $y_k^{(i)}$ and the j-th discharge $q_k^{(j)}$ have an influence on the m-th water level $\hat{y}_{k+1}^{(m)}$, $\forall i, m \in \{1, \ldots, n_y\}$ and $\forall j \in \{1, \ldots, n_u\}$. On the other hand, (B.12), which was derived from the IDZ model, considers that only the i-th water level and all discharges $q_k^{(j)}$ have an influence on the same i-th water water level $\hat{y}_{k+1}^{(i)}$. This assumption leads to a *free* model formulation, as all the relationships among variables are permitted, which is more

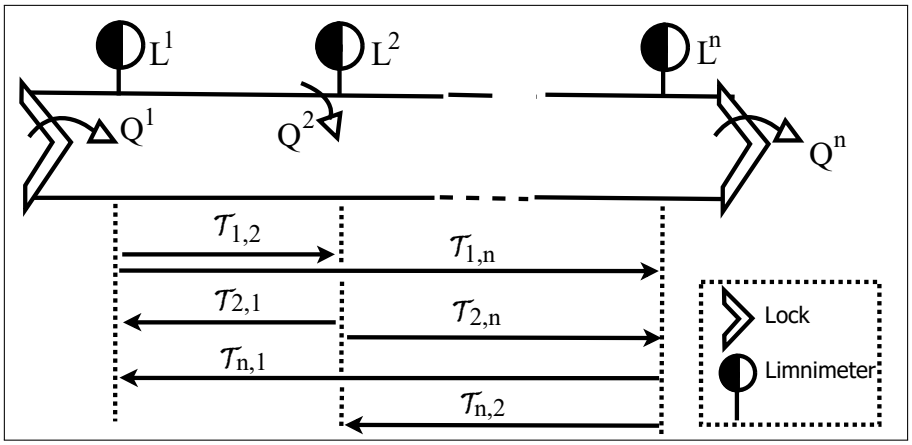

Figure B.1: Time delays τ_{ij} between each pair of measurement points

general than the IDZ formulation.

— With regard to the statement above, it is assumed that matrices $\tilde{\mathbf{A}}$ and $\tilde{\mathbf{B}}$ are composed of a set of blocks $\tilde{\mathbf{A}}^{(i)}$ and $\tilde{\mathbf{B}}^{(i)}$, respectively. Then, the pair $\left(\tilde{\mathbf{A}}^{(i)}, \tilde{\mathbf{B}}^{(i)}\right)$ links the levels y_k and the discharges q_k with the i-th level estimation $\hat{y}_{k+1}^{(i)}$. Furthermore, in order to particularize (B.13) to the IDZ case, only one term in $\mathbf{A}^{(i)}$ should be different from 0, namely $a^{(i,i)}$.

— The input variables $\overline{\mathbf{q}}_{k|\kappa} \in \mathbb{R}^{(n_u \times n_\kappa)\times 1}$ correspond to a combination of the components of the input vector $\mathbf{q}_k = \left[q_k^{(1)} \dots q_k^{(n_u)}\right]^T$ with convenient delays, where $q_k^{(l)} = Q_k^{(l)}\ \forall l = 1, ..., n_u$ are the different discharges along the canal. Similarly, the output variables $\overline{\mathbf{y}}_{k|\kappa} \in \mathbb{R}^{(n_y \times n_\kappa)\times 1}$ correspond to a combination of the components of the output vector $\mathbf{y}_k = \left[y_k^{(1)} \dots y_k^{(n_y)}\right]^T$ with convenient delays, where $y_k^{(i)} = L_k^{(i)}$ $\forall i = 1, ..., n_y$ are the different level measurements along the canal. More precisely:

- The vector $\overline{\mathbf{y}}_{k|\kappa}$ is expressed as

$$\overline{\mathbf{y}}_{k|\kappa} = \left[\overline{\mathbf{y}}_{k|\kappa}^{(1)}\ \overline{\mathbf{y}}_{k|\kappa}^{(2)}\ \cdots\ \overline{\mathbf{y}}_{k|\kappa}^{(n_y)}\right]^\intercal, \tag{B.14}$$

  with $\overline{\mathbf{y}}_{k|\kappa}^{(i)} = \left[L_{k-\kappa_{i,1}}^{(1)}\ L_{k-\kappa_{i,2}}^{(2)}\ \cdots\ L_{k-\kappa_{i,n_\kappa}}^{(n_\kappa)}\right]$.

- The vector $\overline{\mathbf{q}}_{k|\kappa}$ is expressed as

$$\overline{\mathbf{q}}_{k|\kappa} = \left[\overline{\mathbf{q}}_{k|\kappa}^{(1)}\ \overline{\mathbf{q}}_{k|\kappa}^{(2)}\ \cdots\ \overline{\mathbf{q}}_{k|\kappa}^{(n_u)}\right]^\intercal, \tag{B.15}$$

  with $\overline{\mathbf{q}}_{k|\kappa}^{(i)} = \left[Q_{k-\kappa_{i,1}}^{(1)}\ Q_{k-\kappa_{i,2}}^{(2)}\ \cdots\ Q_{k-\kappa_{i,n_\kappa}}^{(n_\kappa)}\right]$.

— The estimation of the delays in the network for the grey-box model is not addressed in this thesis. Instead, it is assumed that these are characterized by the relationships in [LF09] in a precise manner. As the system is considered to be working within the interval [NNL, HNL] during the simulation, it is assumed that their variation is not so large. In the future, an extension with varying operating conditions could be carried out, thus being necessary to re-estimate all the model parameters, and not only the delays.

Remark B.2. (B.12) and (B.13) could also be expressed in terms of openings and elevations by introducing the relationships given in (3.10) and (3.11), as appropriate. However, the available input data are in terms of the discharges and not the openings, which justifies the proposed notation. □

Bibliography

[ABQ+99] F. Allgöwer, T. A. Badgwell, J. S. Qin, J. B. Rawlings, and S. J. Wright. Nonlinear predictive control and moving horizon estimation — an introductory overview. In Paul M. Frank, editor, *Advances in Control*, pages 391–449, London, 1999. Springer London.

[ÁRRS13] A. Álvarez, M. A. Ridao, D. R. Ramírez, and L. Sánchez. Constrained predictive control of an irrigation canal. *Journal of Irrigation and Drainage Engineering*, 139(10):841–854, 2013.

[AvORT17] B. E. Aydin, P. J. van Overloop, M. Rutten, and X. Tian. Offset-Free Model Predictive Control of an Open Water Channel Based on Moving Horizon Estimation. *Journal of Irrigation and Drainage Engineering*, 143(3):B4016005, 2017.

[BBM10] M. Breckpot, T. Barjas Blanco, and B. De Moor. Flood control of rivers with nonlinear model predictive control and moving horizon estimation. In *49th IEEE Conference on Decision and Control (CDC)*, pages 6107–6112, Dec 2010.

[BBPE02] Y. Bolea, J. Blesa, V. Puig, and T. Escobet. Identification of an open canal: parametric black-box vs Muskingum approaches. In *IEEE International Conference on Systems, Man and Cybernetics*, volume 5, Oct 2002.

[BFR07] O. Begovich, J. C. Felipe, and V. M. Ruiz. Real-time implementation of a decentralized control for an open irrigation canal prototype. *Asian Journal of Control*, 9(2):170–179, 2007.

[BHD+14] J. Blesa, K. Horváth, E. Duviella, V. Puig, Y. Bolea, L. Rajaoarisoa, and K. Chuquet. Model-based sensor supervision in inland navigation networks: Cuinchy-fontinettes case study. *Journal of Maritime Research*, 11(2):81–88, 2014.

[BKLS06] M. Blanke, M. Kinnaert, J. Lunze, and M. Staroswiecki. *Diagnosis and fault-tolerant control*. Springer-Verlag Berlin Heidelberg, 2006.

[BLKM06] N. Bedjaoui, X. Litrico, D. Koenig, and P. O. Malaterre. H_∞ observer for time-delay systems. Application to FDI for irrigation canals. In *Proceedings of the 45th IEEE Conference on Decision and Control*, pages 532–537, 2006.

[BMGGMG09] Y. Bolea, R. Martínez-González, A. Grau, and H. Martínez-García. An LPV Fractional Model for Canal Control. *IFAC Proceedings Volumes*, 42(10):1786 – 1791, 2009. 15th IFAC Symposium on System Identification.

[Boe14] M. Boegli. *Real-Time Moving Horizon Estimation for Advanced Motion Control. Application to Friction State and Parameter Estimation.* PhD thesis, KU Leuven, Leuven, Belgium, 2014.

[BP16] Y. Bolea and V. Puig. Gain-scheduling multivariable LPV control of an irrigation canal system. *ISA transactions*, 63:274–280, 2016.

[BPB10] J. Blesa, V. Puig, and Y. Bolea. Fault detection using interval LPV models in an open-flow canal. *Control Engineering Practice*, 18(5):460–470, 2010.

[BPB14] Y. Bolea, V. Puig, and J. Blesa. Linear parameter varying modeling and identification for real-time control of open-flow irrigation canals. *Environmental Modelling & Software*, 53:87–97, 2014.

[BRB+07] O. Begovich, V. M. Ruiz, G. Besançon, C. Aldana, and D. Georges. Predictive control with constraints of a multi-pool irrigation canal prototype. *Latin American Applied Research*, 37(3):177–185, 2007.

[BW11] N. Bedjaoui and E. Weyer. Algorithms for leak detection, estimation, isolation and localization in open water channels. *Control Engineering Practice*, 19(6):564 – 573, 2011.

[CB98] E. F. Camacho and C. Bordons. *Model Predictive Control*. Springer, London, 1998.

[CGH17] D. A. Copp, R. Gondhalekar, and J. P. Hespanha. Simultaneous model predictive control and moving horizon estimation for blood glucose regulation in Type 1 diabetes. *Optimal Control Applications and Methods*, 39(2):904–918, 2017.

[CH17] D. A. Copp and J. P. Hespanha. Simultaneous nonlinear model predictive control and state estimation. *Automatica*, 77:143–154, 2017.

[Cho59] V. T. Chow. *Open-channel hydraulics*. McGraw-Hill Book Co. Inc, New York, 1959.

[CJKT02] E. Camponogara, D. Jia, B. H. Krogh, and S. Talukdar. Distributed model predictive control. *IEEE Control Systems Magazine*, 22(1):44–52, Feb 2002.

[CN09] X. Chen and I. M. Navon. Optimal control of a finite-element limited-area shallow-water equations model. *Studies in Informatics and Control*, 18(1):41–62, 2009.

[CP99] J. Chen and R. J. Patton. *Robust model-based fault diagnosis for dynamic systems*. Kluwer Academic Publishers, 1999.

[CSMndlPnL13] P. D. Christofides, R. Scattolini, D. Muñoz de la Peña, and J. Liu. Distributed model predictive control: A tutorial review and future research directions. *Computers & Chemical Engineering*, 51:21–41, 2013.

[DBSM+13] E. Duviella, L. Bako, M. Sayed-Mouchaweh, J. Blesa, Y. Bolea, V. Puig, and K. Chuquet. Inland navigation channel model: Application to the Cuinchy-Fontinettes reach. In *2013 10th IEEE International Conference on Networking, Sensing and Control (ICNSC)*, pages 164–169. IEEE, 2013.

[DCCC05] E. Duviella, P. Charbonnaud, P. Chiron, and F. J. Carrillo. Supervised internal multi-model control of a dam-gallery open-channel system. In *Proceedings of the 44th IEEE Conference on Decision and Control*, pages 1887–1892, 2005.

[Din08] S. X. Ding. *Model-based Fault Diagnosis Techniques: Design Schemes, Algorithms, and Tools*. Springer Science & Business Media, 2008.

[DPC+10] E. Duviella, V. Puig, P. Charbonnaud, T. Escobet, F. J. Carrillo, and J. Quevedo. Supervised gain-scheduling multimodel versus linear parameter varying internal model control of open-channel systems for large operating conditions. *Journal of Irrigation and Drainage Engineering*, 136(8):543–552, 2010.

[DRBC13] E. Duviella, L. Rajaoarisoa, J. Blesa, and K. Chuquet. Fault detection and isolation of inland navigation channel: application to the

Cuinchy-Fontinettes reach. In *52nd IEEE Conference on Decision and Control*, pages 4877–4882, 2013.

[DRBG17] V. Dalmas, G. Robert, G. Besançon, and D. Georges. Simplified non-uniform models for various flow configurations in open channels. *IFAC-PapersOnLine*, 50(1):12320 – 12325, 2017.

[DSMRD12] V. Dos Santos Martins, M. Rodrigues, and M. Diagne. A multi-model approach to Saint-Venant equations: a stability study by LMIs. *International Journal of Applied Mathematics and Computer Science*, 22(3):539–550, 2012.

[DSMWR14] V. Dos Santos Martins, Y. Wu, and M. Rodrigues. Design of a Proportional Integral Control Using Operator Theory for Infinite Dimensional Hyperbolic Systems. *IEEE Transactions on Control Systems Technology*, 22(5):2024–2030, 2014.

[dSV71] A. J. C. Barré de Saint-Venant. Théorie du mouvement non permanent des eaux, avec application aux crues des rivières et à l'introduction des marées dans leurs lits. *Comptes Rendus des séances de l'Académie des Sciences*, 73:237–240, 1871.

[FMH+14] F. Fele, J. M. Maestre, S. Mehdy Hashemy, D. Muñoz de la Peña, and Eduardo F. Camacho. Coalitional model predictive control of an irrigation canal. *Journal of Process Control*, 24(4):314–325, 2014.

[Ger98] J. Gertler. *Fault Detection and Diagnosis in Engineering Systems*. Marcel Dekker, New York, 1998.

[GL81] A. George and J. W. Liu. *Computer Solution of Large Sparse Positive Definite*. Prentice Hall Professional Technical Reference, 1981.

[GOMP17a] J. M. Grosso, C. Ocampo-Martínez, and V. Puig. A distributed predictive control approach for periodic flow-based networks: application to drinking water systems. *International Journal of Systems Science*, 48(14):3106–3117, 2017.

[GOMP17b] J. M. Grosso, C. Ocampo-Martínez, and V. Puig. Non-centralized Predictive Control for Drinking-Water Supply Systems. In *Real-time Monitoring and Operational Control of Drinking-Water Systems*, pages 341–360. Springer, 2017.

[GOMPJ14] J. M. Grosso, C. Ocampo-Martínez, V. Puig, and B. Joseph. Chance-constrained model predictive control for drinking water networks. *Journal of Process Control*, 24(5):504–516, 2014.

[GRM02] M. Gómez, J. Rodellar, and J. Mantecón. Predictive control method for decentralized operation of irrigation canals. *Applied Mathematical Modelling*, 26(11):1039–1056, 2002.

[HBD+14] K. Horváth, J. Blesa, E. Duviella, L. Rajaoarisoa, V. Puig, and K. Chuquet. Sensor fault diagnosis of inland navigation system using physical model and pattern recognition approach. *IFAC Proceedings Volumes*, 47(3):5309–5314, 2014. 19th IFAC World Congress.

[HDB+14] K. Horváth, E. Duviella, J. Blesa, L. Rajaoarisoa, Y. Bolea, V. Puig, and K. Chuquet. Gray-box model of inland navigation channel: application to the Cuinchy-Fontinettes reach. *Journal of Intelligent Systems*, 23(2):183–199, 2014.

[HDLM10] B. Hamroun, A. Dimofte, L. Lefèvre, and E. Mendes. Control by Interconnection and Energy-Shaping Methods of Port Hamiltonian Models. Application to the Shallow Water Equations. *European Journal of Control*, 16(5):545 – 563, 2010.

[HRD+15] K. Horváth, L. Rajaoarisoa, E. Duviella, J. Blesa, M. Petreczky, and K. Chuquet. Enhancing inland navigation by model predictive control of water levels: the Cuinchy-Fontinettes case. In *Transport of Water versus Transport over Water*, pages 211–234. Springer, 2015.

[Int14] Intergovernmental Panel on Climate Change. *Climate Change 2014 – Impacts, Adaptation and Vulnerability: Regional Aspects*. Cambridge University Press, 2014.

[Ise06] R. Isermann. *Fault Diagnosis Systems: An Introduction from Fault Detection to Fault Tolerance*. Springer, New York, 2006.

[JDOMC14] B. Joseph-Duran, C. Ocampo-Martínez, and G. Cembrano. Output-feedback control of combined sewer networks through receding horizon control with moving horizon estimation. *Water Resources Research*, 51(10):8129–8145, 2014.

[JWH05] A. L. Juloski, S. Weiland, and W. P. M. H. Heemels. A Bayesian approach to identification of hybrid systems. *IEEE Transactions on Automatic Control*, 50(10):1520–1533, 2005.

[Kal60] R. E. Kalman. A new approach to linear filtering and prediction problems. *Trans. ASME, Journal of Basic Engineering*, 82(1):35–45, 1960.

[KB61] R. E. Kalman and R. S. Bucy. New results in linear filtering and prediction theory. *Trans. ASME, Journal of Basic Engineering*, 83(1):95–108, 1961.

[KFK+13] T. Kraus, H. J. Ferreau, E. Kayacan, H. Ramon, J. De Baerdemaeker, M. Diehl, and W. Saeys. Moving horizon estimation and nonlinear model predictive control for autonomous agricultural vehicles. *Computers and Electronics in Agriculture*, 98:25–33, 2013.

[KMJ04] N. R. Kristensen, H. Madsen, and S. B. Jorgensen. Parameter estimation in stochastic grey-box models. *Automatica*, 40(2):225 – 237, 2004.

[KPPC18] F. Karimi Pour, V. Puig, and G. Cembrano. Health-aware LPV-MPC Based on System Reliability Assessment for Drinking Water Networks. In *2018 IEEE Conference on Control Technology and Applications (CCTA)*, pages 187–192. IEEE, 2018.

[LEDC15] L. Lao, M. Ellis, H. Durand, and P. D. Christofides. Real-time preventive sensor maintenance using robust moving horizon estimation and economic model predictive control. *AIChE Journal*, 61(10):3374–3389, 2015.

[LF04a] X. Litrico and V. Fromion. Analytical approximation of open-channel flow for controller design. *Applied Mathematical Modelling*, 28(7):677–695, 2004.

[LF04b] X. Litrico and V. Fromion. Simplified modeling of irrigation canals for controller design. *Journal of Irrigation and Drainage Engineering*, 130(5):373–383, 2004.

[LF06] X. Litrico and V. Fromion. H-infinity control of an irrigation canal pool with a mixed control politics. *IEEE Transactions on Control Systems Technology*, 14(1):99 – 111, 2006.

[LF09] X. Litrico and V. Fromion. *Modeling and Control of Hydrosystems*. Springer, 2009.

[LF12] Y. M. Liu and I. K. Fong. On the controllability and observability of discrete-time linear time-delay systems. *International Journal of Systems Science*, 43(4):610–621, 2012.

[Lju99] L. Ljung. *System identification: theory for the user (2nd Edition)*. Prentice Hall, Upper Saddle River, 1999.

[LMBRB08] X. Litrico, P. O. Malaterre, J. Baume, and J. Ribot-Bruno. Conversion from discharge to gate opening for the control of irrigation canals. *Journal of Irrigation and Drainage Engineering*, 134(3):305–314, 2008.

[LMN+09] J. M. Lemos, F. Machado, N. Nogueira, L. M. Rato, and M. Rijo. Adaptive and non-adaptive model predictive control of an irrigation channel. *Networks and heterogeneous media*, 4(2):303–324, 2009.

[Löf04] J. Löfberg. YALMIP: a toolbox for modeling and optimization in MATLAB. In *IEEE International Symposium on Computer Aided Control Systems Design*, Taipei, Taiwan, 2004.

[Mac02] J. M. Maciejowski. *Predictive control: with constraints*. Pearson education, 2002.

[Mal95] P. O. Malaterre. Regulation of irrigation canals. *Irrigation and Drainage Systems*, 9(4):297–327, Nov 1995.

[Man91] R. Manning. On the flow of water in open channels and pipes. *Transactions of the Institution of Civil Engineers of Ireland*, 20:161–207, 1891.

[MDB14] P. O. Malaterre, D. Dorchies, and J. Baume. Automatic tuning of robust PI controllers for a cascade of rivers or irrigation canals pools. In *2014 European Control Conference (ECC)*, pages 2780–2785, June 2014.

[MN14] J. M. Maestre and R. R. Negenborn. *Distributed model predictive control made easy*, volume 69. Springer Sciene & Business Media, 2014.

[MPE10] J. Meseguer, V. Puig, and T. Escobet. Fault diagnosis using a timed discrete-event approach based on interval observers: Application to sewer networks. *IEEE Transactions on Systems, Man, and Cybernetics Part A:Systems and Humans*, 40(5):900–916, 2010.

[NDSH08] R. R. Negenborn, B. De Schutter, and J. Hellendoorn. Multi-agent model predictive control for transportation networks: serial versus parallel schemes. *Engineering Applications of Artificial Intelligence*, 21(3):353 – 366, 2008.

[NMB12] J. L. Nabais, L. Mendonça, and M. A. Botto. New fault isolation architecture for irrigation canals. *IFAC Proceedings Volumes*, 45(20):450 – 455, 2012. 8th IFAC Symposium on Fault Detection, Supervision and Safety of Technical Processes.

[NPLGC17] L. Nguyen, I. Prodan, L. Lefèvre, and D. Genon-Catalot. Distributed Model Predictive Control of Irrigation Systems using Cooperative Controllers. *IFAC-PapersOnLine*, 50(1):6564–6569, 2017.

[NS70] J. E. Nash and J. V. Sutcliffe. River flow forecasting through conceptual models part I: a discussion of principles. *Journal of Hydrology*, 10(3):282–290, 1970.

[NvODS09] R. R. Negenborn, P. J. van Overloop, and B. De Schutter. Coordinated model predictive reach control for irrigation canals. In *Proceedings of the European Control Conference 2009*, pages 1420–1425, August 2009.

[NvOKDS09] R. Negenborn, P. J. van Overloop, T. Keviczky, and B. De Schutter. Distributed model predictive control of irrigation canals. *Networks and Heterogeneous Media*, 4(2):359–380, 2009.

[Oga02] K. Ogata. *Modern Control Engineering, 5th Edition.* Prentice Hall, 2002.

[OMBP11] C. Ocampo-Martínez, S. Bovo, and V. Puig. Partitioning approach oriented to the decentralised predictive control of large-scale systems. *Journal of Process Control*, 21(5):775 – 786, 2011.

[OMBPB12] C. Ocampo-Martinez, D. Barcelli, V. Puig, and A. Bemporad. Hierarchical and decentralised model predictive control of drinking water networks: Application to Barcelona case study. *IET Control Theory & Applications*, 6(1):62 –71, 5 2012.

[OMPCQ13] C. Ocampo-Martínez, V. Puig, G. Cembrano, and J. Quevedo. Application of predictive control strategies to the management of complex networks in the urban water cycle. *IEEE Control Systems Magazine*, 33(1):15–41, 2013.

[ON08] S. Olaru and S. I. Niculescu. Predictive control for linear systems with delayed input subject to constraints. *IFAC Proceedings Volumes*, 41(2):11208 – 11213, 2008.

[OW01] S. K. Ooi and E. Weyer. Closed loop identification of an irrigation channel. In *Proceedings of the 40th IEEE Conference on Decision and Control (Cat. No.01CH37228)*, volume 5, pages 4338–4343, Dec 2001.

[PB13] V. Puig and J. Blesa. Limnimeter and rain gauge FDI in sewer networks using an interval parity equations based detection approach and an enhanced isolation scheme. *Control Engineering Practice*, 21(2):146–170, 2013.

[PCL+10] V. T. Pham, B. Chopard, L. Lefèvre, D. Anda Ondo, and E. Mendes. Study of the 1D lattice Boltzmann shallow water equation and its coupling to build a canal network. *Journal of Computational Physics*, 229(19):7373 – 7400, 2010.

[PGB14] V. T. Pham, D. Georges, and G. Besançon. Infinite-dimensional predictive control for hyperbolic systems. *SIAM Journal on Control and Optimization*, 52(6):3592–3617, 2014.

[PLGB14] V. T. Pham, L. Lefèvre, D. Georges, and G. Besançon. Decentralized predictive control for 1D cascaded systems of conservation laws. *IFAC Proceedings Volumes*, 47(3):5163 – 5168, 2014. 19th IFAC World Congress.

[POMN15] V. Puig, C. Ocampo-Martínez, and R. R. Negenborn. Model predictive control for combined water supply and navigability/sustainability in river systems. In *Transport of Water versus Transport over Water*, pages 13–33. Springer, 2015.

[PQE+05] V. Puig, J. Quevedo, T. Escobet, P. Charbonnaud, and E. Duviella. Identification and Control of an Open-flow Canal using LPV Models. In *Proceedings of the 44th IEEE Conference on Decision and Control*, pages 1893–1898, Dec 2005.

[PRQ+09] V. Puig, J. Romera, J. Quevedo, C. M. Cardona, A. Salterain, E. Ayesa, I. Irizar, A. Castro, M. Lujan, P. Charbonnaud, P. Chiron, and J. L. Trouvat. Optimal predictive control of water transport systems: Arret-Darre/Arros case study. *Water science and technology*, 60(8):2125–2133, 2009.

[QCH15] S. A. P. Quintero, D. A. Copp, and J. P. Hespanha. Robust UAV coordination for target tracking using output-feedback model predictive control with moving horizon estimation. In *Proceedings of the American Control Conference*, pages 3758–3764, 2015.

[RA10] M. Reble and F. Allgöwer. Stabilizing design parameters for model predictive control of constrained nonlinear time-delay systems. *IFAC Proceedings Volumes*, 43(2):361 – 366, 2010.

[Rao00] C. V. Rao. *Moving horizon strategies for the constrained monitoring and control of nonlinear discrete-time systems*. PhD thesis, University of Wisconsin–Madison, 2000.

[RM09] J. B. Rawlings and D. Q. Mayne. *Model predictive control: theory and design*. Nob Hill Pub. Madison, Wisconsin, 2009.

[RPFBCGLS14] R. Rivas-Pérez, V. Feliu-Batlle, F. J. Castillo-García, and A. Linares-Sáez. Mathematical model for robust control of an irrigation main canal pool. *Environmental Modelling & Software*, 51:207 – 220, 2014.

[RRL01] C. V. Rao, J. B. Rawlings, and J. H. Lee. Constrained linear state estimation – a moving horizon approach. *Automatica*, 37(10):1619–1628, 2001.

[RRM03] C. V. Rao, J. B. Rawlings, and D. Q. Mayne. Constrained State Estimation for Nonlinear Discrete-Time Systems: Stability and Moving Horizon Approximations. *IEEE Transactions on Automatic Control*, 48(2):246–258, 2003.

[RS08] J. B. Rawlings and B. T. Stewart. Coordinating multiple optimization-based controllers: New opportunities and challenges. *Journal of Process Control*, 18(9):839 – 845, 2008.

[SBB95] J. Schuurmans, O. H. Bosgra, and R. Brouwer. Open-channel flow model approximation for controller design. *Applied Mathematical Modelling*, 19(9):525 – 530, 1995.

[SBD+18a] P. Segovia, J. Blesa, E. Duviella, L. Rajaoarisoa, F. Nejjari, and V. Puig. Sensor fault diagnosis in inland navigation networks based on a grey-box model. *IFAC-PapersOnLine*, 51(24):742–747, 2018.

[SBD+18b] P. Segovia, J. Blesa, E. Duviella, L. Rajaoarisoa, F. Nejjari, and V. Puig. Sliding window assessment for sensor fault model-based diagnosis in inland waterways. *IFAC-PapersOnLine*, 51(5):31–36, 2018.

[SBH+18] P. Segovia, J. Blesa, K. Horváth, L. Rajaoarisoa, F. Nejjari, V. Puig, and E. Duviella. Modeling and fault diagnosis of flat inland navigation canals. *Proceedings of the Institution of Mechanical Engineers, Part I: Journal of Systems and Control Engineering*, 232(6):761–771, 2018.

[Sca09] R. Scattolini. Architectures for distributed and hierarchical Model Predictive Control - a review. *Journal of Process Control*, 19(5):723 – 731, 2009.

[SCD+99] J. Schuurmans, A. J. Clemmens, S. Dijkstra, A. Hof, and R. Brouwer. Modeling of irrigation and drainage canals for controller design. *Journal of irrigation and drainage engineering*, 125(6):338–344, 1999.

[SFCB+17] A. Soldevila, R. M. Fernández-Cantí, J. Blesa, S. Tornil-Sin, and V. Puig. Leak localization in water distribution networks using Bayesian classifiers. *Journal of Process Control*, 55:1 – 9, 2017.

[SFMC01] S. Sawadogo, R. M. Faye, and F. Mora-Camino. Decentralized adaptive predictive control of multireach irrigation canal. *International Journal of Systems Science*, 32(10):1287–1296, 2001.

[SHR+17] P. Segovia, K. Horváth, L. Rajaoarisoa, F. Nejjari, V. Puig, and E. Duviella. Modeling of two sub-reach water systems: application to navigation canals in the north of France. In *14th International Conference on Informatics in Control, Automation and Robotics (ICINCO)*, pages 459–467, 2017.

[Sil11] D. D. Siljak. *Decentralized control of complex systems*. Courier Corporation, 2011.

[SLNRA12] T. L. M. Santos, D. Limón, J. E. Normey-Rico, and T. Álamo. On the explicit dead-time compensation for robust model predictive control. *Journal of Process Control*, 22(1):236 – 246, 2012.

[SNRL10] T. L. M. Santos, J. E. Normey-Rico, and D. Limón. Explicit input-delay compensation for robustness improvement in MPC. *IFAC Proceedings Volumes*, 43(2):384 – 389, 2010.

[SRD+17] P. Segovia, L. Rajaoarisoa, E. Duviella, J. Blesa, F. Nejjari, V. Puig, and K. Horváth. Fault detection and isolation in flat navigation canals. In *2017 4th International Conference on Control, Decision and Information Technologies (CoDIT)*, pages 427–432, 2017.

[SRN+] P. Segovia, L. Rajaoarisoa, F. Nejjari, E. Duviella, and V. Puig. A distributed model predictive control and moving horizon estimation approach for the optimal management of inland waterways. *To be submitted.*

[SRN+17] P. Segovia, L. Rajaoarisoa, F. Nejjari, V. Puig, and E. Duviella. Decentralized control of inland navigation networks with distributaries: application to navigation canals in the north of France. In *American Control Conference*, pages 3341–3346. IEEE, 2017.

[SRN+18a] P. Segovia, L. Rajaoarisoa, F. Nejjari, E. Duviella, and V. Puig. Distributed Input-Delay Model Predictive Control of Inland Waterways. In Goffredo La Loggia, Gabriele Freni, Valeria Puleo, and Mauro De Marchis, editors, *HIC 2018. 13th International Conference on Hydroinformatics*, volume 3 of *EPiC Series in Engineering*, pages 1893–1901. EasyChair, 2018.

[SRN+18b] P. Segovia, L. Rajaoarisoa, F. Nejjari, E. Duviella, and V. Puig. Input-delay model predictive control of inland waterways considering the backwater effect. In *2018 IEEE Conference on Control Technology and Applications (CCTA)*, pages 589–594. IEEE, 2018.

[SRN+18c] P. Segovia, L. Rajaoarisoa, F. Nejjari, V. Puig, and E. Duviella. Modeling of interconnected flat open-channel flow: application to inland navigation canals. In *Advances in Hydroinformatics*, pages 75–90. Springer Singapore, 2018.

[SRN+19a] P. Segovia, L. Rajaoarisoa, F. Nejjari, E. Duviella, and V. Puig. A communication-based distributed model predictive control approach for large-scale systems. In *2019 IEEE Conference on Decision and Control (CDC)*, 2019. Submitted.

[SRN+19b] P. Segovia, L. Rajaoarisoa, F. Nejjari, E. Duviella, and V. Puig. Model predictive control and moving horizon estimation for water level regulation in inland waterways. *Journal of Process Control*, 76C:1–14, 2019.

[SZL+95] J. Sjöberg, Q. Zhang, L. Ljung, A. Benveniste, B. Delyon, P. Y. Glorennec, H. Hjalmarsson, and A. Juditsky. Nonlinear black-box modeling in system identification: a unified overview. *Automatica*, 31(12):1691 – 1724, 1995.

[TOMCP18] F. Tedesco, C. Ocampo-Martínez, A. Casavola, and V. Puig. Centralized and Distributed Command Governor Approaches for Water Supply Systems Management. *IEEE Transactions on Systems, Man, and Cybernetics: Systems*, 48(4):586–595, 2018.

[TOML+11] R. Toro, C. Ocampo-Martínez, F. Logist, J. Van Impe, and V. Puig. Tuning of predictive controllers for drinking water networked systems. *IFAC Proceedings Volumes*, 44(1):14507–14512, 2011.

[TR02] M. J. Tenny and J. B. Rawlings. Efficient moving horizon estimation and nonlinear model predictive control. In *Proceedings of the 2002 American Control Conference*, volume 6, pages 4475–4480, May 2002.

[VGH+15] M. Vukov, S. Gros, G. Horn, G. Frison, K. Geebelen, J.B. Jorgensen, J. Swevers, and M. Diehl. Real-time nonlinear MPC and MHE for a large-scale mechatronic application. *Control Engineering Practice*, 45:64–78, 2015.

[vO06] P. J. van Overloop. *Model predictive control on open water systems*. PhD thesis, Delft University of Technology, Delft, The Netherlands, 2006.

[vOB12] P. J. van Overloop and X. Bombois. Identification of properties of open water channels for controller design. In *IFAC Symposium on System Identification*, volume 16, pages 1019–1024, 2012.

[vOCS+10] P. J. van Overloop, A. Clemmens, R. Strand, R. Wagemaker, and E. Bautista. Real-time implementation of model predictive control on Maricopa-Stanfield irrigation and drainage district's WM canal. *Journal of Irrigation and Drainage Engineering*, 136(11):747–756, 2010.

[vOHA14] P. J. van Overloop, K. Horváth, and B. E. Aydin. Model predictive control based on an integrator resonance model applied to an open water channel. *Control Engineering Practice*, 27:54 – 60, 2014.

[vOMB+10] P. J. van Overloop, I. J. Miltenburg, X. Bombois, A. J. Clemmens, R. Strand, and N. van de Giesen. Identification of resonance waves in open water channels. *Control Engineering Practice*, 18(8):863–872, 2010.

[VONDSVDG10] P. J. Van Overloop, R. R. Negenborn, B. De Schutter, and N. C. Van De Giesen. Predictive control for national water flow optimization in The Netherlands. *Intelligent Infrastructures*, 42:439–461, 2010.

[VTSM19] P. Velarde, X. Tian, A. D. Sadowska, and J. M. Maestre. Scenario-Based Hierarchical and Distributed MPC for Water Resources Management with Dynamical Uncertainty. *Water Resources Management*, 33(2):677–696, 2019.

[Wey01] E. Weyer. System identification of an open water channel. *Control Engineering Practice*, 9(12):1289 – 1299, 2001.

[Whi99] F. M. White. *Fluid Mechanics*. McGraw-Hill, New York, 1999.

[WJ95] M. Wooldridge and N. R. Jennings. Intelligent agents: theory and practice. *The Knowledge Engineering Review*, 10(2):115–152, 1995.

[WOP16] Y. Wang, C. Ocampo-Martínez, and V. Puig. Stochastic model predictive control based on Gaussian processes applied to drinking water networks. *IET Control Theory & Applications*, 10(8):947–955, 2016.

[WPC17] Y. Wang, V. Puig, and G. Cembrano. Non-linear economic model predictive control of water distribution networks. *Journal of Process Control*, 56:23–34, 2017.

[ZCMR+11] A. Zafra-Cabeza, J. M. Maestre, M. A. Ridao, E. F. Camacho, and L. Sánchez. A hierarchical distributed model predictive control approach to irrigation canals: a risk mitigation perspective. *Journal of Process Control*, 21(5):787–799, 2011.

Model-based control and diagnosis of inland navigation networks

This thesis addresses the problem of optimal management of water resources in inland navigation networks from a control theory perspective. The main objectives to be attained consist in guaranteeing the navigability condition of the network, minimizing the operational cost and ensuring a long lifespan of the equipment. However, their complex dynamics, large time delays and negligible bottom slopes complicate their management. In order to achieve the optimal management, the efficient control of the hydraulic structures must be ensured. To this end, a control-oriented modeling approach is derived. The resulting formulation belongs to the class of delayed descriptor systems, for which model predictive control and moving horizon estimation can be easily adapted, as well as being able to deal with physical and operational constraints in a natural manner. However, a centralized implementation is often neither possible nor desirable. As these networks are strongly coupled systems, a distributed approach is followed, featuring a communication protocol among agents. Despite the optimality of the solutions, any malfunction can lead to an inefficient system management. Therefore, the last part of the thesis regards the design of supervisory strategies that allow to detect and isolate faults. All the presented approaches are applied to a realistic case study based on the inland navigation network in the north of France to validate their effectiveness. ***Keywords:*** inland navigation networks, large-scale systems, time-delay systems, Saint-Venant equations, control-oriented modeling, model predictive control, moving horizon estimation, system partitioning, distributed control and state estimation, fault diagnosis.

Contrôle et diagnostic à base de modèles des voies navigables

Cette thèse contribue à répondre au problème de la gestion optimale des ressources en eau dans les réseaux de navigation intérieure du point de vue de la théorie du contrôle. Les objectifs principales à atteindre consistent à garantir la navigabilité des réseaux de voies navigables, veiller à la réduction des coûts opérationnels et à la longue durée de vie des équipements. Lors de la conception de lois de contrôle, les caractéristiques des réseaux doivent étre prises en compte, à savoir leurs dynamiques complexes, des retards variables et l'absence de pente. Afin de réaliser la gestion optimale, le contrôle efficace des structures hydrauliques doit être assuré. À cette fin, une approche de modélisation orientée contrôle est dérivée. Cependant, la formulation obtenue appartient à la classe des systèmes de descripteurs retardés, pour lesquels la commande prédictive MPC et l'estimation d'état sur horizon glissant MHE peuvent être facilement adaptés à cette formulation, tout en permettant de gérer les contraintes physiques et opérationnelles de manière naturelle. En raison de leur grande dimensionnalité, une mise en œuvre centralisée n'est souvent ni possible ni souhaitable. Compte tenu du fait que les réseaux de navigation intérieure sont des systèmes fortement couplés, une approche distribuée est proposée, incluant un protocole de communication entre agents. Malgré l'optimalité des solutions, toute erreur peut entraîner une gestion inefficace du système. Par conséquent, les dernières contributions de la thèse concernent la conception de stratégies de supervision permettant de détecter et d'isoler les pannes des équipements. Toutes les approches présentées sont appliquées à une étude de cas réaliste basée sur le réseau de voies navigables du nord de la France afin de valider leur efficacité. ***Mots-clés:*** réseaux de voies navigables, systèmes à grande échelle, systèmes à retard, équations de Saint-Venant, modélisation orientée contrôle, commande prédictive, estimation d'état sur horizon glissant, partitionnement de systèmes, commande et estimation d'état distribuées, diagnostic de pannes.